

Biomimetic Bilayer Membranes Made from Polymers and Lipids

Dissertation
zur Erlangung des Grades
„Doktor der Naturwissenschaften“
im Promotionsfach Chemie

am Fachbereich Chemie, Pharmazie und Geowissenschaften
der Johannes Gutenberg - Universität Mainz

vorgelegt von

Jan Dorn
geboren in Frankfurt am Main

Mainz, 2010

Die vorliegende Arbeit wurde in der Zeit von März 2007 bis Februar 2010 in der Arbeitsgruppe Materialforschung am Max-Planck-Institut für Polymerforschung angefertigt.

Dekan:

1. Berichterstatter:

2. Berichterstatter:

Tag der mündlichen Prüfung: 15.03.2010

Viele Dinge sind nicht unmöglich,..... bis man sie ausprobiert hat.

Terry Pratchett

Table of Contents

Motivation	1
1. General Introduction	3
1.1. The Cell Membrane	3
1.2. General Aspects of Biomembrane Models	4
1.2.1. Black Lipid Membranes (BLM).....	6
1.2.2. Vesicles	6
1.2.3. Supported Bilayer Lipid Membranes	7
1.2.4. Tethered Bilayer Lipid Membranes	8
1.3. Polymer Bilayers	9
1.4. Proteins in Polymer Bilayers	11
1.5. Objectives of this Thesis.....	13
2. Materials and Methods	15
2.1. Materials	15
2.2. Methods	18
2.2.1. Atomic Force Microscopy (AFM)	18
2.2.2. Surface Plasmon Resonance Spectroscopy (SPR)	21
2.2.3. Electrochemical Impedance Spectroscopy (EIS)	25
2.2.4. Fluorescence Correlation Spectroscopy (FCS)	30
3. Supported Polymer Membranes through Langmuir-Blodgett Film Transfer.....	35
3.1. Introduction	35
3.2. Experimental Section.....	37
3.3. Results and Discussion	39
3.3.1. Monolayers at the Air-Water Interface	39
3.3.2. Monolayers on Gold.....	40
3.3.3. Bilayer Membranes on Gold	43
3.3.4. Membrane Stability	47
3.4. Summary.....	51
4. Biomimetic Planar Polymer Bilayers through Vesicle Spreading	53
4.1. Introduction	53
4.2. Experimental.....	57
4.3. Results and Discussion	58
4.3.1. Vesicles on Hydrophobic Support.....	59

4.3.2.	Vesicles on Hydrophilic Support	60
4.3.3.	Vesicle Spreading on Gold through Covalent Interactions	63
4.3.4.	Interactions of Proteins and Peptides with the Supported Polymer Bilayer	74
4.4.	Summary & Conclusion	79
5.	Single Molecule Diffusion in Giant-Unilamellar-Polymer-Vesicles	81
5.1.	Introduction	81
5.2.	Materials and Methods	85
5.2.1.	Materials	85
5.2.2.	Single Particle Tracking (SPT)	88
5.2.3.	Fluorescence Correlation Spectroscopy (FCS)	89
5.3.	Results and Discussion	91
5.3.1.	Diffusion in Lipid Bilayers	92
5.3.2.	Diffusion in Polymer Bilayers.....	94
5.3.3.	Diffusion of the Model Peptide FGFR3-(TM).....	98
5.4.	Summary and Outlook.....	105
6.	On the Preparation of Planar Lipid Bilayers on Peptide Support	107
6.1.	Introduction	107
6.2.	Experimental.....	109
6.3.	Results and Discussion	112
6.3.1.	Analysis of the Existing Surface Preparation Procedure	112
6.3.2.	A New Route to Peptide Tethered Lipid Bilayers.....	116
6.3.3.	Bilayer Formation via Rapid Solvent Exchange	117
6.3.4.	Interactions of Valinomycin with the Bilayer Membrane.....	121
6.4.	Summary.....	123
7.	General Summary and Conclusion.....	125
8.	Outlook.....	127
9.	References	129
10.	Appendix	145
	Acknowledgement.....	147
	Publications	148

Abbreviations

AC	Alternating Current
AFM	Atomic Force Microscopy
α -HL	α -Haemolysin
ATRP	Atom Transfer Radical Polymerization
BAM	Brewster Angle Microscopy
BFP	Back Focal Plane
BLM	Black Lipid Membrane
BSA	Bovine Serum Albumin
CMC	Critical Micelle Concentration
CPE	Constant Phase Element
CT	Cholera toxin
DCM	Dichloromethane
DiPhyPC	Diphytanoylphosphatidylcholine
DMAP	Dimethylaminopyridin
DMF	Dimethylformamide
DOPC	Dioleoylphosphatidylcholine
DOSY	Diffusion Ordered Spectroscopy
DPTL	Diphytanyl-glycerol-tetraethylene glycol-lipoic acid ester lipid
EDC	1-Ethyl-3-(3-dimethylaminopropyl)carbodiimid
EIS	Electrochemical Impedance Spectroscopy
FGFR3	Fibroblast Growth Factor Receptor
FGFR3-(TM)	Fibroblast Growth Factor Receptor- Transmembrane Domain
FRAP	Fluorescence Recovery After Photobleaching
GM1	Monosialotetrahexosylganglioside
GPC	Gel Permeation Chromatography
GUV	Giant Unilamellar Vesicle
HEPES	(4-(2-hydroxyethyl)-1-piperazineethanesulfonic acid)
HPLC	High Pressure Liquid Chromatography
ITO	Indium Tin Oxide
LA	Lipoic Acid
LB	Langmuir-Blodgett
LS	Langmuir-Schaefer
LUV	Large Unilamellar Vesicle

MEK	Methyl-Ethyl-Ketone
MSD	Mean Square Displacement
NA	Numerical Aperture
NHS	<i>N</i> -Hydroxysuccinimide
NMR	Nuclear Magnetic Resonance
OCD	Oriented Circular Dichroism
OmpF	Outer Membrane Protein F
PB	Polybutadiene
PB-PEO	Polybutadiene-Polyethylenoxide
PBS	Phosphate Buffered Saline
PDI	Polydispersity Index
PDMS	Polydimethylsiloxane
PEE-PEO	Polyethylethylene-Polyethylenoxide
PEG	Polyethyleneglycol
PEO	Polyethyleneoxide
PFP	Pentafluorophenole
QCM	Quartz Crystal Microbalance
SAM	Self Assembled Monolayer
SBLM	Supported Polymer Bilayer
SEM	Scanning Electron Microscope
SOPC	Stearoyl-Oleoyl- Phosphatidylcholine
SPM	Scanning Probe Microscopy
SPR	Surface Plasmon Resonance
SPT	Single Particle Tracking
SUV	Small Unilamellar Vesicle
TEM	Transmission Electron Microscope
THF	Tetrahydrofuran
TIRF	Total Internal Reflection Fluorescence
TM	Transmembrane
TMR	Tetramethylrhodamine
TSG	Template Stripped Gold

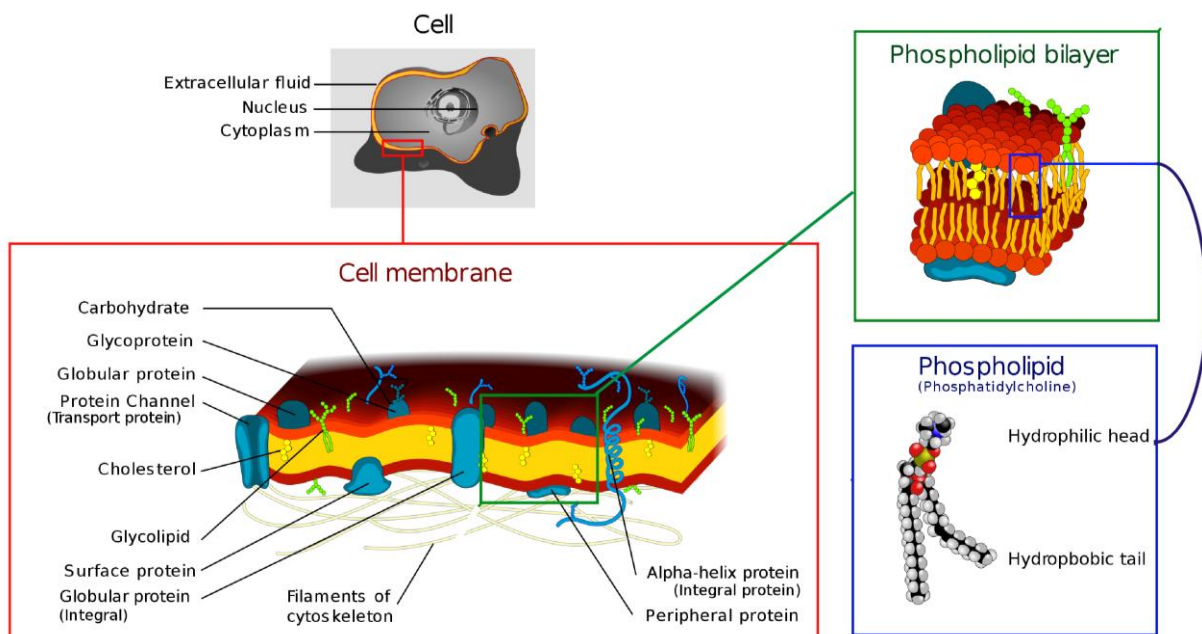
Motivation

There is a great need for model systems of cellular membranes to study membrane proteins outside the complex natural environment. For this purpose a wide range of lipid based model systems has been developed over the past decades. Such membrane models are for example employed as efficient screening platforms in pharmaceutical research because today 60% of all approved drugs on the market target membrane proteins. Biosensing is another field where membrane models are used. The basic principle of such a biosensor is to exploit the specific recognition properties of membrane bound receptors in a device which can be read out upon analyte binding. The main requirements to these systems are to omit the complexity of the natural cell membrane while ensuring the full functionality of the embedded proteins. A general drawback of lipid based model membranes is that they show a lack of mechanical stability necessary for long term use and many technical applications. Therefore new concepts for stable model membrane systems have to be developed. The motivation of the work presented here is to explore the field of amphiphilic polymers as the constituents of artificial model systems for the incorporation of membrane proteins. The main focus was on surface supported systems because they have several advantages over vesicular and free standing systems like additional stability and accessibility to a wide range of surface sensitive techniques.

1. General Introduction

1.1. The Cell Membrane

Native biological membranes are one of the key structures of all living organisms. They pose a barrier between the interior and the exterior of cells controlling and maintaining concentration gradients for molecules of all kinds. The cell membrane consists of numerous components like lipids, integral and peripheral proteins and cholesterol to mention just a few. The main components that form the matrix are lipids. These amphiphilic molecules form extended two-dimensional structures via self-assembly. Lipids consist of a hydrophilic head group and a hydrophobic tail. In a selective solvent like water the hydrophobic acyl ester moieties associate with other molecules to form aggregates wherein the unpolar moieties are grouped together to reduce their contact area to water. The packing of hydrophobic chains is energetically and entropically favoured because hydrocarbon chains cannot form hydrogen bonds with water which reduces the number of possible arrangements of water molecules around them. This is the basis for the so called hydrophobic effect. Within the lipid matrix consisting of over 100 different lipid species there are proteins incorporated or attached to it. Besides that small molecules like cholesterol and large structures of the cytoskeleton also play their cooperative role (Scheme 1).



Scheme 1: Simplified structure of the cell membrane and its components.^[1]

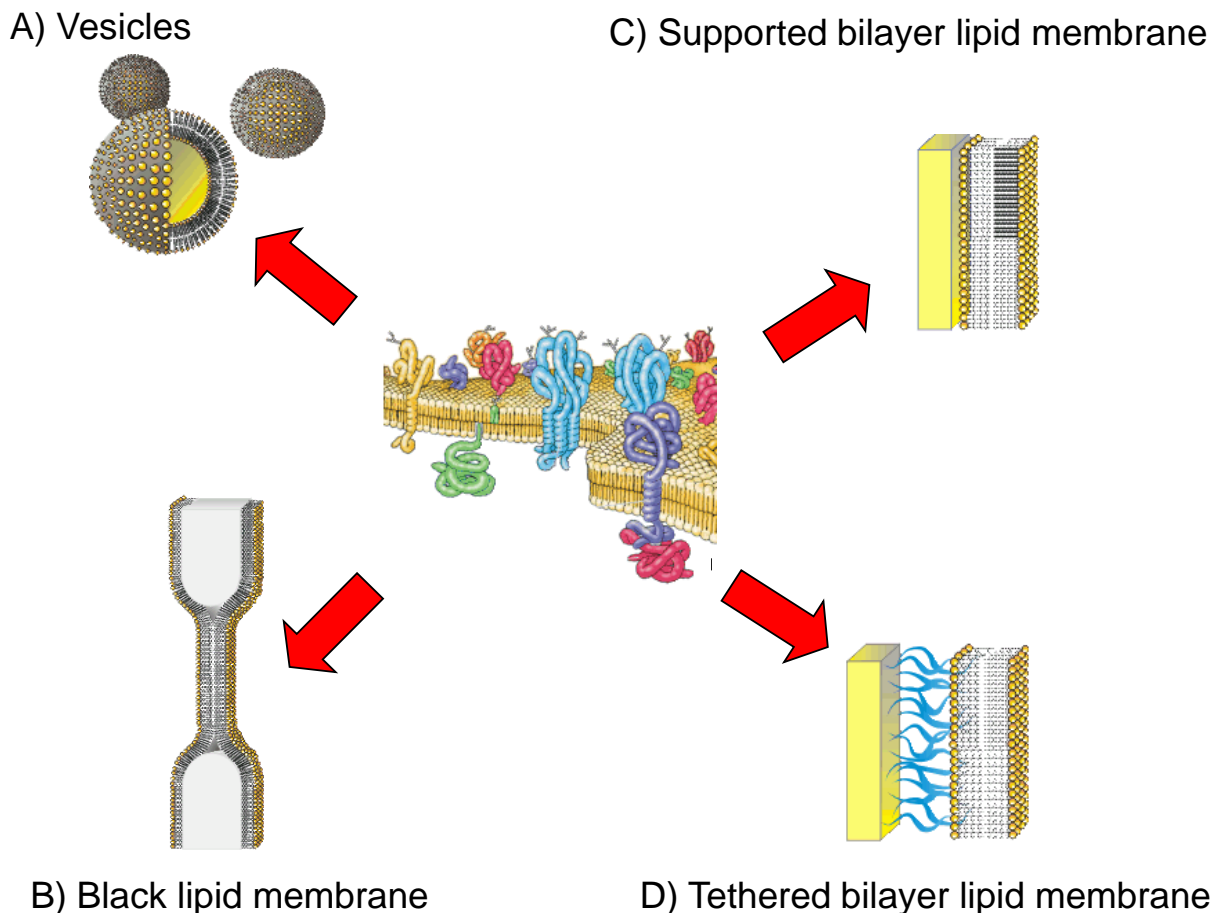
This complex structure composed of a mixture of cell components allows for a selective interplay of the cell with its environment. Among the functions the membrane is involved in are cellular differentiation, growth, and interactions with the environment like signalling. These functions result from many dynamic processes within the cell membrane. A concept suggested by Singer and Nicholson describes the biological membrane as a fluid mosaic where proteins can diffuse freely in the two dimensional viscous liquid represented by the lipid bilayer.^[2] During the past almost four decades since this model was proposed a lot of research has been carried out to elucidate membrane structures and functions. Today it is known that fluidity is not as free as was initially thought. Now it is generally believed that non random co-distribution patterns of specific kinds of membrane proteins and lipids form small-scale clusters at the molecular level and large-scale clusters at the micrometre scale. Such groups of clusters or islands at the sub-micrometer level determine membrane behaviour.^[3] For example the existence of transiently formed lipid islands – also termed rafts - can favour enrichment of a protein in these phases which can be important for processes like enzyme activation or ligand receptor recognition. Cell membranes are perfectly suited to maintain the delicate balance between flexibility and stability. Nature can even sacrifice some stability to favour dynamics because there are highly sophisticated membrane repair mechanisms that can heal defects caused by mechanical or chemical perturbation.^[4-5] As one can notice many natural biomembranes are highly complex structures where the presence and interplay of different components supports the functions that enable life. The many membrane components and processes interacting at the same time make membrane research of isolated aspects often difficult or even impossible.

1.2. General Aspects of Biomembrane Models

For direct investigations of membrane-related processes on the molecular level it is necessary to resolve this complexity into its compounds. For this purpose the development of simplified model systems has attracted attention in laboratories all over the world. Such membrane models offer great potential in fundamental scientific research, especially for investigating structure and function of membrane proteins. Drug research field for example is one field where artificial membrane models. Since many biochemical processes in cells happen in or at the membrane today over 60% of approved drugs on the market target membrane proteins.^[6] Therefore, platforms for efficient drug screening are needed which enable the separate

investigation of specific membrane proteins. One general aspect that has to be considered is that every membrane structure and membrane process is optimized *in vivo* for a native intact complex system. By focusing on one isolated species one might “oversimplify” the subject of investigation. An example for this is the discovery of lipid rafts. In the beginning, phase behaviour of lipid mixtures was studied in supported lipid bilayers where domain sizes of several micrometers were observed.^[7] These domains were very stable. Later on one realized that such extended rafts cannot be found *in vivo* because non-considered lipid and protein species have an influence on the upper limit of domain size and lifetime.^[8]

Therefore, it is absolutely necessary to choose a realistic model system for the aspect of membrane research under investigation. To date a wide variety of lipid model membrane systems for the study of membrane related processes exists as visualized below in Scheme 2.



Scheme 2: Different model membrane systems. (A) Vesicular system; (B) free standing black lipid bilayer (BLM); (C) supported bilayer lipid membrane (SBLM); tethered bilayer lipid membrane (tBLM).^[9]

1.2.1. Black Lipid Membranes (BLM)

The free standing lipid bilayer as it is sketched in Scheme 2 B spans the aperture of a Teflon film. This creates an interaction free membrane model and is accessible from both sides. The name *black lipid bilayer* (BLM) is derived from the fact that the lipid film appears black when it is spanning the aperture. The black “colour” is the result of destructive interference between the reflected light at the two respective hydrophilic/hydrophobic interfaces. The first preparation of BLMs was reported in 1962^[10] where an organic lipid solution was “painted” across such an aperture. After the successful bilayer formation some solvent still remains inside the hydrophobic core so that it can interfere with sensitive membrane proteins. A solvent free^[11] method was first developed by Montal *et al.*. By lowering the aperture through a monomolecular Langmuir film at the air water interface a lipid monolayer is spanned over the hole from both sides resulting in a bilayer. BLM proved to be especially useful for electrochemical measurements investigating membrane pores^[12] and of proton pumps.^[13] A general disadvantage of BLMs is the low mechanical stability. BLM setups have to be installed in a vibration free environment but still last only several hours.^[14]

1.2.2. Vesicles

Vesicles as shown in Scheme 2 A represent an alternative to free standing BLMs. They also have a bilayer structure and can be thought of as a bilayer sheet where the edges are folded together to form a spherical particle. A wide range of vesicle sizes can be prepared with diameters from ~ 20 nm to 100 μm . Their rough classification is as follows: small unilamellar vesicles (SUV) $\text{\O} < 100 \text{ nm}$, large unilamellar vesicles (LUV) $\text{\O} 100 \text{ nm} - 1 \mu\text{m}$, giant unilamellar vesicles (GUV) $\text{\O} > 1 \mu\text{m}$. SUVs are mainly used for protein research in suspension^[15] where many aggregates are present. They are also used as precursors for supported lipid bilayer (discussed later). Due to the diffraction limit they cannot be used for single objects measurements. In contrast to that LUVs and GUVs can be resolved in a brightfield microscope which allows easy handling. When they are labelled with a dye they can also be visualized in fluorescence microscopy which is often done in biological experiments. One typical application for GUVs are measurements of lateral diffusion of components^[16] or lipid phase behaviour^[17] within the membrane plane. Furthermore they proved to be an excellent system for the *in vitro* expression of membrane proteins^[18] and the

investigation of protein-lipid interaction^[19] In some cases it can be useful to tether vesicles to a planar surface. This produces lipid bilayer structures free from perturbations from the surface because the vesicle components can diffuse freely along the vesicle shell. Moreover a strict surface localization necessary for surface sensitive measurement techniques is achieved. This was realized by Boxer and co-workers through binding vesicles via oligonucleotide recognition to a supported lipid bilayer.^[20] Vesicles in general are more stable than BLMs with lifetimes from days to weeks without alteration. A drawback is that the vesicle interior is not accessible as an ion/analyte reservoir which makes them unsuitable for electrochemical methods.^[21]

1.2.3. Supported Bilayer Lipid Membranes

In cases where high localization of the model membrane system on the surface is required, so called supported bilayer lipid membranes (sBLM) can be prepared.^[21] Here a single bilayer film is in direct contact with a solid support as shown in Scheme 2 C. This kind of membrane model was first reported in the mid 80s.^[22-23] There are several ways to generate such structures. The first one which was used by McConnell and co-workers is vesicle fusion.^[24] For this method a concentrated suspension of SUVs is prepared through rehydration of a lipid film followed by extrusion or sonification. When vesicles are added to a hydrophilic support like a clean glass slide, they adsorb and subsequently burst to form planar patches on the surface. Due to the high lateral mobility individual patches fuse together to create extended bilayer films. The vesicle fusion process was studied in great detail by quartz crystal microbalance (QCM)^[25], surface plasmon resonance spectroscopy (SPR)^[26] and atomic force microscopy (AFM).^[27] The two substantial advantages over BLMs and vesicles are the good applicability of surface analytical techniques and the additional stability of the structure because of the solid support underneath. SBLMs are for example used to study cell adhesion^[28] or lipid phase behaviour.^[29]

Sometimes the close proximity to the support can also cause problems since there is only a very thin water film between bilayer and substrate. Especially when transmembrane proteins are introduced the interaction with the substrate can strongly influence the protein structure or behaviour under study. For example a membrane spanning protein with bulky intracellular domains can interact with the substrate so that diffusion is slowed down or even the native membrane structure may be denatured.

1.2.4. Tethered Bilayer Lipid Membranes

A method to prevent this influence of the surface is to decouple the bilayer from the supporting surface which can be achieved by so called tethered lipid bilayers (tBLM) as depicted in Scheme 2 D^[30] Another advantage apart from creating space for proteins is that tethering of a bilayer to a support by covalent coupling increases the stability of the system against detachment and decomposition. Different tethered bilayer lipid membranes have been developed over the years and shown usefulness in membrane protein research. All related architectures have an underlying layer in common consisting of a material which is known to have no or only very weak interactions with proteins. A straight forward way was developed by Schiller *et al.* who used a lipid which carries a polyethylene glycol (PEG) spacer group and a sulphur functionality which can bind to gold.^[31-32] This technique allows to generate very densely packed layers of the lower membrane sheet which makes it a convenient system for electrochemical measurements. Other approaches use a more loose tethering of the bottom layer where only scattered anchor groups are present on the surface. The latter allows a better rearrangement of the tether layer when bulky transmembrane proteins are introduced. Membrane systems were developed where a thin polymer layer is deposited underneath the lipid bilayer.^[33] This polymer layer can even be covalently bound to glass via silane chemistry^[34] or to gold with sulphur chemistry^[35] to make sure that the whole architecture is not rinsed off.

While in some cases the tBLM from a thiolipid self assembled monolayer is still too densely packed to incorporate proteins the anchoring in polymer supported systems can be too loose to form extended 2D architectures. Therefore a third kind of anchor group to decouple a membrane from the surface is the peptide tethered lipid bilayer.^[36] Here a short peptide sequence is attached to the surface by self-assembly and subsequently functionalized with a lipid via active ester chemistry. The stiffness and defined length of the spacer peptide create a defined reservoir but at the same time it does not form tightly packed crystalline layers. The subsequent formation of the bilayer is achieved by vesicle spreading on to the hydrophobic support. The whole activation procedure of the underlying layer is done in an organic solvent (dimethylformamide, DMF). In addition the tethering group has no unfavourable interactions with introduced TM-proteins.

The membrane models described above do not only serve as platforms for basic research but they are also highly relevant for technological applications, including sensor technologies.^[37-38] An example for a transmembrane protein based optical biosensor is the detection of cholera

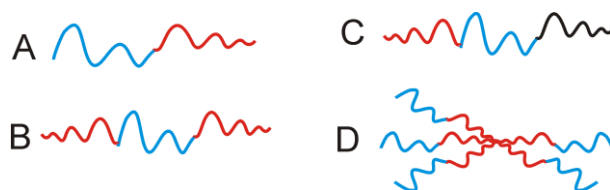
toxin (CT) that selectively binds to fluorescently labelled ganglioside (GM1).^[39] When the analyte is present, CT binds to several GM1 proteins inducing self quenching which is read out as a reduction in fluorescence intensity. A prerequisite for a successful application of such a membrane model in a device is a certain stability and robustness to allow easy handling of the system in a technical process. For this purpose methods have been developed to increase the stability of membrane model systems while preserving protein function. What has to be kept in mind whenever a bilayer model is stabilized is that it potentially loses part of its biomimetic properties.

A field pioneered by Ringsdorf deals with polymerized lipid bilayers.^[40] For this, synthetic lipids have been introduced that carry cross-linkable units like acetylene groups. After bilayer formation the double or triple bonds can be photopolymerized with UV-light. This concept was applied to planar lipid bilayers^[41-42] as well as vesicular structures.^[43-45] It could even be shown that rhodopsin can be reconstituted into polymerizable bilayer lipid membranes and can even be photoactivated after bilayer crosslinking.^[46] In some cases the irradiation of model membranes might be problematic because strong UV-light can alter protein structure. Therefore, other systems have to be developed to meet the need for increased stability. It could also be shown that model membranes can be formed from prepolymerized lipid amphiphiles.^[47] Another useful approach is the stabilization of lipid bilayers through hydrogels. Interesting examples are the encapsulation of free standing bilayers with a photopolymerizable polymer^[48-49] and the coating of functionalized hydrogel beads with lipid bilayer membranes.^[50]

1.3. Polymer Bilayers

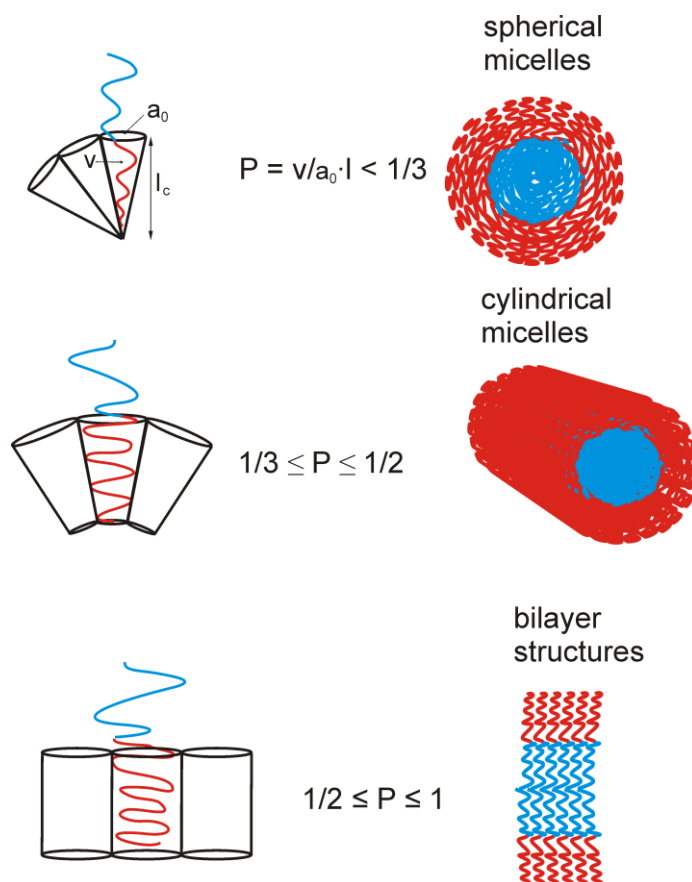
In the above paragraph it was shown that clever use of polymer chemistry can introduce additional stability in lipid bilayers. One can even go one step further and completely replace natural amphiphiles like lipids by synthetic polymers. Amphiphilic diblock copolymers show a phase behaviour in water that is comparable to lipids.^[51] The range of polymers which self assemble to more complex superstructures is much higher than for low molecular weight amphiphiles. This is a big advantage because with the help of polymer synthesis a wide range of new structures is accessible. These structures can be tailored to study questions in basic research e.g. of self assembly or for new applications like drug delivery. In Scheme 3 some

examples of block copolymer architectures can be seen that are able to self assemble in water to form superstructures on much longer length scales than their molecular size.



Scheme 3: Potential bilayer forming polymer structures. AB diblock copolymer (A); ABA triblock copolymer (B); ABC triblock copolymer (C); multiarm star shaped block copolymers (D)

With the help of some simple geometrical considerations borrowed from lipid self assembly^[52] it is possible to predict the morphology of polymers in water.^[53] A few examples are shown below in Scheme 4.



Scheme 4: Graphic illustration of the impact of the packing parameter.

To an amphiphilic polymer – and in fact every amphiphile – a packing parameter P can be attributed representing the shape of the molecule. P is calculated from the volume v the molecule demands divided by the head group area a_0 and the chain length l_c .

$$P = \frac{v}{a_0 \cdot l}$$

Equation 1

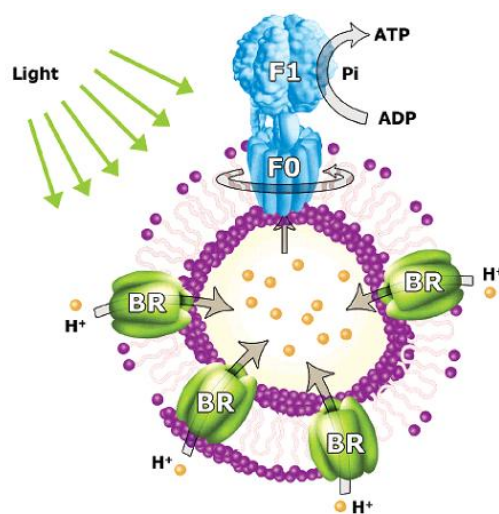
This packing parameter determines the morphology of the aggregates formed in a selective solvent as illustrated in Scheme 4. When P is $<1/3$ the molecule has a conical shape and this is leading to spherical micelles. Between $P = 1/3$ and $P = 1/2$ cylindrical micelles are obtained and between $P = 1/2$ and $P = 1$ the morphology is a planar or vesicular bilayer. Due to the increased hydrophobic block length the structures formed by polymers have a much higher thickness than natural lipids. For block-polybutadien-block-polyethylenoxide vesicles a hydrophobic thickness between 8 and 14.8 nm was observed in cryo-TEM measurements. This is about two to three times thicker than natural lipid structures. As a result of the larger thickness of these membranes they are about 10 times less permeable to water.

Detailed studies on the physicochemical properties of vesicular polymer membranes like bending, rigidity^[54], and maximal areal strain they can withstand^[55] indicate an increased overall mechanical stability compared to lipid systems. The bilayer membrane of such polymer films is also about 10 times less permeable to water than natural membranes. The explanation for the increased toughness was subject to theoretical^[56] as well as experimental investigations.^[57] It is generally believed that the chains in a bilayer induce increased interactions of two kinds which both get stronger with increasing hydrophobic chain length. The first one is interdigitation. Due to the less dense packing compared to lipids the hydrophobic tails of the polymer can reach into the opposing membrane sheet to interact with the molecules there. Secondly the hydrophobic polymer chains are longer and more flexible than fatty acid chains of lipids so that they do not stay stretched but bend backwards into the direction of the hydrophilic block. This causes entanglement of chains within the same membrane plane.

1.4. Proteins in Polymer Bilayers

Since polymer bilayers behave in many ways like natural structures it was only consequent to incorporate transmembrane proteins and see how they behave. To date there are mainly two different polymer types that showed interactions with biological membrane spanning species. The first one is a b-polyoxazoline-b-polydimethylsiloxane-b-polyoxazoline (POXA-PDMS-POXA) triblock copolymer.

Either methyl- or ethyl-oxazoline was used in all these cases in literature. In their pioneering work Meier and co-workers successfully introduced outer membrane protein F (OmpF) and maltoporin in a free standing black polymer bilayer as was shown in electrochemical measurements.^[58] Moreover Wong *et al.* performed quantitative single molecule measurements of alamethicin pores and OmpG in these planar polymer bilayers.^[59] A more sophisticated example is the functional reconstitution of F_0F_1 -ATPase and bacteriorhodopsin in vesicles (Scheme 5).^[60] First the bacteriorhodopsin creates a proton gradient between the interior and the exterior of the vesicle which is then used to drive the ATPase.

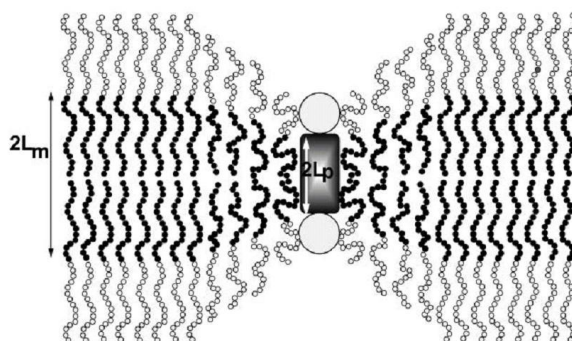


Scheme 5: Bacteriorhodopsin and F_0F_1 -ATPase incorporated in a PMOXA-PDMS-PMOXA vesicle.^[60]

The other polymer with which successful incorporation of a membrane species was demonstrated is polyethylethylen-block-polyethyleneoxide (PEE-PEO). In this example it was shown by the Discher group that the α -helical peptide alamethicin spontaneously incorporates into the vesicle membrane of GUVs.^[61] When alamethicin is inserted correctly it forms a dimeric pore allowing the flux of ions across bilayer. The membrane incorporation was proved by calcein leakage assay, optical microscopy and circular dichroism.

Because of the longer hydrophobic chain length of polymers the membrane core is much thicker than in a lipid environment. On the other hand integral membrane proteins were optimized by nature to match the thickness of the cell membrane of about 4 nm. This thickness mismatch is unfavorable for the insertion of proteins into synthetic membranes. In various experiments still the transport of ions or small molecules across the polymer membrane was demonstrated. This is a clear sign that the involved channels or pores reach all the way through the bilayer. The question is how can this happen? The assumed explanation so far is that membrane thinning happens around the incorporated species as shown in

Scheme 6. It was theoretically calculated that even bilayers with a hydrophobic core with double the thickness of a protein can still host these species.^[62]



Scheme 6: Effect of membrane thinning around a transmembrane protein as suggested in literature.^[62]

So far all work of protein functionalization was done either in vesicular or in free standing systems because this ensures free diffusion of the bilayer constituents. The mobility allows transmembrane species to adopt their desired configuration in the polymer film. Unfortunately neither pore spanning bilayers nor vesicles are very suitable for technological applications. Therefore it would be desirable to have supported polymer bilayer systems as they are superior in stability and accessibility for analytical techniques.

1.5. Objectives of this Thesis

In this work supported two bilayer model membrane systems were developed, one consisting of amphiphilic polymers and one made from lipids.

The first question in this work was if it is possible to generate supported polymer bilayers from derivatives of the amphiphilic diblock copolymer b-polybutadien-b-polyethyleneoxide (PB-PEO) on a planar support. Two different strategies were followed to obtain these structures. On the one hand consecutive transfer of the individual membrane sheets by Langmuir monolayer transfer was used. On the other hand vesicle spreading was utilized to prepare the bilayer structures in a convenient one step process.

After successful preparation the question was how stable the architectures are. Especially the stability against air was tested because this is highly relevant for possible technological applications. Furthermore the biomimetic properties of the surface architectures had to be

evaluated. This was done by monitoring the interaction of the prepared bilayer architectures with membrane peptides and proteins by impedance spectroscopy.

For many membrane proteins the incorporation into a membrane structure alone is not enough but they have to be laterally mobile to function. Therefore another objective was to elucidate the diffusion dynamics of membrane constituents and an α -helical transmembrane model peptide on the single molecule level.

As indicated above in this work also a peptide tethered lipid bilayer was developed. The aim was the revision and in-depth characterisation of an existing lipid bilayer system. Based on the obtained results the question was if it is possible to develop a new route to a peptide tethered lipid bilayer system circumventing the previously observed shortcomings. Finally the aim was to prove the applicability of the developed lipid membrane system as a platform for electrochemical measurements of proteins. This was done by using the ion carrier peptide valinomycin in an electrochemical impedance spectroscopy experiment.

2. Materials and Methods

2.1. Materials

Cleaning procedures. Microcrown glass slides (Menzel GmbH, Germany) were sonicated in a detergent solution (2 % Hellmanex II in ultrapure water) for 15 min. Then substrates were rinsed 10 times with ultrapure water and afterwards sonicated in water for another 15 min followed by 15 min of sonication in ethanol absolute (HPLC grade, Sigma Aldrich, Germany) and stored in ethanol for further use.

Pre-cut silicon wafers (CrysTec GmbH, Berlin, Germany) were deprotected from wafer foil and put into a staining box. The slides were subsequently immersed in a 5:1:1 mixture of ultrapure water, NH_3 and H_2O_2 (35%) and heated for 90 min to 70°C. Slides were then washed ten times with ultrapure water and stored in ethanol until further use.

Plasma cleaning. Plasma treatment of pre-cleaned glass substrates was carried out on a 200-G Plasma System (Technics Plasma GmbH, Germany). Substrates were cleaned for 15 min at 300 Watt input power and an oxygen pressure of 0.2 mbar.

Gold substrate preparation. Clean slides were dried under a stream of nitrogen and directly installed in a thermal evaporation chamber (Edwards FL 400, Edwards Vacuum Ltd., UK). First a 2 nm thin adhesion layer of chromium was evaporated which is then followed by a 50 nm thick gold layer. Evaporation rate was kept between 0.6 and 1.0 Å/s.

Template stripped gold (TSG). Surfaces were prepared according to a procedure developed by Butt *et al.* ^[63] and extended by Naumann *et al.* ^[64] where 50 nm thin gold films were deposited by electrothermal evaporation (0.8-1 Å/s; 5×10^{-6} mbar) on clean silicon wafers (CrysTec, Germany) and glued with epoxy glue (EPO-TEK 353ND4, USA) to clean BK7 glass slides (Menzel, Germany). The glued slides were cured for 1 h at 150 °C and stored until further use. To obtain fresh and ultrasmooth gold films the substrate sandwich was cleaved at the silicon gold interface directly before an experiment.

Polymer Synthesis and Functionalization.

Synthesis of the polymers used in this work was done by Serena Belegriou in the group of Prof. Wolfgang Meier at the University of Basel.

Chemicals. All chemicals and solvents were purchased from Sigma Aldrich or Fluka (Switzerland) with the highest purity grade and, unless otherwise stated, used as received. Tetrahydrofuran (THF) for polymerization and the monomers 1,3-butadiene and ethylene oxide were purified as reported elsewhere.^[65] Dichloromethane (DCM) was dried for 12 h over CaH₂ and freshly distilled prior to use.

Polymer synthesis. Poly(butadiene)-*b*-poly(ethylene oxide) (PB-PEO-OH) block copolymers were synthesized by sequential living anionic polymerization following a procedure utilizing the phosphazene base *t*-BuP₄[‡].^[65-66] This base prevents the strong association of the living PEO chain ends with the Li⁺ counter-ions from the initiator and therefore allows for a sequential one-step polymerization without intermediate steps. Polymerizations were carried out in a thoroughly flame-dried customized glass vacuum apparatus under inert gas atmosphere. The synthesis was described in detail elsewhere.^[65] After purification by repeated precipitations in cold acetone (-30 °C), the hydroxyl-terminated diblock copolymer was esterified with lipoic acid (LA). LA (269 mg, 1.3 mmol), *N*-(3-dimethylaminopropyl)-*N'*-ethylcarbodiimide hydrochloride (EDC·HCl; 250 mg, 1.3 mmol) and 4-(dimethylamino)pyridine (DMAP; 12 mg, 0.1 mmol) were added to a flame-dried flask. The solids were dried under vacuum for 2 h. The mixture was dissolved in 15 mL absolute DCM. In a second flame-dried flask, PB-PEO-OH (4 g, 1 mmol) was dried under vacuum for 2 h and dissolved in 20 mL absolute DCM. After triethylamine (0.2 mL, 1.4 mmol) was added, the solution was injected into the first flask and the reaction mixture was stirred at room temperature for 72 h. Afterwards, the solution was washed with saturated NaHCO_{3aq}, 10% HCl_{aq}, and distilled water (three times each). The organic phase was dried over MgSO₄, filtered, and the solvent was evaporated.

Polymer functionalization. PB-PEO-OH polymers were end-functionalized by esterification with carboxyl group-containing compounds, such as lipoic acid (LA) or biotin. Unless otherwise stated, the general synthetic route was as follows: The carboxyl group-bearing compound, a coupling compound (EDC·HCl or Dicyclohexylcarbodiimide (DCC)) and 4-(dimethylamino)pyridine (DMAP) were added to a flame-dried flask. The solids were dried

under vacuum for 2 h. The mixture was dissolved in absolute DCM, which was freshly distilled from CaH_2 prior to use. In a second flame-dried flask, PB-PEO was dried under vacuum for 2 h and dissolved in absolute DCM. After NEt_3 was added, the solution was injected into the first flask and the reaction mixture was stirred at room temperature for 72 h. Afterwards the solution was washed with saturated $\text{NaHCO}_{3\text{aq}}$, 10% HCl_{aq} , and distilled water (three times each). The organic phase was dried over MgSO_4 , filtered, and the solvent was evaporated.

The functionalization of the amphiphilic diblock copolymer PB-PEO-OH under classical esterification conditions with lipoic acid provided an easy synthetic route to a sulphur-functionalized polymer with 86% yield. As the sulphur is integrated as disulfide in a dithiolane ring, no special precautions have to be taken and handling is much easier than with the more sensitive free thiols. A similar anchor group was used for tethering phospholipids to ultrasmooth gold substrates.^[31] Two-dimensional diffusion ordered spectroscopy (DOSY) was applied to prove covalent linkage of PB-PEO-OH to all lipoic acid present in the system after the work-up procedure. The diffusion coefficients ascribed to distinct signals from the polymer backbone and the lipoic acid end-group are in the same order of magnitude, indicating the same diffusion behaviour for backbone and end-group, respectively, in the applied field gradient. Thus, end-functionalization of the polymer was successful. Diffusion coefficients and further analytical results are summarized in Table 1.

polymer formula	^a M_n (g/mol)	^b PDI	^c DF %	^d δ_{PBPEO} (m^2/s)	^d δ_{LA} (m^2/s)
$\text{PB}_{52}\text{PEO}_{29}\text{-OH}$	4100	1.07			
$\text{PB}_{52}\text{PEO}_{29}\text{-LA}$	4300	1.09	86	2.16×10^{-10}	2.18×10^{-10}

Table 1: Polymer characterization data obtained by GPC and NMR: ^aNumber average molecular weight calculated from GPC and ¹H-NMR. ^bPDI (polydispersity index) obtained from GPC. ^cDF (degree of functionalization) calculated from ¹H-NMR. ^d δ (diffusion constants) obtained from DOSY measurements.

The subscripts are assigned to clearly identified peaks of the polymer backbone (PB-PEO) and the functional group (LA), respectively.

Fluorescence labelling. PB-PEO-OH and the fluorescent dye tetramethyl rhodamine-5-carboxylazide (Molecular Probes) were dried separately under vacuum for 2 h. The components were dissolved in 3 mL methyl-ethyl ketone (MEK) each. After the polymer solution was added to the fluorophore solution, the reaction mixture was refluxed at 80 °C for

72 h (the azide was converted *in situ* in a Curtius reaction to an intermediate isocyanate, which forms stable carbamates with the hydroxyl polymer end groups). The solvent was evaporated under vacuum and the pink crude product was dissolved in DCM and extracted with several litres of water until the aqueous phase was colourless.

Compound	M / g·mol ⁻¹	n / mol	m / mg
PB-PEO-01 OH	4100	6.0	24.6
TMR-dye	455.47	18	8.2

Table 2: Amounts used for functionalization of PB-PEO-OH 01 with a tetramethylrhodamine fluorophore.

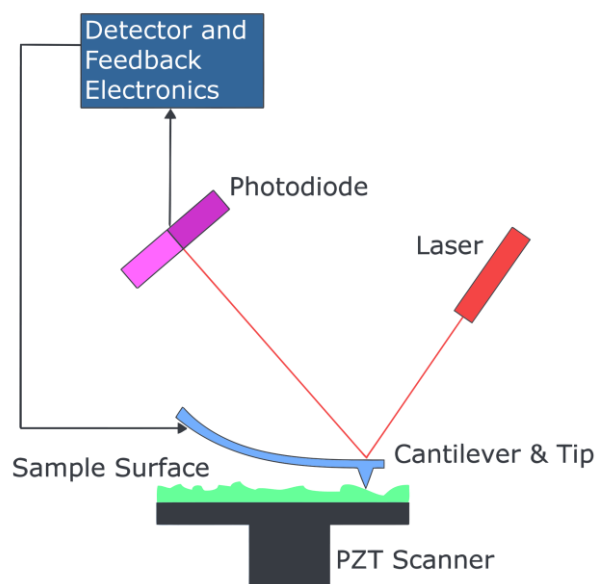
Polymer characterization. The molecular weight of the block copolymer was determined by GPC and ¹H-NMR. First, a PB aliquot, drawn prior to the sequential copolymerization, was analyzed by GPC with THF as eluent. Narrow polybutadiene standards (PSS Polymer Standards Service, Germany) were used to calculate M_n , M_w , and the polydispersity index (PDI) of the PB block. The number of the ethylene oxide repeating units, thus the molecular weight, was calculated from the integral ratios in the ¹H-NMR spectrum of the block copolymer. The degree of functionalization of the lipoic acid-modified polymer (PB-PEO-LA) was determined by ¹H-NMR. Covalent attachment of the end-group to the polymer was proven by DOSY analysis.

2.2. Methods

2.2.1. Atomic Force Microscopy (AFM)

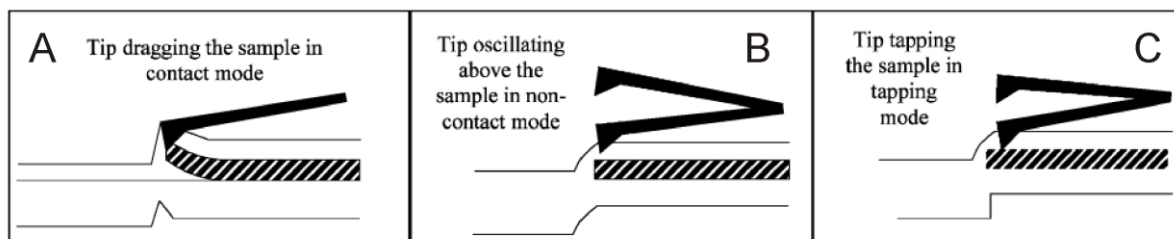
AFM is a special method of scanning probe microscopy (SPM) which is able to measure surface topography, mechanical properties and interactions with the surface with nanometre resolution.^[67] A nanometre sharp tip attached to a cantilever is scanned over the surface and the deflection of the cantilever due to objects or interactions with the substrate is read out by measuring the position of a laser beam reflected from the backside. AFM is a method image surfaces with a resolution which is up to 1000 times higher than in optical microscopy. In addition it does not require labelling and is non-invasive. There are two main fields of application. The first is molecular metrology especially in the field of semiconductor research

and testing. Apart from this, AFM has found its way into biological science. The huge advantage of AFM over high resolution techniques like scanning electron microscopy (SEM) is the ability to measure in water at physiological conditions in a non-invasive fashion. It can even be used to monitor biological processes like cell migration *in situ*. All the named features have made AFM a highly flexible method that is used in research labs all over the world.



Scheme 7: Working principle of a scanning probe microscope. Image take from Wikipedia.com.^[68]

There are three basic measurement modes for AFM. The first one is the so called contact mode where the tip is scanned over the surface at constant force by applying a feedback mechanism (Scheme 8 A). This mode is comparably insensitive to perturbations through the environment and is mostly used for hard and dry surfaces. The only drawback of this method is that the tip can alter the surface through scratching.^[69]



Scheme 8: Three different operation modes in SPM. (A) contact mode, (B) non-contact mode and (C) tapping mode.^[69]

An alternative is the operation in the non-contact mode (Scheme 8 B). For this the cantilever is excited to oscillate at its resonance frequency with small amplitude. It is then brought into

close proximity above the surface. When the tip starts to interact with the surface through van-der-Waals forces the oscillation is damped. By mapping the damping relative to the lateral-position of the cantilever surface images are obtained. This method is mainly used for very soft samples like cells because there is no danger of alteration of the sample by the cantilever. It is possible to get very high resolution images but therefore low oscillation amplitudes and flat surfaces are needed. A major disadvantage of non-contact mode AFM is the susceptibility to perturbations through the environment. An example is the thin water film due to humidity which is almost always present when measuring in air. Due to the very low exerted force on the sample the cantilever will only stick to that liquid film without mapping the actual topography.

A method to get the best out of the two operation modes is the tapping mode – also termed intermittent contact mode (Scheme 8 C). Again the cantilever is actively excited by a piezoelectric element to vibrate at or close to its resonance frequency. Then unlike in non-contact mode it is brought so close to the surface that it starts to tap on the sample which results in a lowered resonance amplitude. By mapping the amplitude versus the lateral position it is possible to extract exact height information of a sample. Because the cantilever is only in contact with the surface for a very short time the likelihood of changing the sample with the tip is reduced. Due to the stronger oscillation compared to non-contact mode it is less susceptible to perturbation through the environment. Furthermore there is a second information available which is the phase of the oscillation. Depending on the mechanical properties of the surface the cantilever oscillation is shifted in phase relative to the excitation frequency. A soft surface results in a higher phase shift than a hard one so that mechanical contrast can be extracted from the phase image.

Another field of application of AFM apart from imaging is force spectroscopy.^[70] This is a direct way to measure the surface interactions as a function of the tip-sample separation. The result is a so called force-distance (F-d) curve. Typically these force distance curves are recorded by repeatedly approaching and retracting the cantilever at a fixed lateral position. The resulting F-d curves can give detailed information about capillary, Coulomb, van der Waals, double-layer, solvation, hydration, hydrophobic forces and many more. Force-distance measurements are nowadays also widely used in biology to investigate forces between single DNA strands or proteins.^[71]

Data acquisition. Atomic Force Microscopy (AFM) was carried out mainly on a Nanowizard (JPK Instruments, Berlin, Germany), installed on an inverted microscope (Axiovert; Zeiss,

Germany). Measurements were performed in intermittent contact mode in liquid environment. For imaging and force-distance measurements, oxide sharpened silicon nitride tips (NP-S; Veeco Instruments, Germany) with a nominal spring constant of 0.32 N/m were used. For scratching experiments silicon cantilevers (OMCL-AC240TS; Olympus, Germany) with a nominal spring constant of 2 N/m were utilized. Typical scan rates ranged from 0.8–1.2 Hz and the z-range was between 3 μm and 5.8 μm . Cantilevers were not calibrated for force-distance measurements but the nominal spring constant was chosen. Force-distance measurements were carried out at a vertical scan speed of 500 nm/s. The z-scan range varied between 500 and 800 nm. Additional measurements of the peptide tethered lipid architecture prepared by vesicle fusion (chapter 6) were carried out on a Veeco Bioscope II (Veeco Instruments Inc.) by Alexandre Berquand at Veeco GmbH in Mannheim.

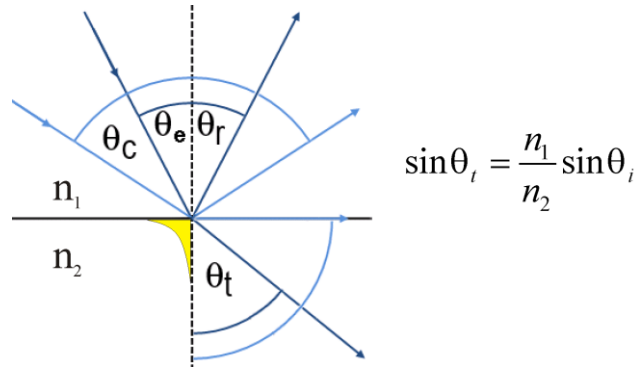
Images were processed using free *Gwyddion* 2.14 software (<http://gwyddion.net/>). Images were 1st order flattened and horizontal error lines were removed. Height information was extracted from profiles along the indicated lines.

2.2.2. Surface Plasmon Resonance Spectroscopy (SPR)

Surface plasmon resonance (SPR) Spectroscopy is a widely used optical technique to non-invasively characterize thin films close to metal surfaces. The high sensitivity in combination with the label free detection makes it a prominent method for biosensor applications. It is for example possible to monitor the binding kinetics of biological molecules as well as the film thickness and swelling behaviour of thin polymer films.

Surface plasmons (SP's) are collective and resonant motions of quasi-free electrons at a dielectric to metal interface, in response to an incident optical field. They can be described as surface electromagnetic waves decaying exponentially to both sides of the interface but propagating parallel to the interface. Under certain conditions it is possible to couple electromagnetic radiation to the surface plasmon. The conditions under which light can be coupled to a thin metal film to create a surface plasmon are very sensitive to the dielectric properties of the surrounding medium. By monitoring the changes of the coupling conditions it is possible to make changes in the local environment visible^[72]

When a light beam hits the interface between a high refractive index (e.g. glass) and a low refractive index medium (e.g. air) it is partly reflected and the transmitted light is refracted according to Snell's law (Scheme 9).



Scheme 9: Graphical and mathematical illustration of Snell's law (dark blue arrows). The special case of total internal reflection is depicted as light blue arrows. n_1 =high refractive index material n_2 = low refractive index material, θ_c = critical angle, θ_e = incident angle, θ_r = reflected angle, θ_t = transmitted angle.

Above a critical angle θ_c which is determined by the material properties of the two media light is completely reflected at the surface. This phenomenon is called total internal reflection (TIR). Directly at the spot where the light is reflected the light intensity does not abruptly drop to zero but it decays exponentially into the lower refractive index medium. As a rule of thumb the penetration depth is assumed to be half the wavelength λ of the excitation light. This is a so called evanescent wave and only reaches about 200 – 300 nm into the medium. When a thin metal film of several tens of nanometres is brought into the evanescent field which has an electric field component perpendicular to the interface, it can induce oscillations of surface charges in the free electron gas and hence generate surface plasmons.

To meet the conditions where light can be coupled to a SP, the wave vector \vec{k}_{photon} of the incident wave and $\vec{k}_{plasmon}$ of surface plasmon wave have to be matched.

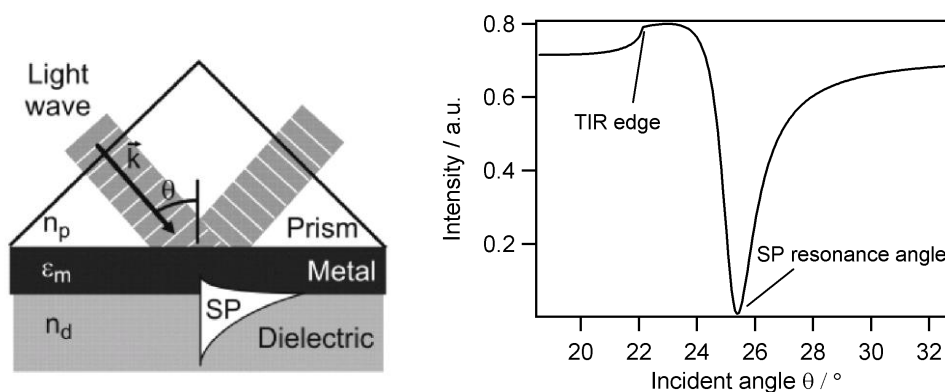
$$k_{photon} = \frac{\omega \sqrt{\epsilon_{prism}}}{c} \sin \theta_i \qquad k_{plasmon} = \frac{\omega}{c} \sqrt{\frac{\epsilon_m \epsilon_d}{\epsilon_m + \epsilon_d}}$$

Equation 2: Wave vectors for the incident light wave and the plasmon respectively. ω = angular laser frequency, c = speed of light, ϵ_{prism} = dielectric constant of the prism, ϵ_m = dielectric constant of the metal, ϵ_d = dielectric constant of the dielectric.

As one can see $\vec{k}_{plasmon}$ at the laser frequency ω is only dependent on the material properties. In contrast to that, the wave vector of the incident light is dependent on the incident angle so that it can be tuned to match $\vec{k}_{plasmon}$. Unfortunately the wave vector of light in air is always smaller than the required $\vec{k}_{plasmon}$ and a surface plasmon cannot be excited by directly shining

light onto a metal film. To excite a SP the incident light has to be coupled through the evanescent wave created by total internal reflection. This can be realised at the base of a prism displayed in Scheme 10 A and is called Kretschmann configuration.^[73]

When incident light and plasmon are in resonance, efficient coupling is achieved and all energy is transferred to the metal film. At this point the reflected intensity almost drops to zero. The intensity is plotted versus the excitation angle θ_i in Scheme 10 B.



Scheme 10: Illustration of the surface plasmon coupling, ϵ_m = dielectric constant of metal, n_d = refractive index of dielectric, n_p = refractive index of glass prism (A) and an example for an angular intensity spectrum (B).

By changing the dielectric environment of the surface plasmon, the wave vector changes which results in a change in plasmon resonance angle θ . This can be used to analyse the adsorption or desorption of molecules to/from the surface. The shift in resonance angle is proportional to the change in adsorbed layer thickness and the contrast between the dielectric constants of the dielectric continuum ϵ_d (e.g. air) and the adsorbed molecules ϵ_{adsorb} . The root term in Equation 4 can be seen as the refractive index contrast.

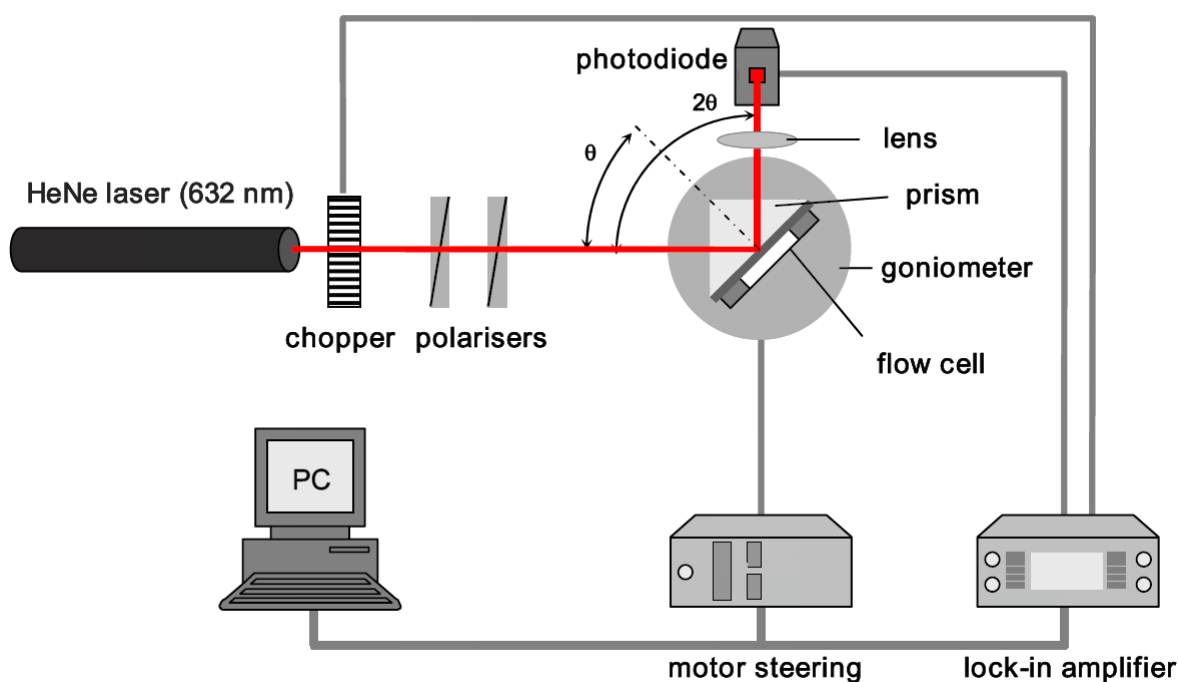
$$\Delta\theta_i \sim n \cdot d$$

Equation 3

When either the dielectric constants or the adlayer thickness are known from complementary methods the respective other variable can be measured with accuracy. SPR spectroscopy can be done in two different measurement modes. To get thickness information one can do angular scans. For kinetic measurements the surface plasmon can be measured at a constant angle with time.

SPR-setup. The setup consists of a p-polarised He/Ne-Laser (632.8 nm) which first passes a chopper to modulate the signal for lock-in detection and afterwards two polarisers for polarisation and attenuation respectively. The beam is reflected at the base of a prism to

which a gold coated glass substrate is coupled by index matching oil. To achieve the high in-plane wave vectors of the exciting light at moderate coupling angles, the microcrown slide was attached to a LaSFN9 Prism ($n=1.845$). The reflected light is collected by a biconvex lens and directed to a photodiode which is connected to the lock-in amplifier. The prism/sample and the detector each are installed on a co-axial goniometer with two independently working arms. In a θ - 2θ geometry the reflected light can be monitored as a function of the incident angle to perform a so called angle scan. It is also possible to monitor the reflected light at a fixed angle as a function of time for kinetic measurements.



Scheme 11: SPR-Setup in the Kretschmann configuration.^[74]

SPR data collection. Measurements were performed using a home-built setup in the Kretschmann configuration with a He/Ne laser ($\lambda = 633$ nm) which is described in literature in detail.^[72] In scan mode, reflectivity is monitored as a function of the incident angle and collected with photodiode.

Data evaluation was done using the free program WINSPALL which was developed at the MPI for Polymer Research.^[75] The analysis is based on a model calculation of the reflectivity $R(\theta)$ from the multilayer system and subsequent fitting these values to the measured data. For each layer, a thickness d and a constant dielectric response $\epsilon = \epsilon' + i\epsilon''$ can be attributed which may be complex-valued. The calculations of spectra from known values are based on Fresnel-equations and are done with a transfer-matrix approach described in detail by Yeh.^[76] First the pure gold layer was measured as a reference and the dielectric constants and

thicknesses obtained from fitting were kept constant for the following polymer film evaluation. Starting values for gold are found in literature.^[77] Spectra of films were fitted using a four layer model including the prism, gold, mono- or bilayer, and the surrounding medium (water or air). A refractive index $n = 1.5$ ($\epsilon' = 2.25$) was assumed for both, mono- and bilayer^[78] so that film thicknesses can be obtained.

2.2.3. Electrochemical Impedance Spectroscopy (EIS)

EIS theory. EIS is a useful method for the characterisation of electrochemical properties of bulk materials and interfaces.^[79] Although impedance spectroscopy was first applied to solid materials like in battery or fuel cell research in recent years it has found steadily increasing interest in biophysics. Especially biomembrane functionalized electrodes are a useful tool for transmembrane protein studies of channel, pores and carriers. The basic measurement principle is as follows. An alternating potential is applied to the system under study and the current response is recorded with potentiostat. For a direct current system Ohms law with a resistance R is fully applicable. For an alternating current (AC) circuit there is an analogue to the resistance which is called impedance. In mathematical terms this can be expressed as a frequency dependent complex-valued quantity $Z(f)$.

$$Z(f) = \frac{U(t)}{I(t)}$$

Equation 4

The driving voltage can be expressed as oscillating sinusoidal potential.

$$\begin{aligned} U(t) &= U_0 \cdot \sin(\omega t) \\ U(t) &= U_0 e^{i\omega t} \end{aligned}$$

Equation 5

With U_0 being the maximum amplitude and ω the driving frequency. The applied potential results in a current flow. It can be expressed as

$$\begin{aligned} I(t) &= I_0 \cdot \sin(\omega t + \theta) \\ I(t) &= I_0 e^{i(\omega t + \theta)} = I_m \cdot e^{i\omega t} \cdot e^{i\theta} \end{aligned}$$

Equation 6

I_0 is the maximum current; ω again is the driving frequency and θ is the phase lag between the driving voltage and the resulting current. Figure 1 displays the driving voltage (black line) and the current response of the system (red line) which is in this example an ideal capacitor which induces a phase lag of $\pi/2$. Typically the driving voltage is chosen in a way that it produces a linear response. This is the case in the range of the thermal energy fluctuation and corresponds to 10-25 mV. To record impedance spectra of an electric circuit the current response to an alternating potential is sequentially measured for different driving frequencies ω .

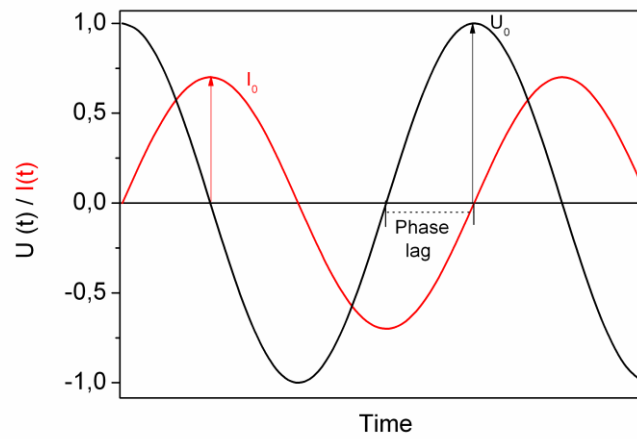


Figure 1: Representation of the sinusoidal driving voltage (black line) and the corresponding current response (red line) at a phase lag of $\pi/2$.

A resistor shows an immediate response to the applied alternating voltage and this can be described by Ohm's law. For a resistor the impedance Z and the direct current resistance R are equal as can be seen by inserting the time dependent potential $U(t)$ and current $I(t)$ into the expression for the impedance (Equation 8).

$$I(t) = \frac{U(t)}{R} = \frac{U_m e^{i\omega t}}{R}$$

Equation 7

$$Z_R = \frac{U(t)}{I(t)} = \frac{U_m e^{i\omega t}}{\frac{U_m e^{i\omega t}}{R}} = R$$

Equation 8

In the case of a capacitor it is different. For a capacitor, the conduction is indirect and results from the attractive or repulsive forces of electrons from the two sides of the capacitor plates as their potential changes. In the case of a capacitor, Z provides a measure of how the passage of ions is impeded by the circuit. This is also graphical displayed in Figure 1. In the ideal case the phase lag for a capacitor is $\pi/2$. The impedance Z can also be expressed in polar coordinates which results in

$$|Z| \angle \phi = \frac{|U| \angle \phi}{|I| \angle \phi}$$

Equation 9

In a capacitor is the stored charge Q is proportional to the applied voltage U and the proportionality constant C is called Capacitance. It is the key characteristic of a capacitor. In mathematical terms it is expressed as $Q = C \cdot U$

To get a relation between current and voltage in a condensator Q has to be differentiated with respect to the time.

$$I \angle \phi = \frac{Q}{dt} = C \frac{dU}{dt}$$

Equation 10

For an alternating current circuit U has to be replaced by the time dependent voltage $U(t) = U_0 e^{i\omega t}$.

$$I \angle \phi = C \frac{dU}{dt} = i\omega C \cdot U_0 e^{i\omega t}$$

Equation 11

When this is inserted into Equation 9 one obtains

$$Z_c = \frac{U(t)}{I(t)} = \frac{U_m e^{i\omega t}}{i\omega C \cdot U_m e^{i\omega t}} = \frac{1}{i\omega C}$$

Equation 12

The response of the capacitor is frequency dependent and 90° out of phase with the response of the resistor.

EIS data collection. Measurements were conducted using an Autolab spectrometer PGSTAT 12 (Eco Chemie, Utrecht, Netherlands). Spectra were recorded for frequencies between 2 mHz and 100 kHz at 0 V bias potential with an ac modulation amplitude of 10 mV. Raw

data were analyzed using the ZVIEW software package (Version 2.90, Scribner Associates). Three electrode measurements were performed with the substrate as the working electrode, a coiled platinum wire as the counter electrode, and a DRIREF-2 reference electrode (World Precision Instruments, Berlin, Germany). The home-built Teflon cells had a buffer volume of 1 mL and an electrochemically active area on the substrates of about 0.28 cm².

EIS data evaluation. Impedance spectra show the combined response of the system to the applied alternating voltage. There are several ways to represent measurement data. The two representations used in this work are the Bode Plot and the admittance plot. In the Bode plot the modulus of the complex impedance $|Z|$ and the phase shift θ are plotted versus the driving frequency. To get quantitative information out of such spectra it is necessary to find a model that reflects the measured system. The possible components from which the circuit models in this thesis were created are summarized in Table 3.


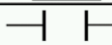

Resistor R		$Z_R(\omega) = R$
Capacitor C		$Z_C(\omega) = \frac{1}{i\omega C}$
Constant phase element		

Table 3: Possible electric components.

The resistor and the capacitor were introduced above. Sometimes real systems cannot be fully described by these two idealised components. Therefore a third one, the constant phase element is introduced. It can be thought of as a distribution of many capacitors and can be used to take surface heterogeneities into account.^[79]

The Bode plot is best suited to get an overview over the whole system response and can help to construct the right model. Frequency regions with a phase angle close to zero and a plateau in the $|Z|$ curve express the dominance of a resistor while frequency regions with a phase angle close to 90° and a slope of -1 are dominated by a capacitor as was shown in the theory section.

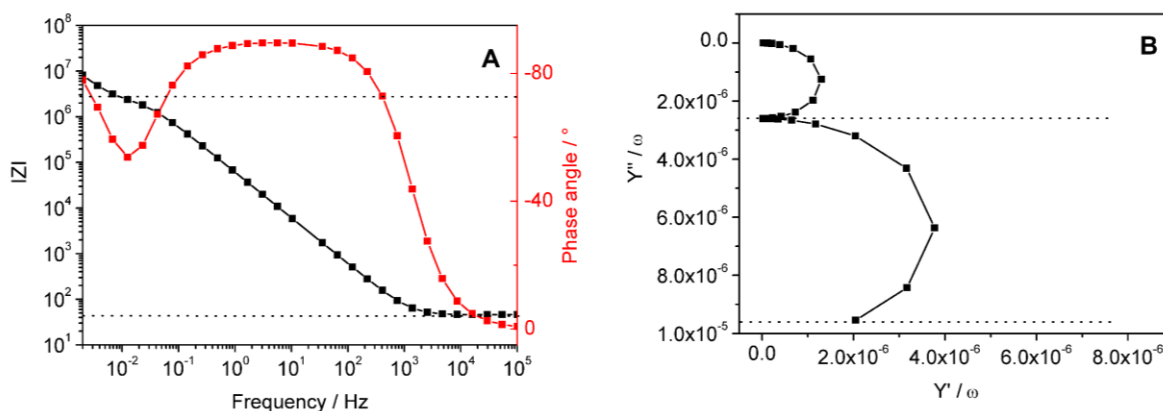


Figure 2: Two different types of data representation for impedance data. (A) Bode plot (B) Admittance plot.

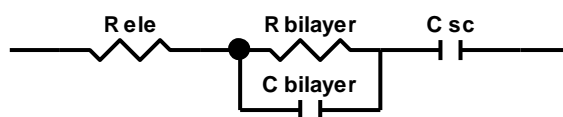
The admittance is the inverse of the complex impedance (Equation 13).

$$Y(\omega) = \frac{1}{Z(\omega)}$$

Equation 13

The frequency reduced admittance plot (Figure 2 B) displays the imaginary part of the admittance Y'' as a function of the real part Y' . Every semicircle represents a capacitance where intersection with the y-axis corresponds to the capacitance values.

By gathering all the information it is possible to construct an equivalent circuit that represents the electrochemical behaviour of the system. The different components can be attributed to the individual parts of the membrane architecture.^[80] To get reliable results from the fit the model should be kept as simple as possible. In the example displayed here the system is best represented with the equivalent circuit shown in Scheme 12. C_{sc} is an element introduced to describe electrochemical processes happening directly at the gold electrode.



Scheme 12: Equivalent circuit model used for the example. R_{ele} = electrolyte resistance, $R_{bilayer}$ = Bilayer resistance, $C_{bilayer}$ = bilayer capacitance, C_{sc} = space charge capacitance.

To fit the impedance data an educated guess for the starting values has to be made. This can be done by eye. From the Bode plot two resistors at 45Ω and $2 \cdot 10^6 \Omega$ can be extracted by reading the $|Z|$ values at the dotted lines. From the admittance plot one can read the two

capacitance values at $2.5 \cdot 10^{-6}$ F and $9.5 \cdot 10^{-6}$ F (dotted lines in Figure 2). After finding the right starting values a least squares fitting algorithm is applied to yield quantitative information from the spectra. In this work two main quantities were analysed. One is the resistance attributed to the bilayer R_{bilayer} which gives information about the large scale sealing properties of a layer. A high value for R_{bilayer} is interpreted as a high surface coverage with a densely packed layer and a small number of defects. The second quantity is the bilayer capacitance C_{bilayer} . It gives information about the amount of material deposited on the surface. Changes in adsorbed mass are visible in a variation in C_{bilayer} . In principle it is possible to calculate layer thicknesses from the capacitance values according to Equation 14.

$$C = \frac{A \varepsilon \varepsilon_0}{d}$$

Equation 14: Relation of the capacitance C to the layer thickness d. A = measured area, ε = dielectric permittivity, ε_0 = permittivity in vacuum.

In this work ε of the complex polymer and lipid bilayer systems is not known so that no quantitative evaluation of the film thickness can be made by electrochemical methods.

2.2.4. Fluorescence Correlation Spectroscopy (FCS)

FCS theory. FCS often also termed fluorescence fluctuation spectroscopy is an optical measurement technique developed by Webb and co-workers in 1972 ^[81] that allows for the analysis of dynamic processes in highly confined volumes. Most commonly, FCS is performed in optical microscopy in a confocal configuration because by focusing light with an objective it is possible to confine light to a very small observation volume. It is used in all fields of science be it physics, chemistry or biology to monitor dynamic processes in a very wide time range (typically 10^{-6} -10 s). The lower limit is given by the number of photons emitted from a molecule, the detection efficiency and the speed of the measurement electronics. The upper limit is only posed by the stability of the measurement setup but if events seldom occur data acquisition takes very long. Although the method is very flexible it has a sever limitation. If the analyte concentration in the observation volume is too high the signal of a single molecule does not cause a detectable intensity fluctuation anymore. A way to circumvent this is to use smaller excitation volumes but due to the diffraction limit the focus cannot be made infinitely small. To date there are some approaches to circumvent this diffraction limitation. ^[82-83]

If a parallel light beam is focused with a high NA objective a high light intensity is created in a small volume. The focal volume of a Gaussian focus is between 200-300 nm in width and has a 2-6 times higher extension along the beam. The approximate radius at the centre can be calculated according to Equation 15.

$$r_{exc} \approx \frac{\lambda}{2NA}$$

Equation 15

This creates an effective volume of about one femtoliter. When fluorescent molecules enter the focal volume they are efficiently excited and emit light while travelling through the focus. At concentrations of 1 nmol/L 0.6 molecules are in average present in this volume. The fact that molecules in solution can diffuse in and out of the focal volume creates a high fluctuation in the emitted fluorescence light. These intensity fluctuations can be recorded with time. From the fluorescence signal of a molecule an autocorrelation function $G(\tau)$ can be calculated which basically calculates the self similarity upon a defined shift in time τ . In Figure 3 d) the decreasing signal overlap with time is displayed graphically.

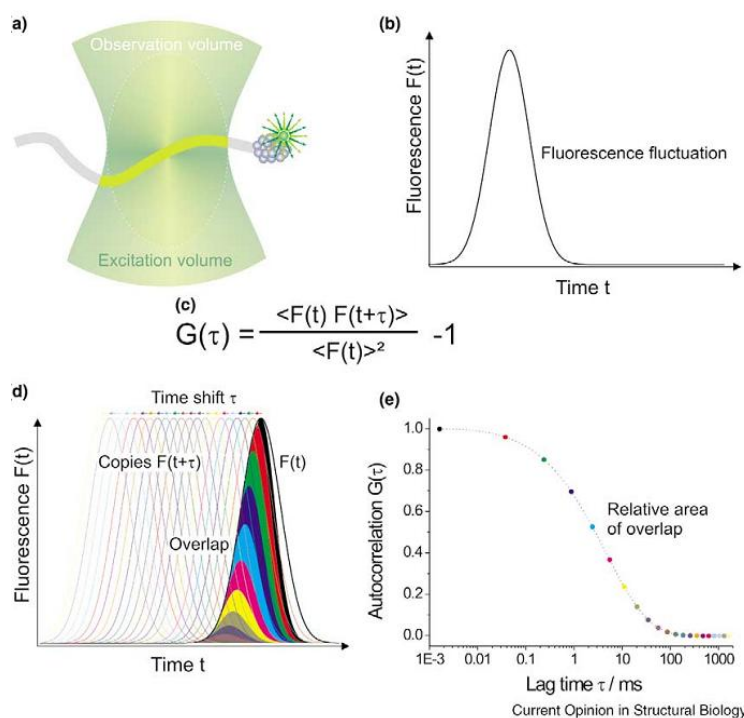


Figure 3: Principle of FCS. Diffusion of the analyte through the observation volume a) Resulting fluorescence signal from the event b) Demonstrating the signal overlap upon increasing lag time d) The resulting autocorrelation curve e) Graphics taken from Haustein *et al.*^[84]

In mathematical terms the autocorrelation function is expressed as follows.

$$G(\tau) = 1 + \frac{\langle \delta F(t) \delta F(t + \tau) \rangle}{\langle F \rangle^2} = \frac{\langle F(t) F(t + \tau) \rangle}{\langle F \rangle^2} - 1$$

Equation 16

The expression $\delta F(t) = F(t) - \langle F(t) \rangle$ stands for the deviation from the mean intensity.

In real life FCS the photon trace is noisy and consists of many events. It looks like the one in Figure 4 A and the calculated autocorrelation curve is depicted in Figure 4 B.

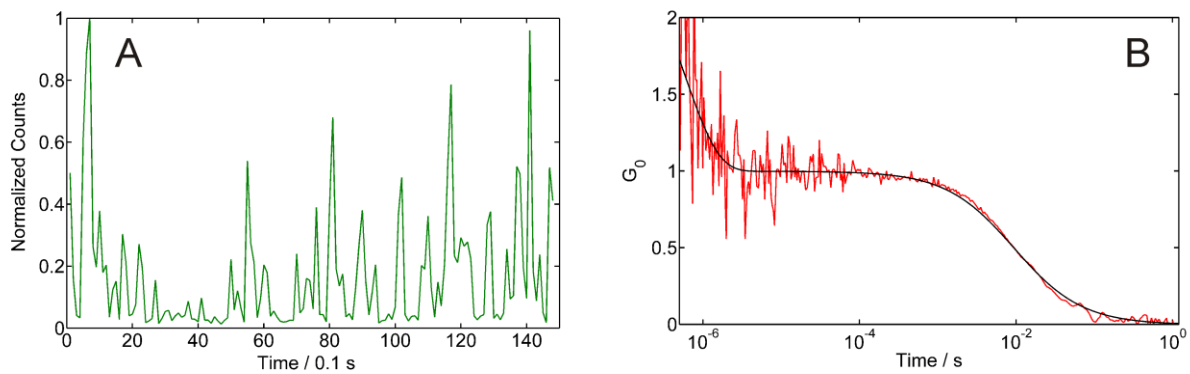


Figure 4: Time dependent fluorescence intensity trace is shown in (A) and the corresponding correlation curve in red (B).

To get quantitative information out of such a correlation curve it has to be fitted to a model. Typically a nonlinear least squares algorithm is used. The simplest model is free diffusion in three dimensions with Gaussian excitation volume. For a comprehensive derivation the reader is referred to a manuscript circulated in the web.^[84]

For a Gaussian 3D-volume $G(t)$ was derived as

$$G(t) = \frac{1}{\langle N \rangle} \frac{1}{1 + \frac{t}{\tau_D}} \frac{1}{\sqrt{1 + S^2 \cdot \frac{t}{\tau_D}}}$$

Equation 17

where $\langle N \rangle$ is the mean number of particles and τ_D is the characteristic residence time in the excitation volume. The experimental lag time is denominated t and the structural parameter S stands for the ratio $(\omega^2 \cdot z^{-2})$. This is a geometrical measure for the size of the sample volume. The drop of $G(t)$ to the half the initial value is a measure for the characteristic diffusion time τ_D . Since the diffusion time is dependent on many experimental factors it is hard to compare

these values among different machines. More convenient is the calculation of the diffusion coefficient according to Equation 18.

$$D = \frac{\omega^2}{4\tau_D}$$

Equation 18

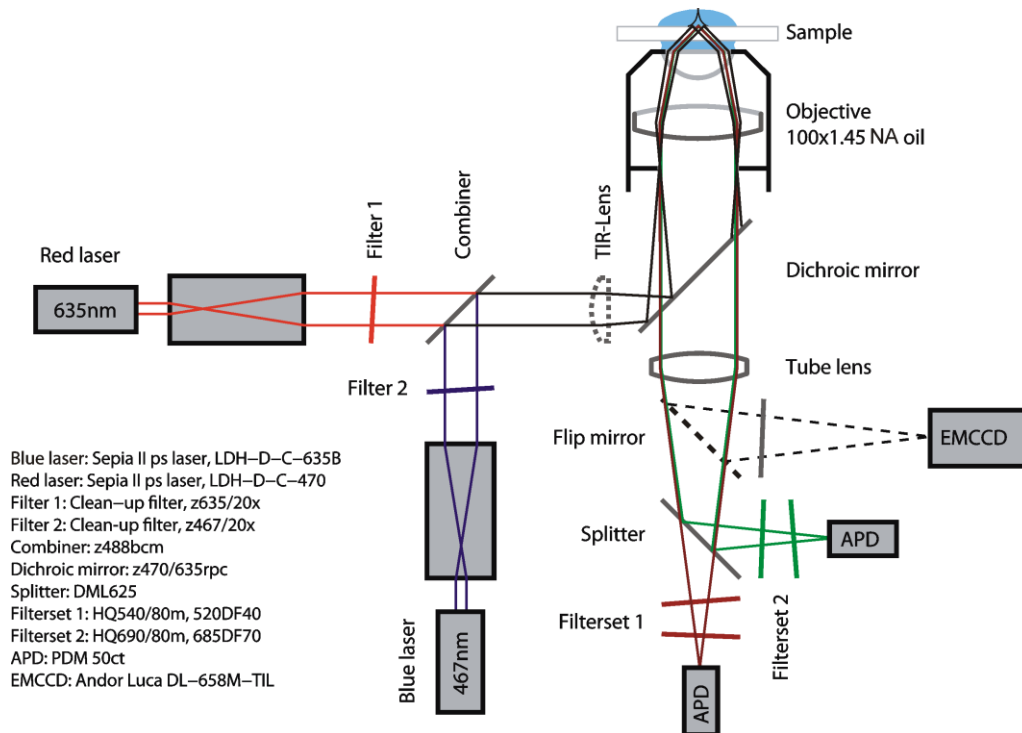
Before D can be calculated it is required to calculate the width of the focal volume. The standard way to this is to conduct a reference measurement on a diffusing species with a known diffusion coefficient. Such reference values are often measured with a complementary technique like NMR or with advanced calibration free FCS methods, e.g. two-focus FCS. When D is known and τ_D is measured, ω can be calculated for a setup. After calibration diffusion coefficients D of unknown species can be measured and compared in labs all over the world. At a fixed temperature D is a characteristic constant for a species in a certain environment and it has SI-units of $\text{m}^2 \cdot \text{s}^{-1}$. The higher D is the faster is the diffusive motion of a component.

FCS-setup. FCS measurements were carried out on a home built microscopy system in the group of Prof. Theo Lasser at the EPFL, Lausanne Switzerland.

Two different laser sources were utilized for FCS measurements. For red excitation at 635 nm a Sepia II picosecond laser system with a LDH-D-C-635B laser head (PicoQuant, Berlin Germany) was used while green excitation was achieved with a frequency doubled Nd:YAG laser at 532 nm (ChangChun New Industries Optoelectronic Tech. Co.laser (CNI) China).

For white light illumination an uncollimated lamp was positioned above the sample for rough sample positioning. The laser beam is passed through a polarization maintaining fiber for cleaning up the lateral beam profile. After collimation to an e^{-2} diameter of ≈ 10 mm (confocal), it is aligned coaxially to the microscope objective using two beam steerers. A laser-line clean-up filter (z635/20x, Chroma) ensures well-defined excitation spectra. For wide field mode an achromatic lens ($f = 130$ mm) focuses the beam into the back-focal plane (BFP) of the high NA oil immersion objective (α -Plan-Fluar 100×1.45 , Carl Zeiss), which results in a circular area with e^{-2} diameters $20 \mu\text{m}$ at the coverslip-sample interface. For confocal excitation the parallel beam was lead directly to the objective. The sample was positioned with a xyz-translation stage (ULTRAlign 561D with μ Drive Controller ESA-C, Newport). A mirror guides the fluorescence light, in the detection pathway. The combination of a dichroic mirror (z470/635rpc, Chroma) and a band-pass filter (Chroma HQ690/80m)

blocks the back-reflected laser light by more than 10 orders of magnitude. In this epi-illumination setup, the fluorescence light is collected with the same high NA objective and focused directly onto the active area of \varnothing 50 μ m of the single photon detector (PDM 50ct, MPD). The fluorescence signal is recorded with a PicoHarp 300 system (PicoQuant) and simultaneously correlated with a hardware correlator (Flex02-08D, Correlator.com). For the experiments in the green, the combining beam splitter has been removed and the main dichroic and emission filters have been replaced by appropriate filters (Dichroic: Q565LP, Chroma and Emission Filter: HQ620/100m, Chroma). For imaging, a flipable mirror redirects the fluorescence light on a sensitive electron-multiplying CCD camera (LucaDL-658M-TIL, Andor).



Scheme 13: Setup for fluorescence correlation spectroscopy and microscopy in the group of Prof Lasser at the EPFL in Lausanne.

3. Supported Polymer Membranes through Langmuir-Blodgett Film Transfer

The work presented here was done in collaboration with Serena Belegriou from the University of Basel within the EU-Project FuSyMem. Polymer synthesis, characterisation and pressure area isotherm measurements were done in the labs of Prof. W. Meier at University of Basel.

3.1. Introduction

As described in chapter 1 there is a high interest in model membrane systems for different purposes. Especially for the use as cell-surface models or in technological applications like biosensing and drug screening architectures are needed that are easy to prepare and accessible for sensitive analytical techniques. For these purposes a wide variety of planar model membrane systems have been developed.

The most straight forward way is to prepare supported lipid bilayers directly on a support by different techniques like vesicle fusion^[24], Langmuir-film transfer^[85] or a combination of both.^[86] Since these model systems only have a very limited life time they are not applicable in technical devices. In the past decades, various attempts were made to design more stable membrane model systems.^[40] An alternative to lipid membranes are systems which are made from amphiphilic block copolymers. With a certain molar mass and hydrophilic to hydrophobic block ratio, they adopt the bilayer structure in water.^[87-88] Polymer synthesis allows for the adjustment of such parameters as block length, molecular weight, chemical composition, hydrophilic/hydrophobic balance, and molecular architecture. This provides new insights to control amphiphilic self-assembly and produces structures of defined morphology, molecular packing, and membrane thickness. Hence, manifold possibilities are accessible to engineer customized block copolymer membranes.^[89-91] Measurements carried out on vesicular systems showed that these polymeric membranes exhibit an up to ten times higher stability, as defined by the maximal areal strain, than lipid membranes.^[92] It was suggested that increased entanglement of molecules within the same bilayer plane as well as partial interpenetration of the opposing membrane layers can contribute to enhanced mechanical stability of polymeric membranes compared to lipid membranes. In diffusion measurements

Lee *et al.*^[93] showed that there seems to be a critical chain length above which strong entanglement and high interpenetration of the layers start to occur. Below that length, the two membrane sheets are rather separated layers standing on top of each other which results in faster polymer self diffusion coefficients than for the longer polymer chains. These observations were also supported by simulations which show that the hydrophobic block length determines the degree of entanglement of opposing chains.^[56] Furthermore, superstructures from amphiphilic block copolymers resemble the ones from lipids and they are suitable to functionally incorporate membrane proteins. Meier and co-workers^[94-95] succeeded to functionalize triblock copolymer vesicles with the channel protein outer membrane protein F (OmpF). However, for many analytical techniques as well as for technological applications it is highly desirable to confine membrane processes to the surface. Besides accessibility the coupling of polymer film to a planar support further enhances the mechanical stability of the system. So far, the closest achievement have been solid-supported amphiphilic polymer membranes from methacrylate based triblock copolymers prepared by vesicle fusion^[96] or a grafting-from approach.^[97] The reported work on vesicle fusion on mica resulted in a polymer layer which is very thin (4 nm) compared to the overall polymer length. This probably stems from the strong interactions of the whole hydrophilic polyelectrolyte block with the freshly cleaved mica surface. From the work presented there it is not sure if the film still consists of separated hydrophilic and hydrophobic blocks. In the grafting-from approach a defined hydrophilic hydrophobic hydrophilic structure is achieved but since this densely packed polymer brush is fully tethered to the surface the structure completely lacks chain mobility. Such a high packing density makes it difficult or even impossible to introduce proteins.

The objective of this work was to prepare supported polymer a bilayer system, by combining covalent attachment of a self-organized macromolecular film to a solid support with hydrophobic interactions between two individual bilayer leaflets. The strong interactions between the individual polymeric leaflets and with the substrate are expected to produce a system of high membrane stability. On the other hand, the non-covalent interactions allow for a certain degree of membrane fluidity necessary for biological applications.

If the two aspects of chain mobility and bilayer stability are well balanced it is possible to create polymeric membranes which might open pathways towards architectures, which are stable in gaseous environment and generally more robust than the so far most commonly used phospholipid-based membrane models.

The polymers employed for this approach consist of hydrophobic polybutadiene (PB) units covalently linked to sulphur-functionalized hydrophilic polyethylene oxide (PEO) blocks. PB-PEO block copolymers were chosen, as they were previously shown to produce fluid vesicular membranes^[98-99] and monolayers at the air-water interface.^[100-101] It was also shown, that vesicles from PB-PEO do not exhibit toxic effects on living cells^[98] and are able to host membrane-active peptides.^[61]

A combination of sequential Langmuir-Blodgett (LB) and Langmuir-Schaefer (LS) monolayer transfer techniques is presented to deposit individual polymeric monolayers on ultrasmooth gold supports as depicted in Scheme 14. Langmuir-Blodgett transfer was developed 80 years ago and is the first technique to deposit monomolecular films on a surface.^[85] For this surface active molecules have to be spread on a gas/liquid interface - typically air/water. The molecules on the surface can then be compressed to the desired configuration and packing density. By dragging a support vertically or horizontally through the monomolecular layer the film can be transferred to a surface. This is a very gentle way to produce ultrathin functional coatings. The method can be applied to any kind of amphiphilic molecule including polymers.^[102] The advantage over other bilayer forming methods is that monomolecular films can be prepared while e.g. with vesicle fusion sometimes multilayers are obtained.

The resulting structures in this work were analysed by contact angle measurements, atomic force microscopy, and surface plasmon resonance spectroscopy to gain insights into morphology, homogeneity, and thickness of the layers.

3.2. Experimental Section

Surface pressure-area isotherms. Monolayers were investigated with a Langmuir TeflonTM trough (KSV Instruments, Finland), area 420 cm², equipped with two symmetric, hydrophilic DelrinTM barriers and a Wilhelmy plate (ashless filter paper strips, perimeter 23 mm) to monitor the surface pressure with an accuracy of 0.1 mN/m. The trough was placed in a plastic cabinet to prevent dust contaminations. All experiments were carried out in an air-conditioned lab (20 °C). Monolayers were spread drop-wise on ultrapure water (18.2 MΩm; Millipore, Germany) surface from chloroform solutions (typically 1-2 mg/mL). The solvent was allowed to evaporate for 15 min, and the monolayers were compressed at the rate of 1 mm/min.

Monolayer transfer. PB-PEO-LA monolayers were transferred onto TSG substrates by the Langmuir-Blodgett (LB) technique, using a KSV 5000 (KSV Instruments, Finland) Langmuir TeflonTM trough (area 1860 cm²), placed on an antivibrational table in a plastic cabinet.

Prior to film spreading, four freshly cleaved TSG substrates were immersed in the subphase using a dipper. After compressing a film to the pressure of 35 mN/m it was left for 15 min in order for the polymer chains to establish their most favourable orientation. Afterwards, a monolayer film was transferred at constant speed (0.3 mm/min) on dipper upstroke.

Two PB-PEO-LA coated slides were used for surface investigations and the other two were subjected to a second monolayer transfer, completing the bilayer membrane. In this way, nearly identical conditions were created for one set of samples.

Bilayer preparation. A compressed PB-PEO-OH film (target pressure 35 mN/m) was produced at the air-water interface of a Langmuir trough. PB-PEO-LA coated slides were placed in the dipper horizontally above the floating monolayer. At constant dipper speed (50 mm/min), the substrate was lowered through the interface. The water surface was thoroughly cleaned before transferring the substrate into a crystallization dish. Great care was taken to keep the bilayer surface under water all the time. When no drying experiment was carried out the assembly of all measurement cells was done in a crystallisation dish under water to keep the architecture permanently hydrated.

3.3. Results and Discussion

3.3.1. Monolayers at the Air-Water Interface

Langmuir monolayer behaviour of the amphiphilic diblock copolymers used in this work, i.e. PB-PEO-OH and PB-PEO-LA, is characterized by surface pressure-area (π - A) isotherms. The isotherms are reproducible and reversible. Additionally, polymer organization at the air-water interface was investigated by Brewster angle microscopy (BAM). The observed monolayers were smooth and did not show any significant features over the whole compression range.

Representative isotherms recorded at 20 °C on ultrapure water as subphase, are presented in Figure 1 (A: PB-PEO-OH, B: PB-PEO-LA). Unlike low molecular weight amphiphiles, polymers usually do not display clear, well-defined phase transitions.^[103] In order to gain deeper insight in possibly occurring transitions, compressibility moduli $C_s^{-1} = -A(\partial\pi/\partial A)_T$ were calculated, using the first order derivatives of the isotherms.^[104]

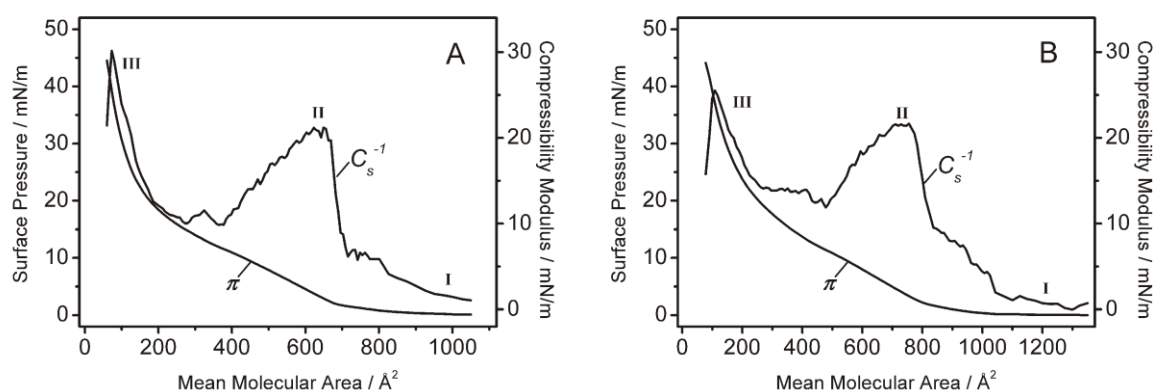


Figure 5: Surface pressure (π) and compressibility modulus (C_s^{-1}) versus mean molecular area for the OH-terminated polymer (A) and the lipoic acid functionalized block copolymer (B). The isotherms were recorded at T = 20 °C. I, II, and III are explained in the text.

At low surface pressures and mean molecular areas $>800 \text{ \AA}^2$ (I) it is assumed that the polymer films are in an expanded state (“pancake” conformation), with the hydrophobic PB blocks lying flat at the air-water interface. The insoluble PB chains are anchored in water by soluble PEO blocks. The PEO segments are assumed to adopt a flattened conformation at the interface.^[105] In this relaxed state, no difference in the π - A -isotherms of the two polymers is recognizable.

Upon compression, an increase in surface pressure and compressibility modulus of both polymers is measured (II), indicating that the films undergo a transition from a gas-like to a more condensed phase. The maxima of the compressibility moduli of both polymers in this phase were calculated to 21 mN/m, corresponding to liquid expanded regimes.^[106] At smaller mean molecular areas, approximately 380 Å² for the OH-terminated polymer (Figure 1 A) and 485 Å² for the LA-terminated polymer (Figure 1 B), a second phase transition is revealed, as characterized by stagnating C_s^{-1} values. These phase transitions do not show any temperature dependence in the range from 14 to 28 °C, which means that the observed transitions are rather related to conformational rearrangements of the PEO blocks in the subphase than to first order phase transitions. As reported before,^[105] such transitions are assigned to the dissolution of the PEO blocks in the subphase. In this region, the PEO blocks extend into the subphase increasing intermolecular interactions by hydrogen bonding^[105] while the water-insoluble PB blocks serve as an anchor to the interface. This “pseudo-plateau” region becomes more pronounced with increasing PEO block length.^[101, 105, 107] The block copolymers used in this work bear only 29 PEO units, and therefore the plateau is not clearly visible. However, the first derivative of the isotherms reveals the constant C_s^{-1} region with proceeding partial PEO dehydration. Further compression leads to a slightly more compressible, i.e. liquid-like, phase with similar C_s^{-1} values for both polymers (III). At a mean molecular area of 100 Å², the compressibility moduli of 30 mN/m for the OH-terminated polymer and 26 mN/m for the LA-terminated polymer, respectively, suggest a qualitatively similar organization pattern for the two polymers. Finally, the surface pressure of both polymers increases steeply until the films collapse at 44 mN/m.

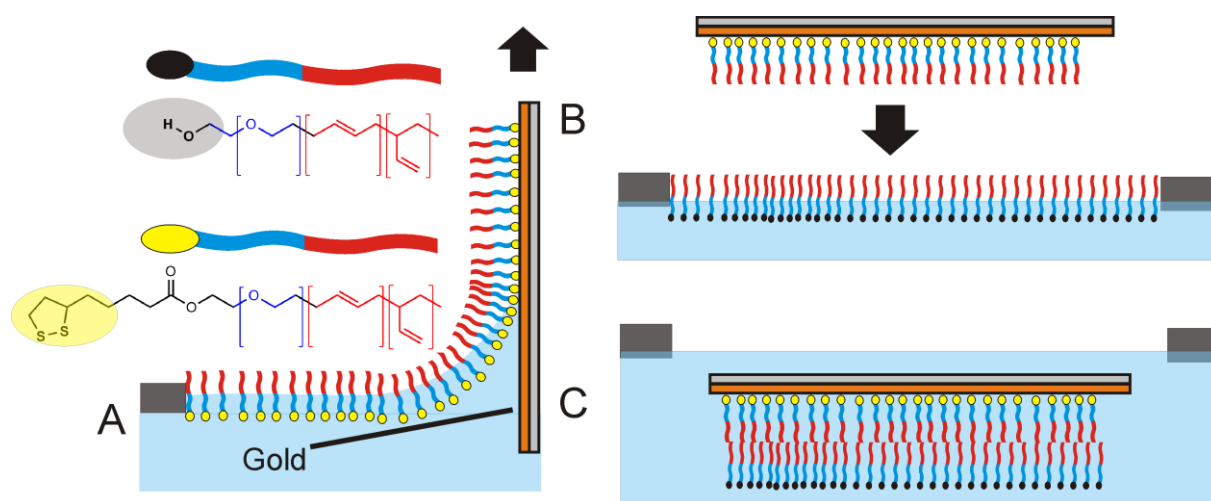
In order to create defect-free bilayers by consecutive Langmuir-Blodgett/-Schaefer film deposition, film stability is crucial. Therefore, the polymer monolayers were compressed to the surface pressure applied in the transfer experiments, which was monitored over time. The compressed monolayers maintained the pressure for longer than 100 min, which was the usual duration for the transfers, indicating high film stability.

3.3.2. Monolayers on Gold

Covalent immobilization of sulphur-containing PB-PEO-LA monolayers was accomplished by LB transfer. A major advantage of the LB transfer technique is the ability to produce highly ordered monolayers without multilayer formation or major defects on very large scales compared to the size of its components. It has been applied for the controlled fabrication of

highly ordered monomolecular films^[85] and has been successfully employed for lipid bilayer preparation.^[23, 80, 108]

Film depositions (Scheme 1 A) were performed at the surface pressure of 35 mN/m which corresponds to 80% of the collapse pressure. The corresponding compressibility modulus of the monolayer is 26 mN/m. In this phase, the polymer films assume the most densely packed brush-like order. The transfer ratios are approximately 1.3. Since the transfer ratio is an approximate indication of the transfer quality,^[109] the moderately deviating value from unity is acceptable and suggests successful monolayer transfer.



Scheme 14: Monolayer and bilayer formation: In (A), the substrate is covalently coated with a monolayer of sulphur-functionalized polymer on dipper upstroke. (B) and (C) show the Langmuir-Schaefer transfer by pressing the monolayer through the air water-interface.

In order to follow the surface functionalization process, contact angle measurements were carried out on the bare gold surface and the transferred LB film. Contact angles increased from 60° for freshly cleaved gold substrates to at least 90° for the PB-PEO-LA-covered substrates. The contact angle values were obtained from at least five different individual measurements on the same sample. The changes towards higher values originates from the hydrophobic polybutadiene blocks facing away from the gold surface.

Monolayer formation was also characterized by surface plasmon resonance spectroscopy (SPR). This optical method allows for non-invasive thin film characterization and is very sensitive to small changes in adsorbed mass. Another major advantage of this technique is the label free detection. Figure 6 shows the representative angular spectrum of a PB-PEO-LA monolayer transferred to an ultrasmooth TSG substrate, a blank gold substrate, and a bilayer. The bilayer spectrum will be discussed later.

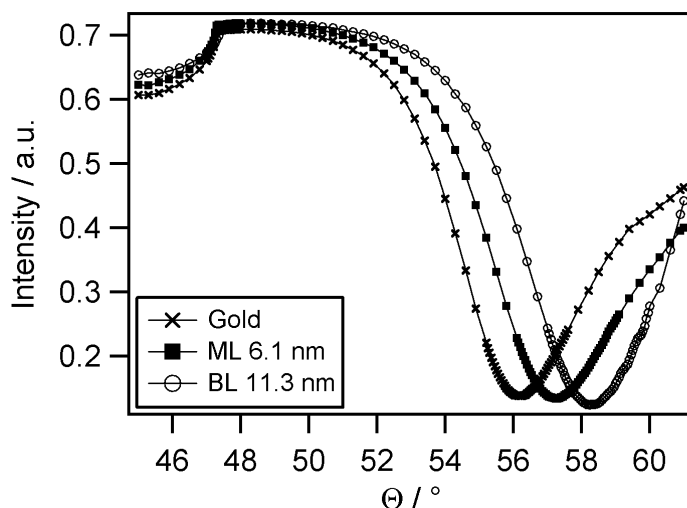


Figure 6: Representative angular SPR spectrum measured in ultrapure water showing the shift of the reflectivity from blank gold to the covalently attached PB-PEO-LA monolayer (ML) and to the bilayer (BL). Curves were fitted using a refractive index for the polymer film of $n = 1.5$ (fit parameters: glass $\epsilon_{\text{real}} = 3.39$; gold: $d = 50.48 \text{ nm}$ $\epsilon_{\text{real}} = -13.2759$, $\epsilon_{\text{imag}} = 2.3799$; polymer: $\epsilon_{\text{real}} = 2.25$; water: $\epsilon_{\text{real}} = 1.77$).

The shift of the reflectivity minimum from the blank gold to the PB-PEO-LA monolayer is clearly visible in Figure 6. From Fresnel equation-based calculations, the optical thickness of the monolayer can be obtained. Assuming a refractive index of 1.5 for the block copolymer, a mean geometrical thickness of $6.1 \pm 0.4 \text{ nm}$ was calculated. The experiments were performed in air as well as in water and data analysis resulted in the same monolayer thickness which means that neither strong swelling nor drying alters the monolayer. It has to be noted that SPR yields average mass thicknesses, meaning that it cannot distinguish rough or patchy films from plane layers.

To study local film morphology, AFM was applied for monolayer characterization. Information about homogeneity, structural defects, and roughness of the monolayers can be obtained by this method. AFM measurements were performed in air as well as in aqueous media. A typical height image and cross section of a measurement in water are presented in Figure 7. The film surrounding the square in the centre of the image remains completely unperturbed, while the part in the middle was scratched with the AFM-tip. The unaltered film does not show any defects on the micrometer scale. Roughness (root-mean-square) does not exceed 0.5 nm over one square micrometer. It has to be mentioned that there is a small amount of material adsorbed on top of the monolayer which might result from impurities during film transfer. What can be seen as well is the monolayer film exhibiting a very fine structure on the length scale of about 10 nm. This might be due to rearrangements of amphiphilic polymers with chain lengths comparable to the size of these microstructures. This

is not surprising since the image was recorded in water so that the hydrophobic polybutadiene chains tend to minimize their free energy by rearranging on the surface. However, the freedom to reorient is limited by the covalent attachment to the substrate. AFM scratching experiments show that the monolayer cannot be scratched away, but some loosely bound material is wiped away by the tip. This loose material likely originates from impurities during film transfer. The dark stripes in the image are cracks in the epoxy-glue underneath the gold which result from cutting large substrates into halves.

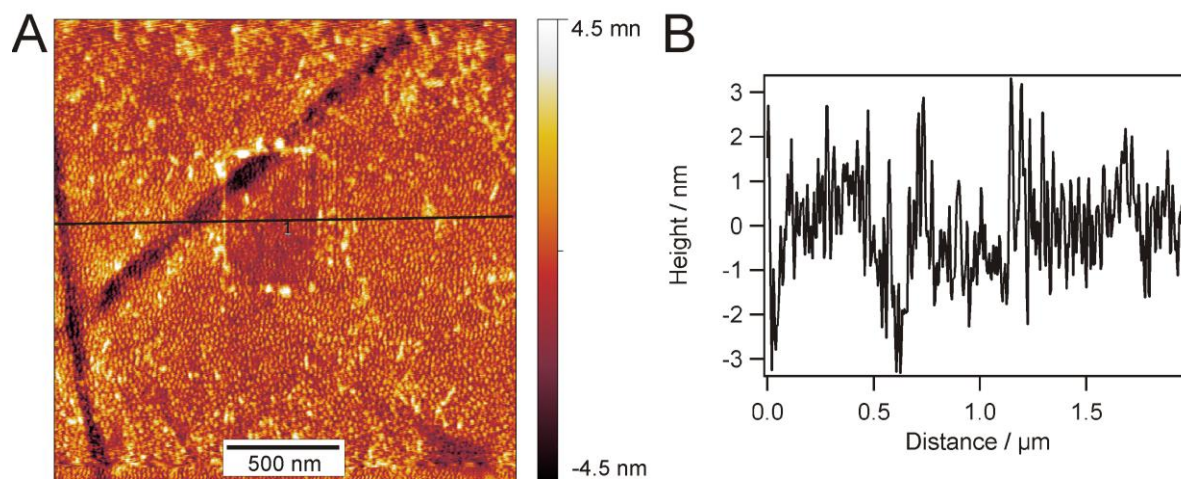


Figure 7: AFM image (A), recorded in water, of the covalently immobilized monolayer which was scratched with a hard cantilever. The two dark stripes result from cracks in the epoxy glue due to cutting the slide prior to monolayer transfer. The corresponding section is shown in (B).

3.3.3. Bilayer Membranes on Gold

The Langmuir-Schaefer (LS) technique was applied for the transfer of the second monolayer to the PB-PEO-LA-covered substrate in order to obtain a complete bilayer membrane. The procedure is depicted in Scheme 1 B and C. A substrate, which had been previously coated with a PB-PEO-LA monolayer, was placed horizontally above a PB-PEO-OH Langmuir film and subsequently pressed through the air-water interface. After transfer, the sample was assembled into the measurement cell and kept hydrated throughout all surface analysis. SPR measurements were performed to investigate the thickness. The angular scan in Figure 6 shows the shift of the minima of the bilayer and the blank gold substrate, respectively. From the fit a mean bilayer thickness of 11.3 ± 0.5 nm was obtained, assuming $n = 1.5$. The doubling of the layer thickness suggests a bilayer structure of the type hydrophilic-hydrophobic-hydrophilic, as depicted in Scheme 1 C. The bilayer thickness is in good agreement with results reported earlier,^[55] where a PB-PEO diblock copolymer was

investigated, having similar molecular weight and a comparable hydrophilic to hydrophobic block ratio to the polymer reported here. Bermudez *et al.*^[55] investigated the vesicular membrane thickness by cryo-TEM and the value of 9.6 nm was obtained. Considering the different membrane preparation methods, resulting in different polymer chain packing densities in vesicles *versus* compressed monolayers, the minor discrepancies are negligible. In the case of the planar bilayers, the chains were forced to stretch by compression at the air-water interface, whereas packing in vesicles occurs basically without area constraints, leading to less stretched polymer chains. Furthermore, the thickness measurements in this work consider the whole polymer length including the hydrophilic blocks and not only the hydrophobic core (as measured by cryo-TEM), which results in higher values for the thickness.

The attachment of the second layer to the previously immobilized monolayer is governed mainly by hydrophobic interactions between the polybutadiene blocks. The resulting membrane architecture is supposed to be an intermediate structure between completely unperturbed chains, like it is the case with low molecular weight amphiphiles, and an interdigitated structure.^[57, 88] However, minor entanglement of the individual polymer chains in the opposing leaflets is expected due to the rather low molecular weight of the polymer.

Homogeneity and roughness of the respective membranes were investigated by AFM measurements in water. The height image presented in Figure 8 A shows a uniform and homogeneous bilayer. Sections across the image (Figure 4 B) and statistical analysis showed the root-mean-squared roughness to be approximately 0.35 nm over an area of $1 \mu\text{m}^2$. High uniformity and smoothness were accomplished on large areas up to several tens of square millimetres.

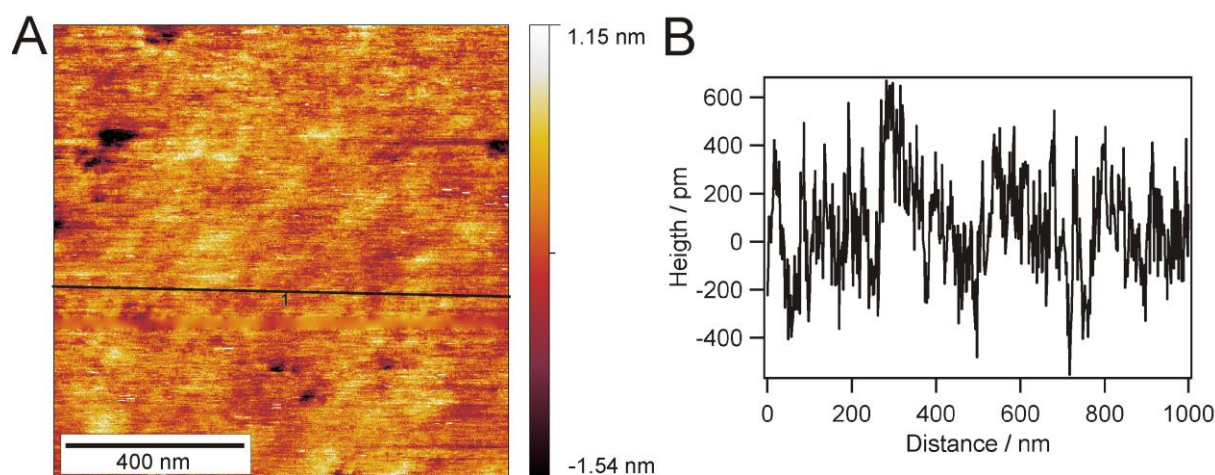


Figure 8: AFM image of the intact bilayer after Langmuir-Schaefer transfer (A) and the corresponding cross section (B) show homogenous transfer over an area of $1 \mu\text{m}^2$ with negligible defects.

Layer transfer of the bilayer without major defects was only accomplished when the monolayer was not treated with organic solvents like THF or chloroform. Whenever the monolayer film was cleaned with THF prior to Langmuir-Schaefer transfer the resulting bilayer exhibits wormlike defect structures as shown in Figure 9. The defects reach all the way through the bilayer film and have a depth of ~ 11.4 nm. Similar structures which have half the height of the complete bilayer were observed for bilayers prepared via vesicle fusion (see chapter 3) and rinsed with organic solvent. It is most likely that polymer chains are rinsed off which cannot couple to the gold substrate because they bare hydroxyl groups at the end. The branched structure results from the fact that the hydroxyl functionalised polymer phase separates from the sulphur terminated one so that it can be collectively rinsed away. Obviously the second layer is not able to back fill the created voids and thus heal the surface structures.

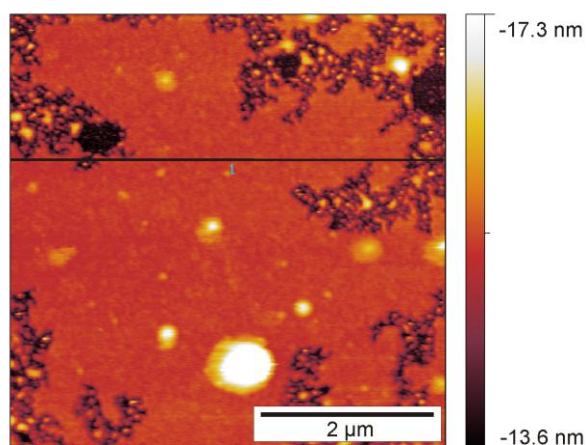


Figure 9: AFM image of a bilayer film on top of a monolayer which was rinsed with THF.

In addition to the height images, force-distance curves provide information about the mechanical properties. By repeatedly approaching and retracting the cantilever from the surface, adhesive and repulsive forces, as well as structural details can be obtained. All force measurements were performed with a bare oxide sharpened silicon nitride AFM tip, known to be hydrophilic. Since structures, such as presented in this work, have not been reported so far, there are no literature references to be compared with. However, a lot is known about force measurements on supported lipid bilayers.^[110] For the monolayer one does not expect any characteristic features since the covalently bound polymer chains have only very limited ability to reorganise upon perturbation by the cantilever. Also the hydrophilic cantilever should be repelled from the hydrophobic surface. Exactly this behaviour can be seen in Figure 10 A.

In the case of the bilayer the situation is different, as shown in Figure 10 B. The molecules of the top layer tend to reorganise when the tip penetrates the surface. Since there is a lateral pressure within the membrane plane that has to be overcome, a rise of the force curve can be observed at the beginning. At a certain point, the applied force is high enough and the cantilever snaps into the bilayer, which can be seen at a distance below 10 nm where the force temporarily decreases until the lower part of the substrate is reached. This step is characteristic for supported bilayers and has been observed for various lipid bilayer systems.^[110] What is also important is that the jump in the force-distance curve appears even after several tens of approach-retract cycles which shows that the membrane is mobile enough to cure the small hole made by the cantilever. The width of the jump corresponds to approximately 7 nm, which is the thickness of an individual polymer layer. Since the cantilever was not calibrated and the nominal spring constant was taken for scaling, it was not possible to determine absolute force values from these measurements. However, a qualitative statement can be made.

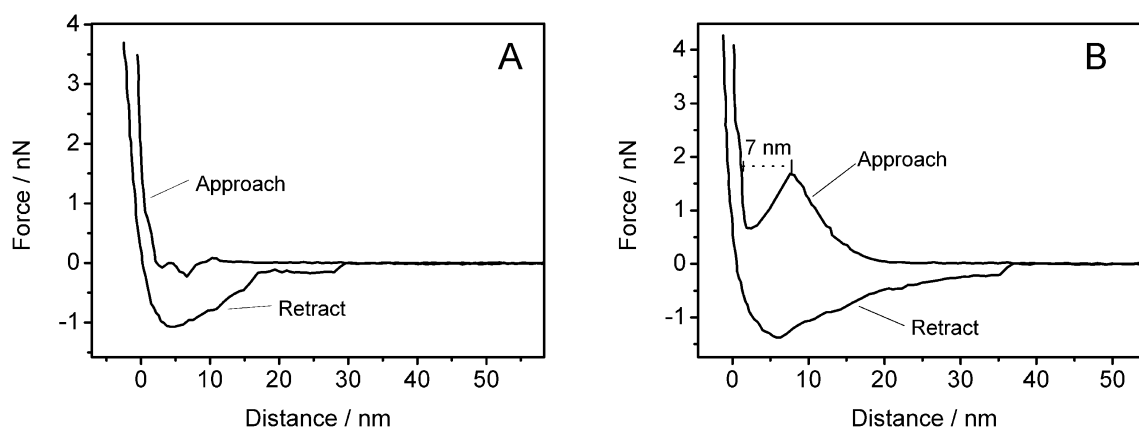


Figure 10: Force-distance curves measured on the monolayer (A) and the bilayer (B). Measurement on the bilayer shows a distinct jump in the approaching curve which indicates the penetration of a distinct layer. Both measurements were performed using the same cantilever.

Scratching experiments. In order to prove the presence of the second polymer monolayer, scratching experiments were performed with a hard cantilever, able to remove material from the surface. Figure 11 A clearly shows that the upper layer can be selectively removed from the surface which is not possible by scratching the covalently attached monolayer (see Figure 7). The corresponding section (Figure 11 B) shows the height difference between monolayer and bilayer more evidently. The formation of a well with a homogeneous depth indicates complete removal of the second layer. However, as shown in Figure 11 B, the section depth of the trace is merely 3 nm. The hard cantilever (2 N/m) used for this experiment is not able to

map the actual height, but partially penetrates the membrane. Unfortunately it is not possible to exchange the hard tip by a soft one without losing the position of the scratch under the microscope. If a soft cantilever (spring constant 0.32 N/m) can be used to image the scratched area, the expected monolayer thickness of approximately 6 nm will be found. The time span between scratching and imaging of the whole area of $2 \times 2 \mu\text{m}$ is about 3 min. This time does not allow the closure of the created defect of $500 \times 500 \text{ nm}$ but the scratched edges are still sharp which points to a low chain mobility of the top layer on these large length scales.

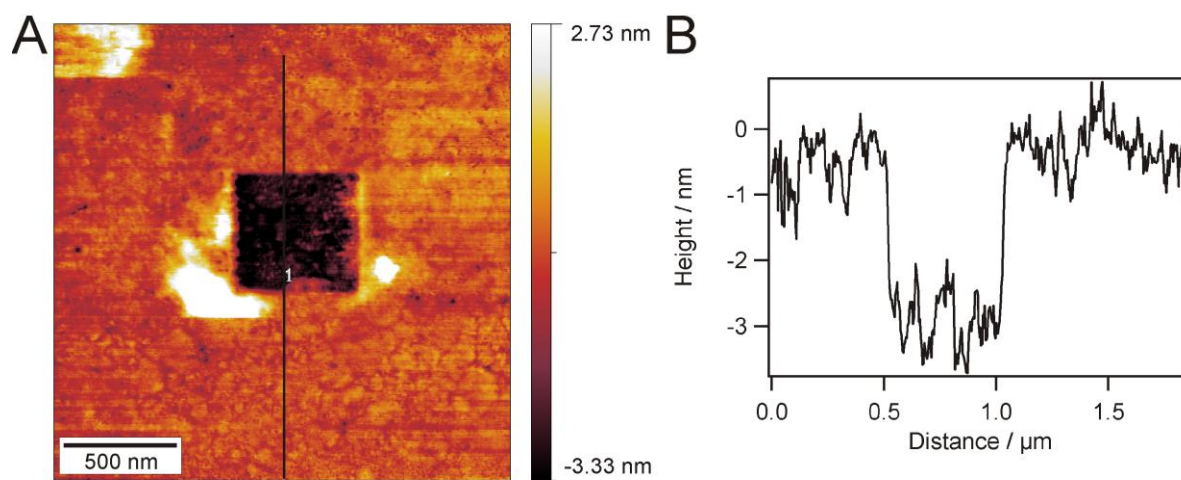


Figure 11: AFM image after a scratching experiment (A) and section through image (A) along the indicated line (B).

3.3.4. Membrane Stability

In order to probe stability, the membrane was heavily rinsed with ultrapure water ($18.2 \text{ M}\Omega \text{ m}$) in a flow cell and SPR reflectivity changes *versus* time at the incident angle of 56° were recorded. For that, the membrane was permanently kept under water. This kinetic measurement did not reveal any changes in reflectivity upon the harsh rinsing process. Consequently, no loss of mass was detected and the membrane stayed intact during and after the rinsing procedure. When rinsing was carried out using an effective solvent for the PB-PEO diblock, such as THF or chloroform, the non-covalently bound upper leaflet of the membrane was washed away and the reflectivity minimum returned to the value obtained for a monolayer as demonstrated in Figure 12.

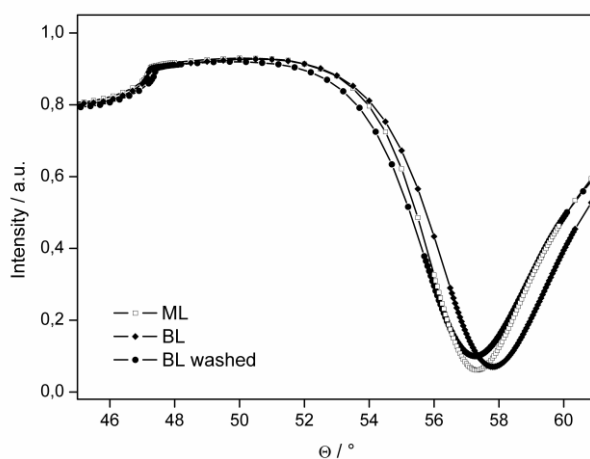


Figure 12: Angular SPR spectrum measured in ultrapure water. After the bilayer was washed with a good solvent such as THF or chloroform, the reflectivity minimum returned to the value obtained for a monolayer.

Furthermore, the membrane stability in air was studied. Therefore the membrane was dried under a stream of nitrogen, left dry for two hours, and later rehydrated with ultrapure water. SPR measurements hardly revealed any shift of the reflectivity minimum after drying and rehydration of the membrane as can be seen in Figure 13.

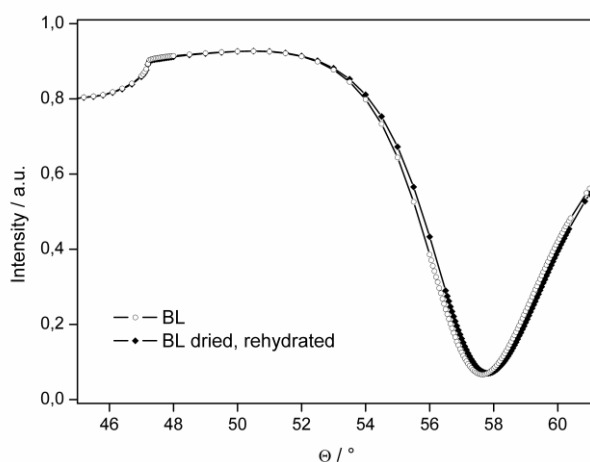


Figure 13: Angular SPR spectrum measured in ultrapure water. A bilayer was dried under a stream of nitrogen and left dry for 2 h prior to rehydration.

This indicates that the material on the surface was not removed during this experiment. In addition to the optical measurements, AFM images in Figure 14 A show that the architecture does not change significantly upon drying for short times up to two hours. This unambiguously proves the high stability of the polymer architecture compared to common

lipid systems. Since the architecture exhibits a certain air stability it was tried to measure contact angle on the freshly dried slides. In theory the contact angle should adopt a small value because hydroxyl groups are facing towards the air. Unfortunately it was not possible to obtain a constant value due to strong drift. Most likely the surface forces at the solid liquid interface are too high so that the drop itself changes the bilayer structure. Usually, supported and tethered lipid bilayers decompose directly when brought into contact with air, whereas solid-supported phospholipid systems resisting a rinsing procedure have already been reported.^[111-112] So far, the closest attempts towards air-stable supported lipid bilayers employed the stabilising effect of sugars^[113] or polymer layers.^[114] However, these approaches have the drawback of potentially hindering the access of proteins or substrates to the membrane. A recent publication from Deng *et al.*^[115] describes an air stable surface tethered membrane via a high density of cholesterol anchor groups which remains fluid after several cycles of drying (2 h) and rehydration.

Drying of the polymeric bilayer for longer than 12 hours leads to a significant change in morphology, as can be seen in Figure 14 C. Objects of 10-20 nm in height are present everywhere on the surface, which suggest the disassembly of the architecture. Most likely the polymer chains reassemble into micellar structures in order to minimize their energy. This assumption is supported by the measured height of these objects, which is in the dimension of a complete bilayer and which should also be the theoretical height of a micelle. Consequently, it is concluded here, that water is still necessary to stabilize the bilayer structure on the long term scale.

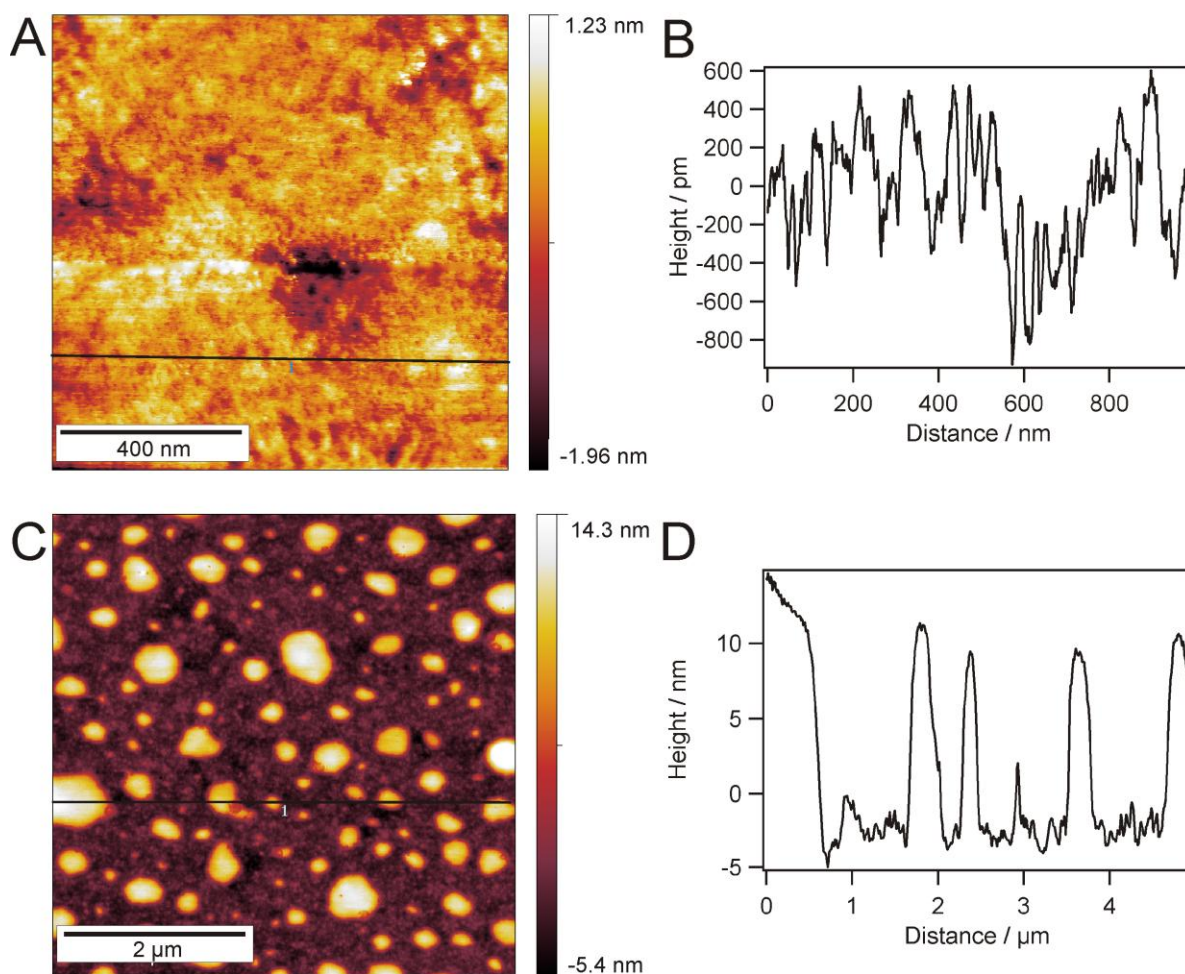


Figure 14: AFM images of the supported polymer bilayer after different drying stages. 1.5 hours of drying (A) with the corresponding section (B). After 12 hours of drying, large objects of 10-20 nm can be seen in the image (C) and the section (D).

An explanation for this observation can be the insufficient coupling between the two individual polymer layers. This suggests a rather low entanglement of the polymer chains which is in accordance with the literature for the particular chain length of the polymers used here.^[93] Probably, membrane stability against drying can be increased by using longer block copolymers. In this case, a higher degree of interdigitation between the two opposing leaflets, thus enhanced membrane stabilization, is expected. On the other hand, a higher degree of entanglement and an increase in thickness, due to the use of longer polymers, might minimize fluidity and hinder incorporation of proteins. This is disadvantageous for the principal purpose of this membrane system, i.e. serving as matrix for protein incorporations.

3.4. Summary

In this chapter a novel planar membrane system composed of the amphiphilic diblock copolymer, *b*-polybutadiene-*b*-polyethylene oxide is described. A standard chemical modification procedure yielded a sulphur-functionalized polymer, which can be covalently attached to ultrasmooth gold substrates by the well-controllable Langmuir-Blodgett monolayer transfer technique. The covalent attachment of the proximal membrane layer to the solid support endows the system with mechanical stability. The second layer was transferred by the Langmuir-Schaefer method and led to an artificial bilayer system consisting of two individual layers, resembling the hydrophilic-hydrophobic-hydrophilic structure of lipid membranes. Due to the non-covalent coupling of the second bilayer sheet the architecture retains a certain degree of mobility as could be shown by measuring repeated force-distance curves at one spot. On the other hand it could be shown by scratching experiments that there is hardly any self-diffusion in the top sheet which is able to close bigger gaps created by the cantilever. SPR results indicate a bilayer thickness of 11.3 nm and AFM measurements proved flatness and homogeneity of the system on several square millimetres. For the first time, a polymeric supported bilayer of defined morphology, molecular packing, and membrane thickness was produced by this straightforward preparation route. Drying experiments implied air stability of the system to a certain extent, however, the presence of water is still required to hydrate the hydrophilic block and stabilize the layered structure in the long term. The polymer used in this work rather falls into the regime where entanglement between opposing layers only starts to occur, which is in agreement with reports from literature for this chain length. Therefore stability of this membrane system could be improved by using longer, thus stronger interpenetrating, polymers. In addition, a mixture of di- and triblock block copolymers could be used as membrane building blocks. Due to their molecular structure (i.e. hydrophilic blocks on both ends of the hydrophobic core), a fraction of the triblocks will span a membrane, thus, further contribute to membrane stability. Nevertheless, the results presented in this work already suggest superior stability of our membranes compared to conventional phospholipid bilayers.

These stable and robust solid-supported polymeric membranes could be a suitable platform to study membrane proteins in a completely artificial environment. Moreover, they offer versatility concerning the application of surface-analytical techniques which might lead to sensing applications in the future.

4. Biomimetic Planar Polymer Bilayers through Vesicle Spreading

4.1. Introduction

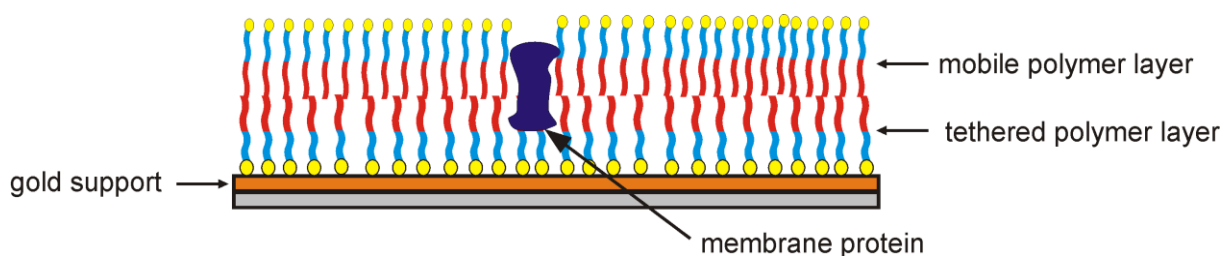
The big advantage of planar model membrane systems compared to others like black lipid bilayers or vesicular structures is the high localisation on the surface. This makes them accessible for a wide range of surface sensitive analytical techniques like atomic force microscopy (AFM)^[27], quartz crystal microbalance (QCM)^[25], electrochemical impedance spectroscopy (EIS)^[80] and surface plasmon resonance (SPR)^[26] spectroscopy. The support also provides extra stabilisation to the system. Most model systems are made from lipids but there are other amphiphiles which are able to produce bilayer membrane structures. One promising alternative are amphiphilic block copolymers which can under certain conditions also form bilayer structures in aqueous environment.^[51] Through polymer synthesis a high structural and chemical diversity of these amphiphiles is available so that bilayer structures can be tailored to specific needs. Polymers and especially those which are biocompatible are promising as substitutes for lipid systems since it was shown that they form mechanically much more stable bilayers. Their maximal areal strain is up to 10 times higher than for lipid systems.^[55]

In the previous chapter a new method to produce biomimetic supported polymer bilayers with the help of consecutive Langmuir-Blodgett and Langmuir-Schaefer transfer was reported.^[116] This method allows for the preparation of a homogenous polymer bilayer over several square millimetres or even square centimetres. It was shown that these bilayers readily form and exhibit a certain stability towards drying. The advantage is the highly defined layer architecture but it is tedious to transfer the two layers on a Langmuir-trough. The question was if it is possible to prepare solid supported polymeric bilayer membranes with a straight forward one step route. For this purpose polymer vesicle fusion was explored.

Vesicle fusion is an established and quick way to produce lipid bilayers on various supports.^[24] The architectures produced by this method have proven useful for studies of various membrane properties like lipid diffusion^[117], cell adhesion^[28] and many more.^[118-120] Depending on the chemistry of the vesicle constituents and the surface properties vesicles can

be spread on hydrophilic surfaces like SiO_2 [24] or hydrophobic surfaces like self assembled monolayers of sulphur tethered lipid analogues. [64]

In this chapter vesicles of a diblock co-polymer were spread where the end group is functionalized with lipoic acid so that it reacts with the gold surface. Since polymer vesicles are more stable than their lipid analogues vesicle spreading is impeded. To promote vesicle bursting sulphur groups on the vesicle surface are introduced which increase the interactions with the gold surface film. By applying this vesicle suspension to the gold, a planar film can be formed. The mechanistic details of vesicle fusion in general are still unclear. The resulting bilayer is only coupled to the surface through the bottom sheet while the upper one is just attached by hydrophobic interactions (Scheme 15). This allows for a certain degree of flexibility which can be favourable for the introduction of membrane probes or proteins.



Scheme 15: Illustration of the supported polymer bilayer structure consisting of two individual leaflets of a diblock copolymer.

Since the bilayer preparation is carried out on a gold film that can serve as an electrode, the resulting polymer film is perfectly suited for electrochemical measurements. This is useful for TM-protein studies like channels or pores because their incorporation has an effect on the overall bilayer resistance. In the future electrochemical techniques might also serve as a read out if the polymer matrix is used in a sensor application.

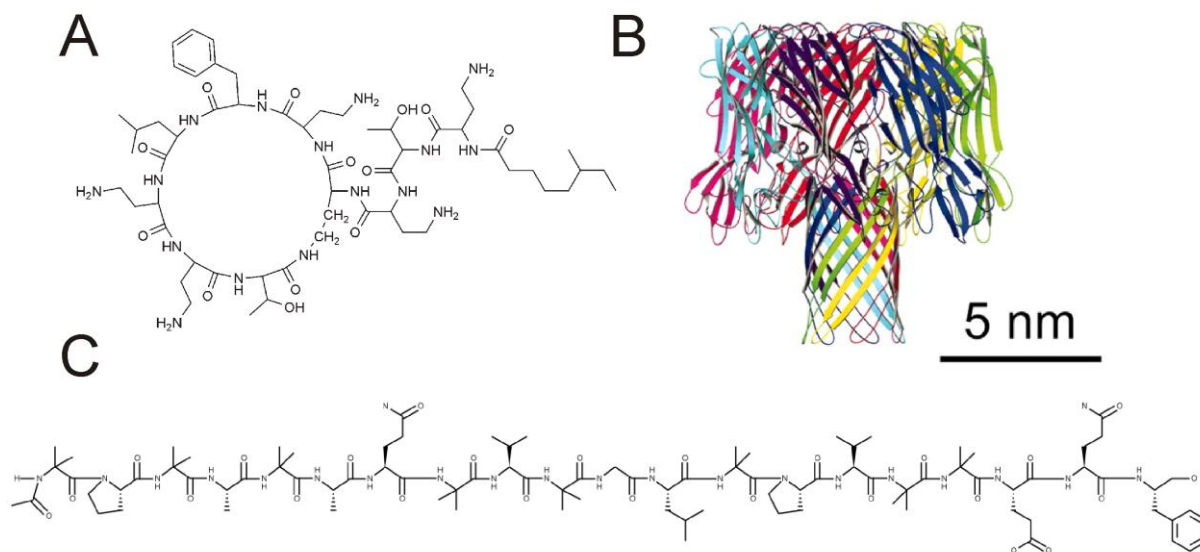
One drawback of membrane architectures on gold is that quenching inhibits fluorescence measurements. Due to strong reflection it also complicates white light optical microscopy. Therefore an alternative route to planar systems on a transparent support was investigated by applying vesicles of PB-PEO 01 with a hydroxyl-functionality to plasma cleaned glass surfaces. The plasma treatment makes the surface very hydrophobic. In this approach the vesicles are forced to spread solely by non-covalent interactions and the resulting polymer bilayer is only physisorbed on the support. For comparison the non-covalent interactions of small unilamellar polymer vesicles with strongly hydrophobic surfaces was also tested.

So far there are just a few studies where supported polymer bilayer systems have been produced and characterized. A grafting from approach by surface-initiated atom transfer

radical polymerisation (ATRP)^[97] and one case where polymer vesicles of an ABA triblock copolymer were adsorbed on solid support and consecutively fused is reported.^[96] In this polymer vesicle fusion approach Rakhmatullina *et al.* used the strong interactions of the hydrophilic block of a polycationic polymer with a freshly cleaved mica surface to spread vesicles. Due to the strong Coulomb interactions of the hydrophilic block of the polymer with the surface this produces very thin films. Most likely they do not resemble the clear hydrophilic – hydrophobic - hydrophilic structure of natural lipids anymore. None of the reported systems on a support was shown to interact with transmembrane proteins or peptides. In the last decade, different approaches lead to protein functionalised polymer bilayers where unperturbed membrane diffusion is possible. For example bacteriorhodopsin was functionally incorporated in vesicular structures^[60] and outer membrane protein F (OmpF) was shown to be hosted by free standing systems^[121]

To evaluate if and how membrane active species interact with the supported bilayer system prepared via vesicle spreading, different species were tested. The covalently bound architecture on gold was investigated by electrochemical impedance spectroscopy (EIS) to monitor the interaction. The species investigated are polymyxin B, alamethicin and α -haemolysin which are all known to spontaneously incorporate into lipid bilayers (Scheme 16). This is a prerequisite if transmembrane species shall be introduced into the bilayer after preparation.

Polymyxin B is a cyclic peptide used as an efficient antibiotic for gram-negative bacteria. It causes alterations in the membrane structure similar to the way detergents do. It especially disrupts membranes consisting of lipopolysaccharides which are a major component of gram-negative bacterial membranes leading to leakage of small ions and molecules and finally causing cell death.^[122] Polymyxin B is a promising candidate to interact with the polymer bilayer structures presented in this work because its natural target structure is chemically similar to hydrophilic PEO-block. In its native environment polymyxin B preferably incorporates into membranes with a high content of lipopolysaccharides. This could facilitate recognition of the artificial bilayer structure by the peptide.



Scheme 16: Structures of the used peptides and proteins. (A) polymyxin B, (B) α -haemolysin taken from Kasianowicz *et al.*^[123] and (C) alamethicin.

The α -haemolysin of the human pathogen *Staphylococcus aureus* consists of a monomeric 33 kDa protein. In its functional form it is a heptameric pore^[124] as depicted in Scheme 16 B. The mechanism of assembly is well understood and consists of three steps.^[125] First a monomeric unit α_1 attaches to the membrane followed by assembly of an unfunctional heptameric structure α_7^* which is finally incorporated into the membrane as a functional transmembrane pore α_7 . α -haemolysin is probably not the easiest protein to introduce into a polymer bilayer because of its size but in case of successful incorporation it causes a very strong decrease in membrane resistance that can be read out by EIS.

Alamethicin is an α -helical transmembrane peptide forming voltage dependent ion-channels consisting of four to six molecules.^[126] It has been extensively studied in the context of lipid-peptide interactions^[127] and pore formation.^[128] Most interesting it was shown that alamethicin is able to induce calcein leakage from polymer vesicles. At high peptide concentrations it was even able to lyse giant unilamellar polymer vesicles as could be demonstrated under a standard light microscope.^[61]

4.2. Experimental

Vesicle preparation and DLS characterisation was done by Serena Belegriou in the group of Prof. W. Meier at the University of Basel.

Vesicle preparation. For the preparation of small unilamellar polymer vesicles 8 mg of polymer were dissolved in 4 mL of tetrahydrofuran (THF). Under vigorous stirring 10 mL of ultrapure water (18.2 M Ω , MilliQ) were slowly added with a peristaltic pump at 100 μ L/min. During addition of water the solution gets turbid while vesicles in a relatively defined size range are forming. The vesicle suspension is stirred for another 3 h. Then stirring speed is reduced and the suspension is left to volatilise THF for another 4 days. The resulting solution with a target concentration of 0.19 mM is consecutively extruded through 800 nm, 400 nm, and 200 nm polycarbonate membranes in a barrel extruder at 5 bar. The automated extrusion is advantageous over manual extrusion because it can extrude at a constant predetermined pressure. This increases comparability between different batches. Dynamic light scattering (DLS) proves the formation of vesicles with hydrodynamic radius of 100 nm with a reasonable size distribution. Vesicle suspensions were kept at 4°C until further use. Typical suspensions were stable for months without any precipitation. The approximate sizes of the used vesicles are presented in Table 4. The extruded vesicles of PB-PEO-01 with an OH-terminus could not be fitted with a monomodal distribution because two modes of motion were clearly visible in the correlation curves. Most likely this second species are micelles.

Sample type	R _h / nm	Dispersity
PB-PEO-01 LS non-extr	115-130	0.2-0.25
PB-PEO-01 OH non-extr	150-300	0.5
PB-PEO-01 LS extr	100	<0.1
PB-PEO-01 OH extr	no fit possible	-

Table 4: Approximate vesicle sizes as determined by dynamic light scattering.

Bilayer preparation. For covalently coupled systems on gold lipoic acid functionalized polymer vesicles were either added directly or were mixed with 8 or 45 mg of NaCl and vortexed until everything was dissolved. Then the suspension was directly given on a freshly cleaved template stripped gold surface. In some cases vesicle fusion was carried out in an

oven at 45°C as described later in the text. For AFM imaging the surfaces were rinsed with ultrapure water or the respective sodium chloride solution prior to the measurement.

For spreading on hydrophobic gold and hydrophilic glass substrates PB-PEO- 01 vesicles were prepared from a polymer bearing hydroxyl end groups at the PEO block. 500 µL of the vesicle suspension were mixed with 45 mg sodium chloride and applied directly to the surface and incubated for roughly 3 h. Then the sample was rinsed with the respective salt solution. For the passivation of the areas of uncovered glass 100 µl of a 6% solution of bovine serum albumin (BSA) were allowed to interact with the surface for 60 min and rinsed afterwards.

Bilayer-peptide interactions. For the peptide insertion experiments the successfully formed polymer bilayer was washed with PBS and allowed to equilibrate for ~14 h inside the EIS cell. The equilibration process was monitored in 1 h time intervals to see when the signal stabilises. In the case of polymyxin B the sample volume was reduced from 1 mL to about 200 µL inside the EIS sample cell before addition of the peptide to prevent strong dilution of the aliquot by the electrolyte. Then 20 µl of the peptide in ultrapure water (1 mg/mL) were added and allowed to incubate for 15 min to 1 h. EIS spectra were recorded directly after addition of peptide. For the α -haemolysin 60 µL of a solution in PBS was added directly to the EIS-sample cell at a concentration of 0.5 mg/mL. The development of the electrochemical impedance spectra was monitored over 14 h within time steps of 30 min to 1 h.

Alamethicin was added to the polymer surface inside EIS sample cell. 50 µl of a peptide solution in ethanol (2 mg/mL) were added after equilibration of the impedance spectra.

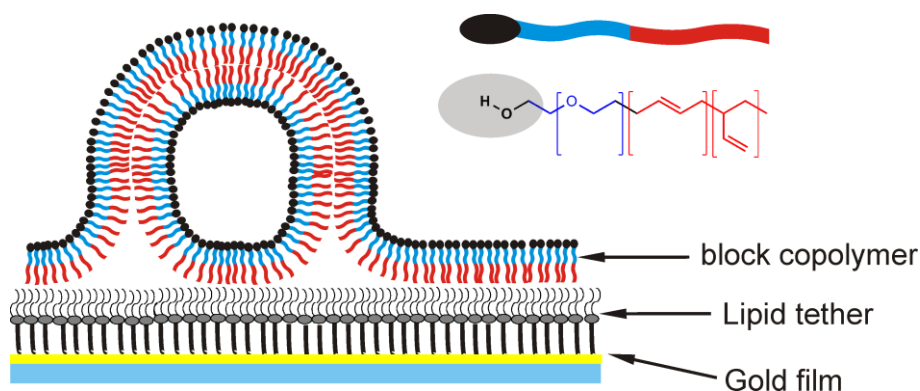
4.3. Results and Discussion

Three different approaches were tested to fuse polymeric vesicles made from poly(butadiene)-*b*-poly(ethylene oxide) on planar surfaces. Different surface forces were used to force the vesicles to spread. On the one hand polymers were added to the support to physisorb on hydrophilic as well as hydrophobic surfaces. Moreover covalent coupling of the bilayer to the surface via sulphur-gold bonds was investigated. The interactions of membrane peptides with the successfully prepared structure on gold were then tested with electrochemical impedance spectroscopy (EIS).

4.3.1. Vesicles on Hydrophobic Support

First experiments were carried out to see if the hydrophobic interactions of polymer vesicles with a hydrophobic support are sufficiently strong to spread films.

Typically lipid vesicles can be fused on a hydrophobic support as for example a self assembled monolayer of alkane thiols^[129] or tethered lipids^[112] on gold. The hydrophilic functionalisation on gold is very convenient because it can be done by self assembly. For this the sample slide only needs to be immersed in an organic solution of the respective molecule over night and rinsed off afterwards. Typical monolayers of these molecules have a contact angle of at least 105° to water. In the case shown here the supporting hydrophobic layer consists of an archae analogue thiolipid SAM.^[31] The same approach of vesicle fusion as for lipids was carried out in this work with polymer vesicles only bearing hydroxyl groups on their shell. In the case of successful vesicle spreading the resulting architecture would be a hybrid membrane with a polymer top layer and a lipid bottom layer as depicted in Scheme 17. In addition the underlying gold film proves to be useful for electrochemical measurements and surface plasmon resonance spectroscopy.



Scheme 17: Hypothetical fusion mechanism and the resulting structure from a polymeric vesicle spreading on hydrophobic support.

Pure and dilutions (1:10 and 1:1) of vesicle suspension and phosphate buffer concentrations were tested by AFM and SPR. Highest mass adsorption in the SPR measurement was observed for the pure vesicle solution in water but no statement can be made about the surface morphology. The AFM image in Figure 15 shows the hydrophobic gold surface after incubation with pure vesicle solution over night. Only very sparsely scattered objects can be found on the substrate but no signs of planar patches. The surface between the objects was checked with force-distance measurement and only a hard repulsion was detectable in the approach and retract curve. This is the typical behaviour for a hard hydrophobic substrate.

This excludes the possibility of a complete defect free bilayer between the objects. In the case of a polymer bilayer between the objects additional repulsive and attractive forces would cause additional features in the fore-distance curve as shown later in this chapter.

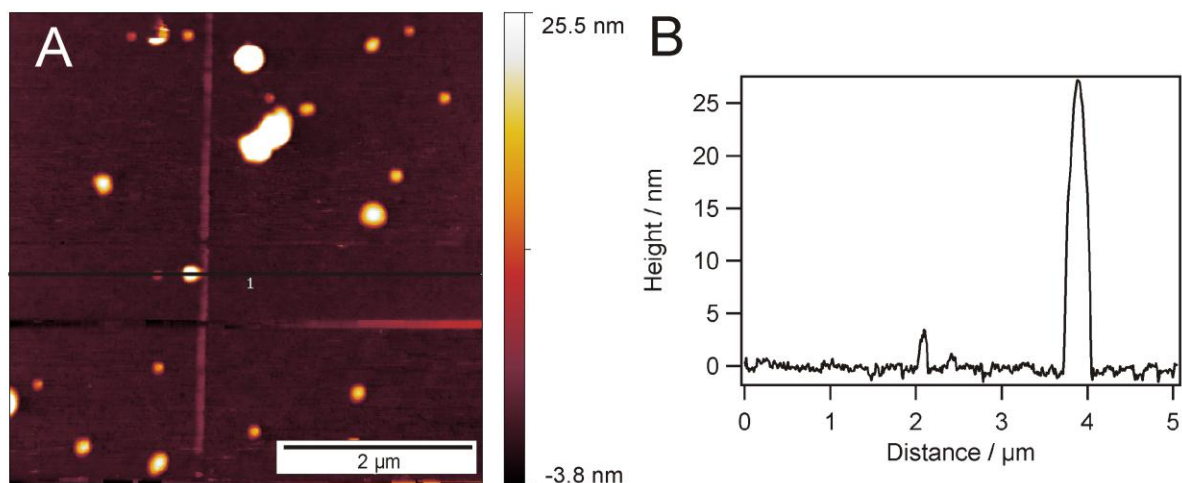


Figure 15: AFM image of OH-functionalized vesicles on hydrophobic support and the corresponding height profile along the indicated line.

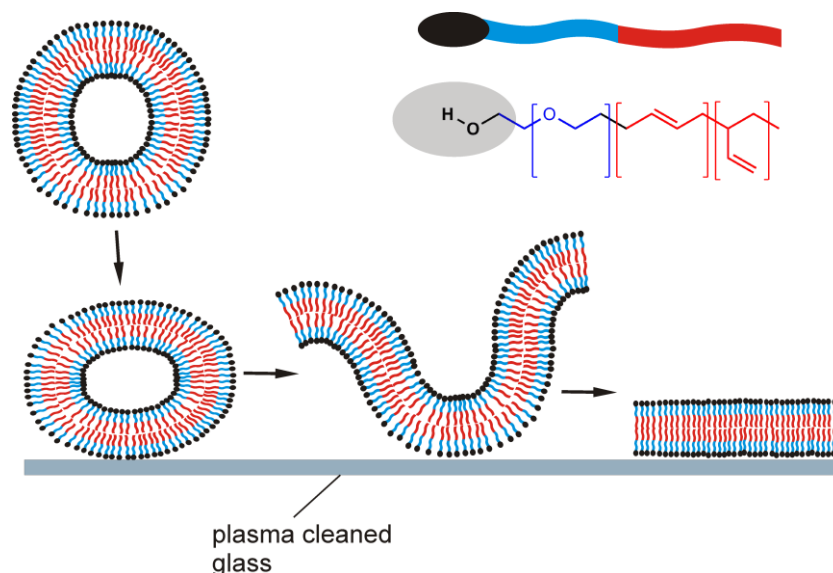
In some cases the tendency of vesicles to spread on a surface can be increased by exerting an osmotic pressure. This is done by dissolving a high concentration of salt in the vesicle suspension directly before application to the substrate. In the case discussed here the addition of salt showed no effect on the adsorption density as could be seen by AFM (not shown).

It can be concluded that the hydrophobic interactions of the polymer vesicles with the hydrophilic support are not strong enough to spread them on the surface. Even the additional destabilisation by applying an osmotic pressure was not sufficient for vesicle fusion.

4.3.2. Vesicles on Hydrophilic Support

To produce planar polymer bilayers on a transparent support and at the same time compare the above studies to bilayer formation on a hydrophilic support, the same kind of vesicles (PB-PEO hydroxyl terminated) was also applied to highly hydrophilic glass slides which were treated with oxygen plasma (Scheme 18). After the plasma treatment the surface bears mainly negatively charged oxygen which is transformed into hydroxyl groups upon contact with water. The exposed OH-groups lead to complete surface wetting upon addition of a water droplet so that no contact angle measurement is possible. Again different vesicle dilutions and

salt concentrations were tested on the surface and the resulting topography was checked with AFM imaging. Best results were obtained for the undiluted vesicle suspension. The vesicles in ultrapure water were mixed with solid sodium chloride to yield a final concentration of 1.5 M directly before addition to the surface.



Scheme 18: Proposed vesicle adsorption and subsequent spreading of hydroxyl functionalised vesicle on glass support.

The result after incubation can be seen in Figure 16. A lot of flat patches with a typical height of ~15 nm can be measured in the section along the indicated line. In cases where a second bilayer is laying on top of the first one the layer thickness of these patches is about the same. One thing has to be kept in mind when the thickness of such soft structures is measured. The hydrophilic polyethylenoxide block of the polymer is highly hydrated. This makes the brush-like structure very soft and flexible so that it cannot be fully detected by the cantilever. The AFM tip partly compresses and protrudes this flexible PEO-layer and therefore the bilayers appear thinner than they actually are.

In the lower part of Figure 16 A an extended patch of around $1 \mu\text{m}^2$ can be seen. In contrast to spreading on hydrophobic support here the vesicles showed higher tendencies to spread on glass when NaCl (1.5 M) was added directly before the experiment instead of adding the pure suspension in water. It also has to be mentioned that there are only very few adsorbed vesicles on the surface. The ones which attach to the surface seem to instantaneously spread to form bilayer patches. This suggests that an even higher surface coverage can be achieved if there are more vesicles available in suspension and on the surface. The patches resulting from vesicle spreading keep their round form and stay mostly separate. Apparently the mobility of chains within such a patch is very low so that there is no tendency to fuse with neighbouring

patches. Unfortunately it is not possible to produce vesicle suspensions with a much higher concentration because sometimes this leads to uncontrolled precipitation of material.

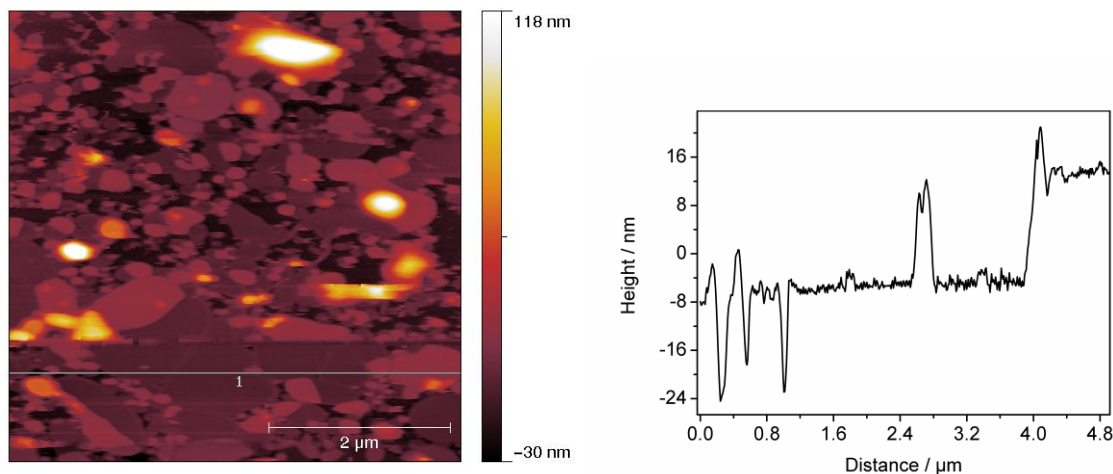


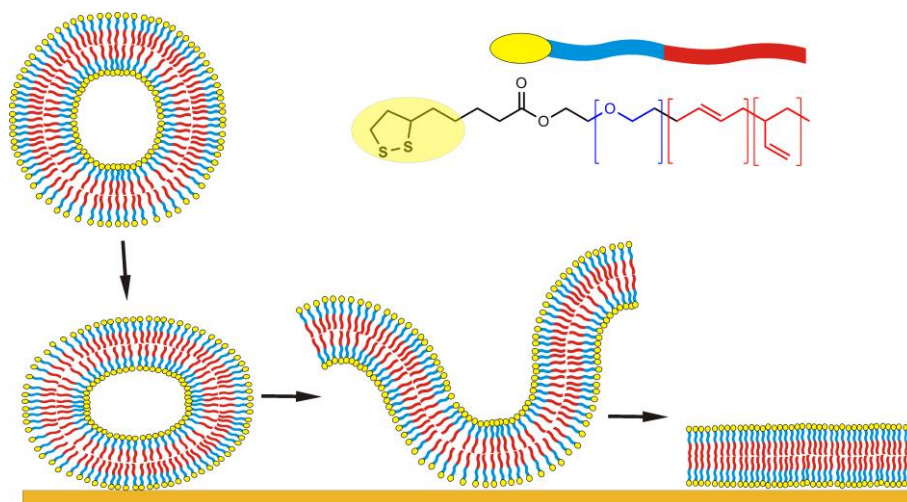
Figure 16: AFM image A) non-extruded vesicles on plasma cleaned glass, 45 mg NaCl were added to the vesicle solution immediately before the addition to the surface. B) The measured layer thickness of the first bilayer from the section is 15.7 nm.

The bilayer system on glass resists extensive rinsing with ultrapure water and phosphate buffer (PBS). As shown in the AFM image in Figure 16 the surface coverage is high but not complete. It would be desirable to use the planar polymer layers on a transparent support for fluorescence microscopy studies of biomolecules. Unfortunately many proteins have a very high affinity to bind unspecifically to glass. In order to make the incomplete surface architecture suitable for studies of biomolecules (e.g. proteins) the uncovered areas on the glass have to be passivated. A common route to block surfaces for unspecific adsorption is to incubate with bovine serum albumin (BSA) because it has a high affinity to glass and at the same time prevents sticking of other proteins.^[130] The addition of 100 μL of a 6% BSA solution to 500 μL of sample volume after successful vesicle spreading did not change the adsorbed polymer layer but it seems that a small amount of protein precipitates and forms bigger aggregates of ~100 nm. They can be easily removed by rinsing. No adsorption of BSA on top of the bilayer structures was observed in the AFM image (not shown). Due to the low amount of unspecifically adsorbed protein this polymer bilayer on transparent support should prove to be useful for interaction studies of the amphiphilic block copolymer with biological species via fluorescence measurements.

4.3.3. Vesicle Spreading on Gold through Covalent Interactions

Next, the question was addressed if the vesicle spreading on the surface can further be enhanced by changing the interactions between polymer vesicles and the surface from purely hydrophobic/hydrophilic to covalent ones which should be significantly stronger.

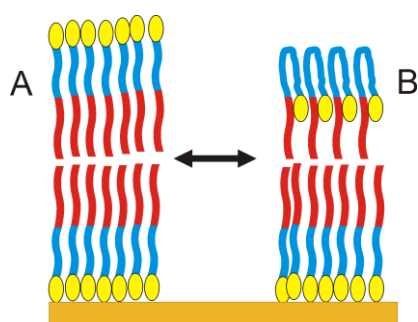
Therefore a covalent coupling approach will be presented to completely tether the resulting bilayer to the surface as seen in Scheme 19. For this route a polymer functionalised with a lipoic acid end group (depicted in yellow) on the hydrophilic block is used to form small unilamellar polymer vesicles. The strong interactions of thiol groups with gold makes the vesicles attach on the substrate and subsequently force them to spread. First the polymer suspension is added directly to a freshly cleaved ultrasmooth gold surface without any further treatment.



Scheme 19: Schematic representation of the proposed polymer vesicle fusion mechanism on gold.

From the AFM image in Figure 17 A it can be seen that already a significant area of the surface is covered with vesicles which directly spread on the gold surface. Because single round patches which correspond to one vesicle are visible this means that vesicles individually fuse on the surface and do not need to adhere in a critical concentration before they can spread. Fusion of single vesicles to the surface was also observed at lower concentrations and resulted in free standing round patches of several hundred nanometres in diameter. The height of the patches was measured to be 11-12 nm which can also be seen in the height profile in Figure 17 B. The measured thickness is about 3 nm lower than for the measured thickness of PB-PEO-OH bilayer patches on glass. The polymer chains for covalent and non-covalent polymer bilayers are exactly the same. Only in the covalent case the head group of the PEO block was modified with a lipoic acid endgroup. This end group has only a

very limited possibility to form hydrogen bonds with water. Two conceivable conformations of the polymer head group of the top layer are shown in Scheme 20. In the first case the end group is pointing towards the surface (A) while in the other case the lipoic acid head can be buried in or close to the hydrophobic core. The second scenario would result in a lower film thickness. The bottom layer has no ability to change conformations because all chains are tethered to the surface. Although the end group of the polymer is small compared to the full chain it seems to play an important role in determining the overall chain conformation. Maskos made a similar observation, when he looked at the phase behaviour PB-PEO block copolymers with different end groups. By changing the chain end from a hydroxyl group to carboxyl group different morphologies in a selective solvent were observed.^[131]



Scheme 20: Two possible configuration of the lipoic acid functionalized polymer in the top layer of the structure. The stretched case is depicted in (A) while the coiled conformation is illustrated in (B).

The patches themselves are as smooth as the underlying gold surface and have a mean surface roughness of 0.4 nm (RMS). In addition to the patches there are also vesicles present which adsorb on top of the present bilayer structures. Almost no large vesicles can be observed which are adsorbed directly to the gold without fusion with the surface so that it can be concluded that they all burst upon contact to gold. In order to increase surface coverage, different parameters were changed to force vesicles to spread.

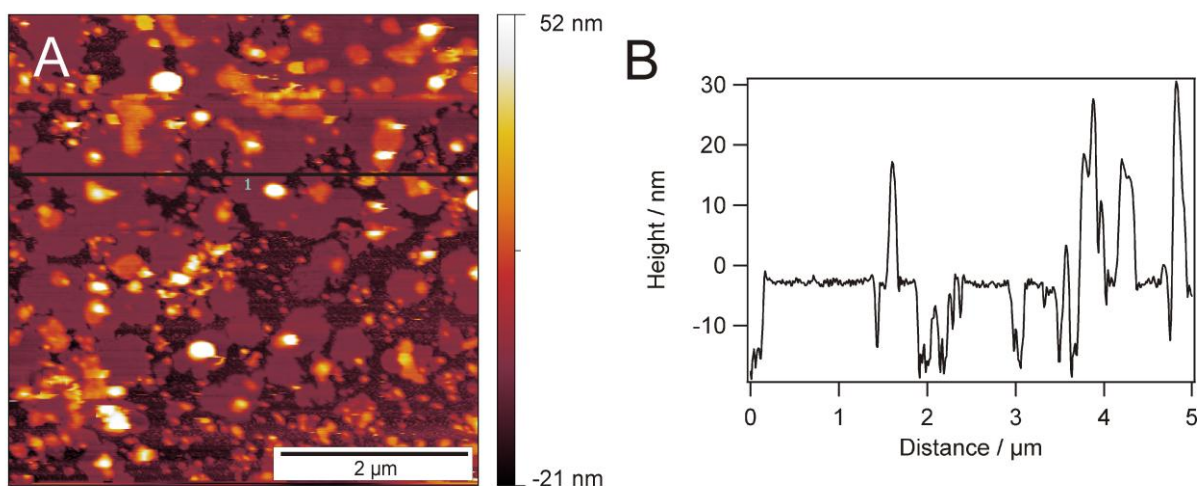


Figure 17: AFM image of a pure vesicle suspension added to a fresh gold surface (A) and the corresponding height profile along the indicated line (B).

The vesicles themselves were prepared in water. To further increase the surface coverage by exerting osmotic pressure on the vesicles, salt was added to the vesicle solution before application to the surface to yield respective concentrations of 0.3 M and 1.5 M in the suspension. After that the samples are directly added to the gold substrate. The effect of the increased osmotic pressure is clearly visible in Figure 18 A and B. While in Figure 18 A there are still gaps between vesicle patches in Figure 18 B it can be seen that the bilayer patches fuse and really form an extended bilayer film. Again the height of the first bilayer on gold is measured to be around 12 nm at defect sites. If one looks closer there are still some grooves visible where adjacent vesicles spread next to each other but do not fully fuse. The fact that the top layer chains cannot close these gaps is a sign for their rather low fluidity of the system. In comparison a lipid system would easily close these gaps. The larger hole at the top right of Figure 18 B most likely originates from impurities in the gold film because not even small aggregates can bind there. Since surface coverage is high everywhere around that region it seems that there are simply no binding sites for the sulphur functionalities in the polymer.

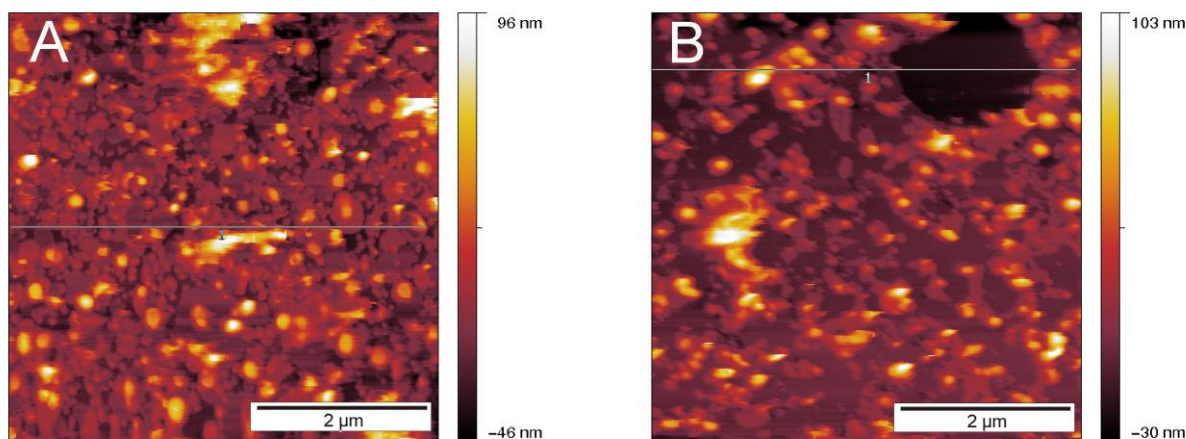


Figure 18: AFM image of vesicles spread on a gold surface at two different salt concentrations. (A) 0.3 M NaCl (B) 1.5 M NaCl.

The glass transition temperature (T_g) of 1,2-poly-butadiene in bulk is relatively high and lies between -28°C ^[132] and 0°C ^[133] depending on the tacticity for bulk materials. For comparison, the T_g of polydimethylsiloxane (PDMS) is about -128°C . These bulk values are certainly not directly transferable to thin films of one single PB-layer since it was shown that film thickness has a significant effect on T_g ^[134] but they give a rough idea about the chain flexibility. The resulting membrane strength which was already confirmed experimentally by Discher and co-workers^[55] is a consequence of the high chain rigidity. On the other hand the increased stability hampers fast and complete vesicle spreading on the surface because the lower mobility reduces the capability to heal small voids between adjacent patches.

In order to further drive the system towards full surface coverage, the vesicle fusion is done in an incubation oven at 45°C again in the presence of 1.5 M NaCl. This increases the fluidity of the membrane, destabilizes it and facilitates the spreading of vesicles. The resulting architecture is shown in Figure 19. Best results were obtained when the vesicle-salt suspension was added to the gold substrate at room temperature and kept for one hour before it was heated for one hour. In the first step vesicles can adsorb on the surface. Once adsorption has taken place the vesicles are destabilized by the mild heating and forced to fuse. Application of heat directly after addition resulted in significantly lower coverage. The resulting bilayer shows hardly any defects anymore but still a lot of loose material is adsorbed on top of the first bilayer. First it was tried to remove the material by strong rinsing with respective salt solution and with ultrapure water but this showed no effect.

In a next step the sample was blown dry under a stream of nitrogen for approximately 20 sec and consecutively rehydrated for the AFM measurement shown in Figure 19. The quick dehydration procedure removes most of the adsorbed material in the form of vesicles or other

aggregates but leaves the bilayer unchanged. Bilayer patches which lie on the first layer (yellow islands in Figure 19 A) cannot be removed by this treatment. The fact that the architecture can stand a relatively harsh drying procedure without detectable alterations is a sign for the increased membrane stability. A lipid system would fully disassemble if subjected to the same kind of experiment. Furthermore the bilayer structure was stored over 14 days in water and no change in bilayer morphology was detectable by AFM imaging.

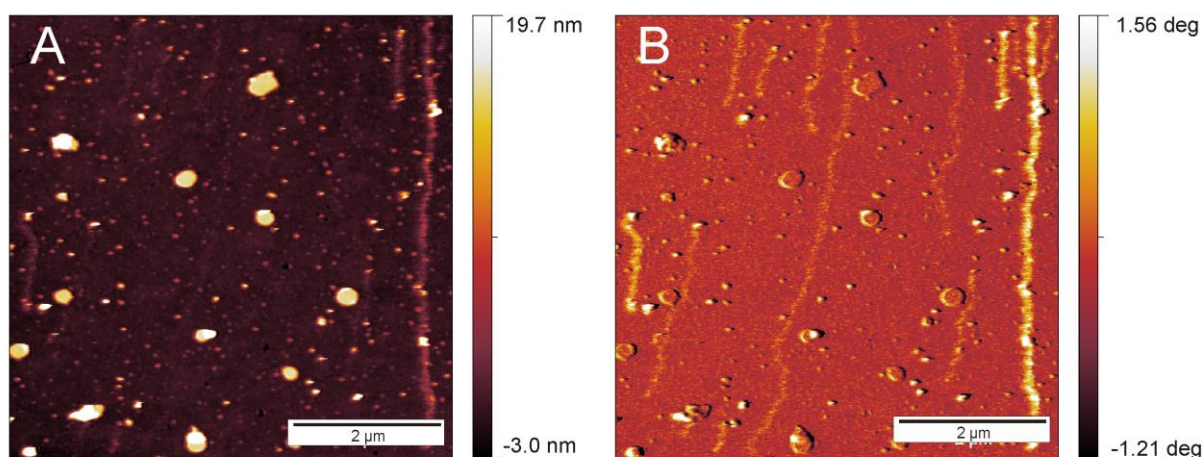


Figure 19: AFM image of vesicles fused on the surface at 45°C at a salt concentration of 1.5 M (A) and the corresponding phase image (B).

In Figure 19 B the phase image shows no phase contrast between the background and the adsorbed islands. This implies that the area between the scattered islands consists of a complete polymer film.

To further validate that the architecture really consists of two individual membrane sheets, the surface has been rinsed with THF which is an effective solvent for the polymer and investigated with AFM after rehydration. The solvent should selectively remove the top layer which is only coupled through hydrophobic interactions. In Figure 20 A one can see that the underlying polymer layer is not defect free. The layer depth of the defects as measured by AFM is about 6 nm which corresponds well to the thickness of one monolayer as already observed in the previous chapter on Langmuir-Blodgett films.^[116]

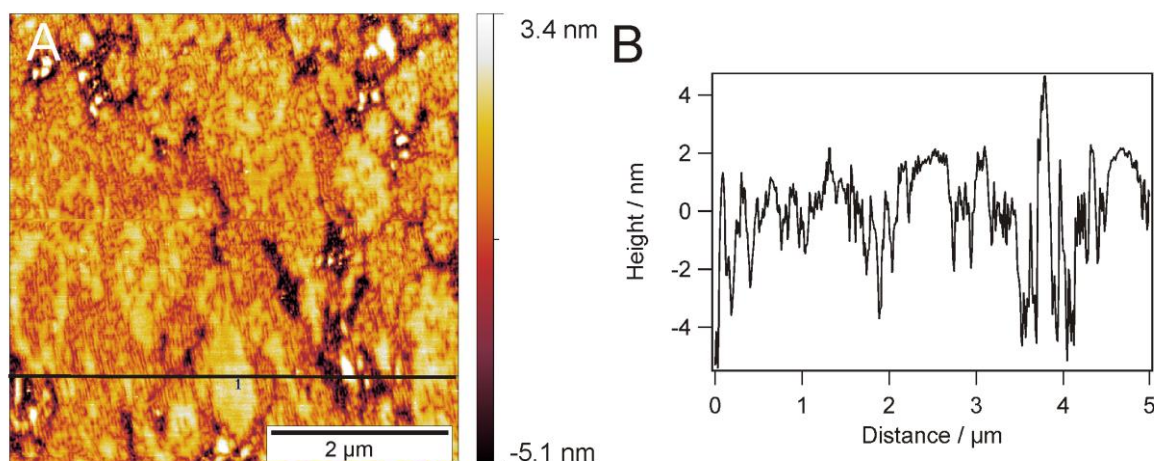


Figure 20: AFM image of the sample rinsed with THF. Section shows layer thickness at defect sites of approximately 6 nm.

Interesting are the numerous wormlike channels inside the layer in Figure 20. These morphologies are not visible in an intact bilayer. Since the functionalisation of the PB-PEO block copolymer with the lipoic acid end group only reaches about 80%, there are still many OH-terminated chains present which cannot covalently bind to gold. The branched structures point towards a phase separation of the two polymer species with different end groups. Similar branched structures are known for the phase separation of lipids^[135] A phase separation between the two PBPEO species would not come as a surprise because Maskos could show in a work on PB-PEO block copolymer that the same polymer adopts different morphologies depending on small changes in the chemistry of the headgroup.^[131] The same channel morphology as seen in Figure 20 but twice as high also appears, when a readily prepared bilayer is heated for times of 12 h or longer as can be observed in Figure 21 B. This can be explained by non-anchored chains in both bilayer sheets which can change their conformation to a more favoured state or detach from the surface. It is remarkable that this channel morphology seems to be a more general property of the used polymer because it also appears in Langmuir films (Figure 21 A) which are described in more detail in chapter 3.

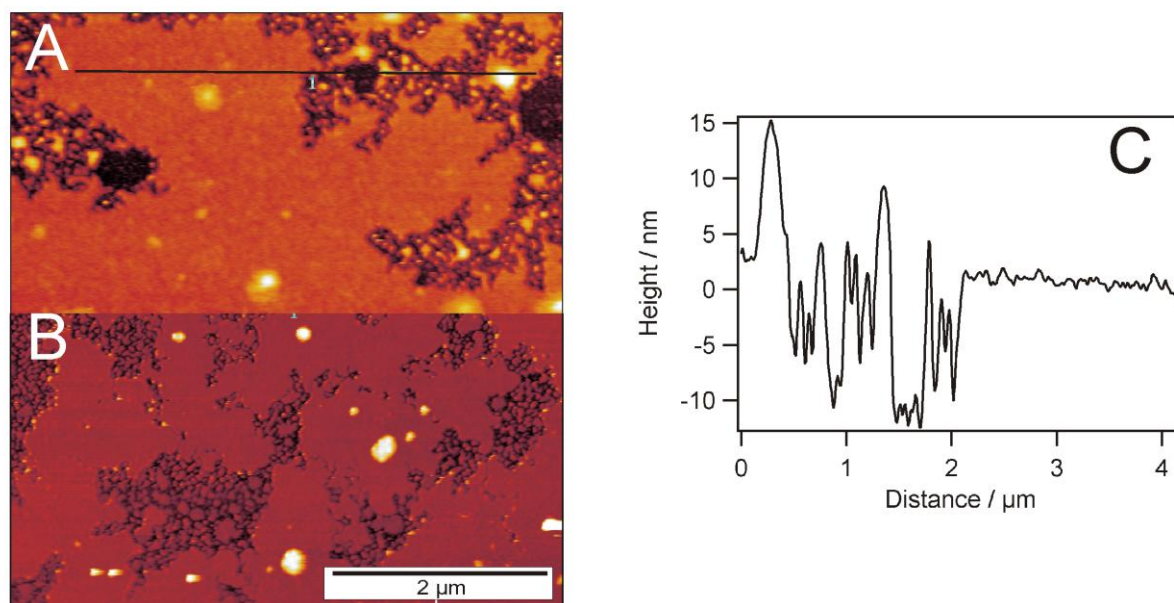


Figure 21: In (A) a polymer bilayer prepared via Langmuir-Blodgett techniques (see chapter 3) is shown after mild heating, and the corresponding height profile (C) which indicates layer thicknesses of around 12 nm. The bilayer architecture prepared by vesicle fusion after heating to 45°C for 12 h is shown in (B).

In addition to the height images, force-distance curves provide information about the mechanical properties. Since structures, such as the ones presented here, have not been reported so far, there are no literature references to compare with. However, a lot is known about force measurements on supported lipid bilayers.^[110] By repeatedly approaching and retracting the cantilever from the surface, adhesive and repulsive forces, as well as structural details along the z -direction (perpendicular to the surface) can be obtained. Since the cantilever was not calibrated and the nominal spring constant was taken for scaling, it was not possible to determine absolute force values from these measurements. However, a qualitative statement can be made. All force measurements were performed with a bare oxide sharpened silicon nitride AFM tip, known to be hydrophilic. In Figure 22 A a force distance curve on a polymer monolayer prepared by rinsing the bilayer structure with THF (Figure 20) is shown. For an intact monolayer one does not expect any characteristic features in the approach and retract curve since the covalently bound polymer chains have only very limited ability to reorganise upon perturbation by the cantilever. Also the hydrophilic cantilever should be repelled from the hydrophobic surface. This repulsion of the tip from the surface can be seen in the approach curve in Figure 22 A. Unexpectedly the adhesion force upon retraction from the monolayer is quite high. A possible explanation for this observation is that the cantilever protrudes the monolayer upon increasing force and interacts with the underlying hydrophilic PEO block facing to the gold surface. Additionally there could be some un-anchored chains

with an OH-terminus left which were not washed away by the organic solvent. These unbound chains can then be detached from the monolayer by the tip.

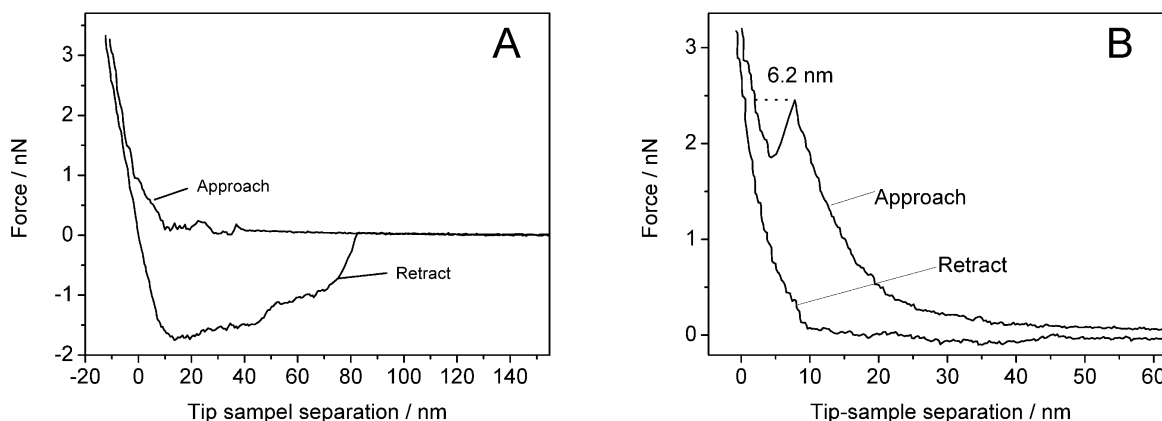


Figure 22: Force-distance measured on the monolayer after rinsing the surface with THF (A) and on the intact bilayer (B).

The bilayer situation is shown in Figure 22 B. This curve was recorded on the architecture shown in Figure 19. The molecules of the top layer tend to reorganise when the tip penetrates the surface. Since there is a lateral pressure within the membrane plane that has to be overcome, a rise of the force curve can be observed at the beginning. At a certain point, the applied force is high enough to overcome the lateral pressure so that the cantilever snaps into the bilayer, which can be seen at a distance below 20 nm where the force temporarily decreases until the lower part of the substrate is reached. This step is characteristic for supported bilayers and has been observed for various lipid bilayer systems.^[110] Importantly the step in the force-distance curve appears even after several approach-retract cycles which shows that the membrane is mobile enough to cure the small hole indented by the cantilever. The width of the step corresponds to approximately 6 nm, which is the thickness of one polymer bilayer sheet. This corresponds well to the values measured in chapter 3.

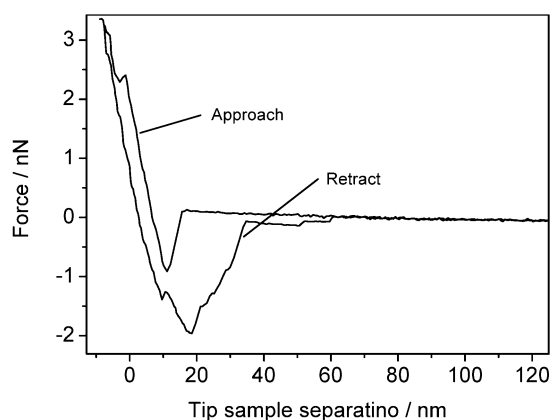


Figure 23: Force-distance curve recorded on a bilayer after about 10 approach-retract cycles.

If the cantilever is kept at one position for more than approximately 10 approach-retract cycles the created indentation cannot cure anymore (Figure 23). This is seen as a small dip in the approaching curve at around 10 nm. The area enclosed by the retract-curve indicates a significant adhesion force. This could be the result from polymer chains that are not covalently anchored to the gold film and can stick to the AFM-tip.

SPR measurement of the layer thickness. SPR spectroscopy provides a complementary method to AFM for film thickness determination. The angle scan after vesicle fusion and rinsing (Figure 24 (□)) shows a strong shift in the plasmon resonance signal compared to the blank slide (●). By fitting the data to a four-layer model based on Fresnel-equations a layer thickness of 13.7 nm was obtained for an assumed refractive index of $n = 1.5$ for the polymer. This value is slightly higher than the value measured above by AFM (11 -12 nm) but still falls in the range measured by AFM.

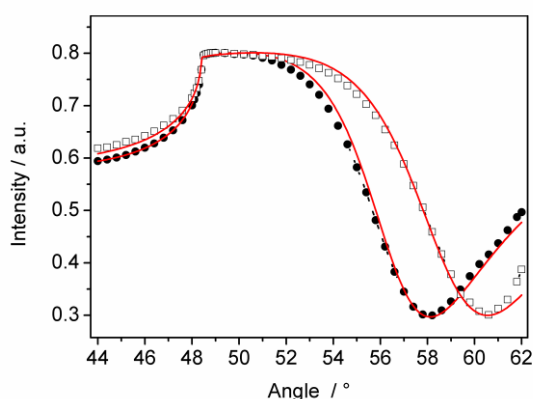


Figure 24: SPR measurements: Angle scan before (●) and after the adsorption process (□) The red lines indicate the fit values. ($\epsilon_{\text{glass}}=3.404$, $d_{\text{gold}}= 32.76$ nm, $\epsilon_{\text{gold}}=-13.55+i0.93$, $d_{\text{poly}}= 13.7$ nm, $\epsilon_{\text{real salt}}=1.81$)

The discrepancy between SPR and AFM measurement can have several explanations. First the cantilever partly protrudes the soft, hydrated PEO layer facing the solution so that AFM measurements tend to underestimate the real thickness value. Additionally the SPR measurement most likely shows an increased thickness because not all of the adsorbed material on top of the first layer is rinsed off in the SPR flow cell configuration. Since SPR is sensitive to mass adsorption within 200 nm above the surface intact vesicles or adsorbed bilayer patches are also detected and result in a slightly higher thickness value.

To follow the kinetics of the spreading process, a vesicle suspension was given in a SPR liquid cell and the signal change during adsorption process was monitored over time at a

constant angle (Figure 25). The kinetic curve shows a steep increase in signal in the first 1 h. After about 3 h the vesicle fusion process is complete. During the rinsing process no significant amount of material gets washed away.

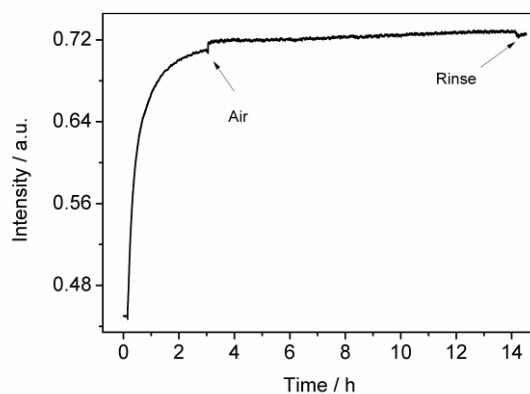


Figure 25: SPR kinetic measurement recorded at a constant angle. The small step in the curve at around 4 h stems from an air bubble which had to be removed by gently shaking the cell.

Electrochemical characterization. Since the polymer bilayers created on gold form stable and homogeneous bilayers this offers the possibility to measure electrochemical properties of this system. Unfortunately it was not possible to measure electrochemical impedance spectroscopy at the high salt concentrations used for optimal vesicle spreading presented in this chapter. Although there was an obvious surface coverage visible in AFM the resistance did not change at all upon addition of the vesicle solution. A reason for that could be that the high electrolyte concentration leads to charge transport going mainly through the defects but not across the polymer bilayer. Instead of the 1.5 M solution the vesicle suspension was mixed with an equal amount of phosphate buffer containing 0.14 M NaCl. This still produces a high surface coverage comparable to the procedure at higher NaCl concentration as can be seen in the AFM-image in Figure 26.

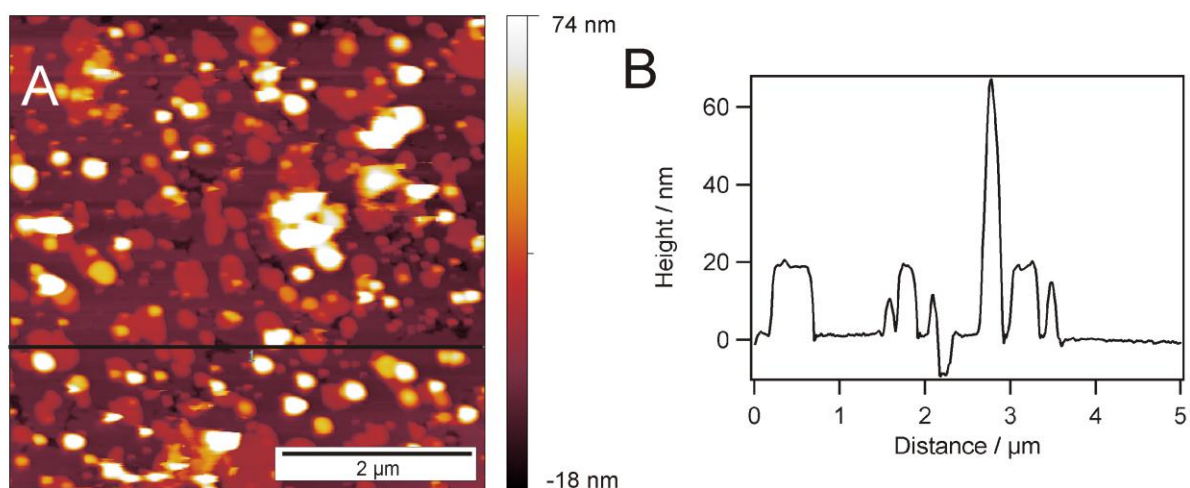


Figure 26: AFM of a polymer bilayer after vesicle fusion diluted in PBS (50:50) and the corresponding height profile. The measured thickness at the defect is 10.8 nm.

By measuring EIS-spectra in 30 to 60 min time steps over the course of 14 h a kinetic curve was recorded which is presented in Figure 27. Quantitative values for the resistance and the capacitance were obtained by fitting the data to the equivalent circuit depicted in Figure 27 B.

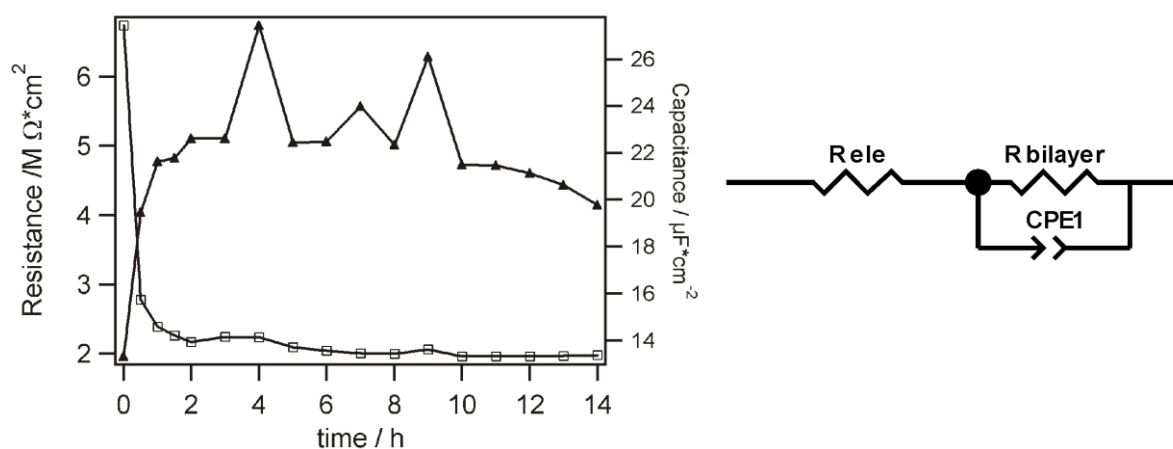


Figure 27: Plot of the fitted resistances (\blacktriangle) and capacitances (\square) for the vesicle fusion process.

The kinetic curve shows that the vesicle fusion process is completed to a degree of 75% after 20 min. After two hours the capacitance which can be related to the amount of material attached to the gold electrode has reached its final value. Qualitatively the kinetics of the EIS measurement shows the same time dependence as in the SPR curve in Figure 25. The resistance of the final architecture goes up to 4-5 $\text{M}\Omega\cdot\text{cm}^2$ while capacitance drops from above 26 $\mu\text{F}/\text{cm}^2$ to 12 $\mu\text{F}/\text{cm}^2$. The resistance needs about 3 h to stabilize and almost reaches the value for a complete lipid bilayer (1-20 $\text{M}\Omega\cdot\text{cm}^2$). The capacitance is higher than the

typical lipid values of $0.8 \mu\text{F}\cdot\text{cm}^{-2}$. One reason for the comparatively high capacitance values can be the low packing density of the hydrophobic block which exists in a mostly coiled conformation but not in a fluid crystalline phase like lipids do. Another factor contributing to the low density is the high degree of hydration of the polyethyleneoxide. This low density due to the two factors is expressed as a low electrical permittivity ϵ which contributes to the capacitance C according to Equation 19

$$C = \frac{\epsilon\epsilon_0 A}{d}$$

Equation 19

Since the absolute values for ϵ are not known it is not possible to calculate layer thicknesses from the measured data.

4.3.4. Interactions of Proteins and Peptides with the Supported Polymer Bilayer

Since it is possible to produce stable polymer bilayers resembling the defined hydrophilic-hydrophobic-hydrophilic structure of lipid bilayers on areas of several square millimetres it is now interesting to test the biocompatibility of this system. The polymer based architectures shown here have several features which are different from natural membrane components and it is interesting to see what influence they have on biological molecules like proteins and peptides. Firstly there is an influence of the increased thickness of the hydrophobic core on the incorporation of transmembrane proteins which has been addressed before theoretically^[62] and experimentally.^[58] Another aspect which also has a big effect on protein-bilayer interactions is the charge distribution. Some membrane forming lipids do not carry an overall charge but still they are zwitterionic like e.g. phosphatidylcholine. In contrast to that the bilayer structures presented here consist of completely neutral components. Therefore it is interesting to see if biological relevant species are able to interact with an uncharged, amphiphilic polymer film.

An additional important aspect is the fluidity in 2D. All studies of proteins in literature so far were done either in vesicular systems or in free standing bilayers so that unhindered diffusion of polymer chains is possible.^[93] The aspect of polymer diffusion will be discussed in more detail in chapter 5. For the newly developed supported polymer bilayers diffusion is strongly hindered. The bottom layer is completely immobilized since it is tethered to the gold support.

Scratching experiments in chapter 3 as well as force distance measurements showed that the ability of the top layer to close intentionally created defects is very limited. This rigidity is certainly disadvantageous to incorporate proteins after the bilayer preparation.

The surface preparation for testing the interactions of the bilayer with polymyxin B was carried out directly in the EIS sample cell. The data representation in the Bode-plot as well as in the admittance plot is shown in Figure 28 A and B. The full squares show the measured data points and the blue lines indicate the fitted values. The relatively high membrane resistance of about $4.4 \Omega \cdot \text{cm}^2$ which can be extracted from fitting of the EIS curve (Figure 28 C) to the equivalent circuit depicted in Figure 28 D shows the successful bilayer formation. The plateau of the phase angle at around 83° is an indication for high homogeneity of the surface architecture. The pure bilayer structure was monitored over 14 h and showed no changes. This is of importance to be able to detect even small changes in the membrane configuration.

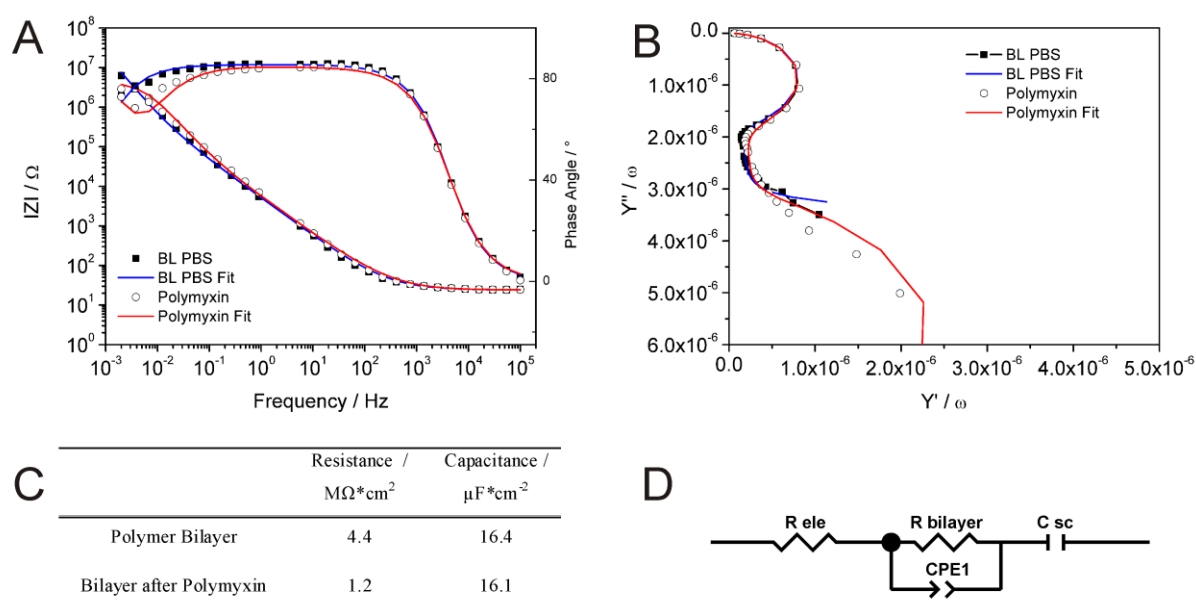


Figure 28: EIS Results from the addition of polymyxin to a polymeric bilayer. Data representation in the Bode plot (A) and in the admittance plot (B). The fitting results are displayed in table (C) and the equivalent circuit used for fitting is shown in (D).

It was reported that transient defects are only created by that peptide at a high local concentration.^[136] To reach a peptide concentration that causes a visible effect on the bilayer in impedance spectra a concentration of 0.1 mg/mL was chosen. Therefore the volume in the cell was reduced to about 200 μL of PBS to which 20 μL of the polymyxin B solution

(1mg/mL in water) were added. Following incubation the cell was rinsed with PBS and EIS spectra were directly measured. The data points after polymyxin B addition are depicted as open circles and the red lines represent the fitted values. In Figure 28 A a clear decrease in the membrane resistance from $4.4 \text{ M}\cdot\Omega\cdot\text{cm}^2$ to $1.2 \text{ M}\cdot\Omega\cdot\text{cm}^2$ can be observed. This reduction of electrochemical sealing by a factor of 3.7 is a clear sign for the creation of additional pathways for charge carriers to travel across the membrane. Polymyxin B was incubated on the surface for 15 to 60 min respectively but no difference was detectable between the long and the short incubation time indicating an immediate effect of the peptide on the bilayer. While a significant change in resistance is obtained, the capacitance stays constantly at around $16 \mu\text{F}\cdot\text{cm}^{-2}$ during the course of the whole experiment. This means that there is no change in the amount of material on the surface or a significant change in polymer packing density. It has to be noted that impedance measurements of the bilayer 7 h after the peptide addition returned to the values before addition. This suggests that polymyxin B does not form a stable transmembrane pore but rather acts in a detergent like fashion. It instantaneously dissolves some of the membrane constituting polymer chains which creates transient defects as was reported in literature for lipid membranes.^[136] With time the holes can then heal so that the curve returns to its initial values. Due to the low polymer mobility within the 2D architecture this process of closing the gaps takes much longer than in a completely fluid film. Another explanation for the recovery of the membrane resistance to a higher value would be that polymyxin B only temporarily binds to the bilayer structure at high concentrations to destabilize it but by diluting the sample with PBS the peptide is washed out again. This hypothesis is supported by a report from Morrison *et al.* that demonstrated that binding of polymyxin B to lipids is reversible^[137] so that there is an equilibrium between membrane bound and unbound species. By dilution the equilibrium would be shifted towards freely dissolved species. To distinguish the two possible cases further investigations of the peptide concentration in solution and on the surface are necessary. The control experiment where only 20 μL of ultrapure water without peptide was applied to the surface showed no change in the EIS spectra at all.

In the experiments with α -haemolysin the layer assembly was carried out outside the EIS sample cell and was first checked by AFM. Then the sample slide was consecutively clamped into the electrochemical sample cell while keeping the surface constantly immersed in water. To check the stability of the layered architecture itself again a time series of spectra was taken over 14 h as a background measurement. Neither resistance nor capacitance changed during

the experiment which means that the system is not susceptible to drift through rearrangement or desorption of material. The final curve of that series is shown in Figure 29 A. Fitting of the curve to the model in Figure 29 C resulted in a resistance of $R_{BL}=1.6 \text{ M}\cdot\Omega\cdot\text{cm}^2$ and a capacitance of $C_{BL}=16.2 \text{ }\mu\text{F}\cdot\text{cm}^{-2}$. The lower bilayer resistance compared to Figure 28 most likely stems from the fact that the surface was prepared externally. By clamping the EIS cell to the slide defects are generated along the O-ring. The drift in the phase angle in Figure 29 A indicates a lower bilayer homogeneity than for the polymyxin experiment.

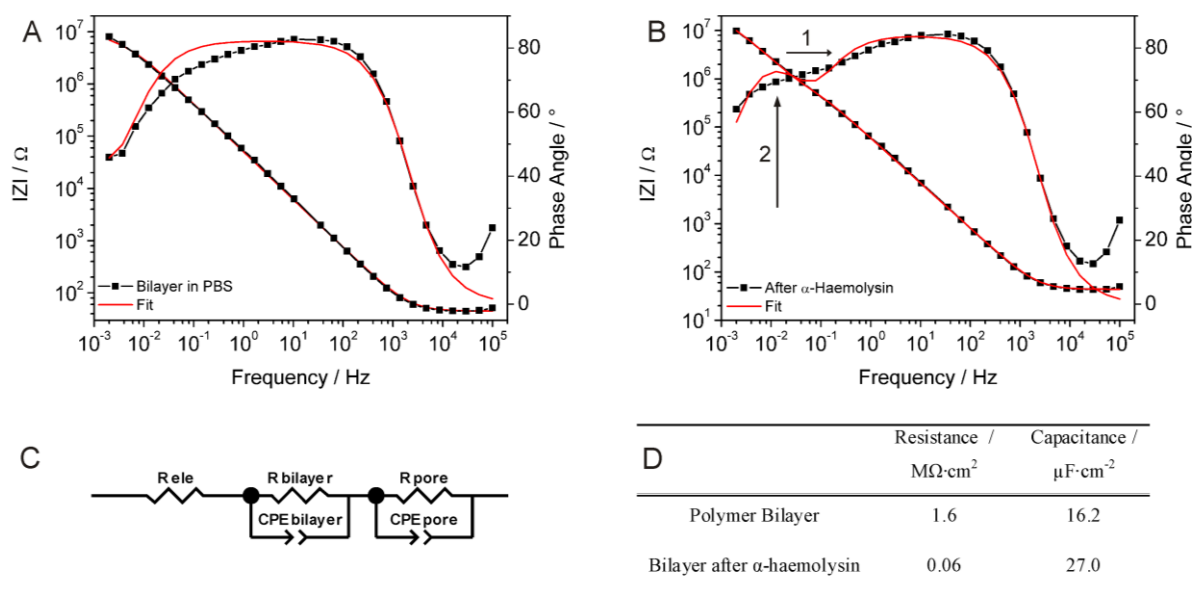


Figure 29: Impedance data in the Bode plot and fitted curves (red) for measurements before (A) and 10 h after addition of α -haemolysin(B). Spectra were fitted to the equivalent circuit depicted in (C) and the obtained fit results are summarized in (D).

After α -haemolysin addition there are two processes visible in the measurement curve (Figure 29 B). First the bilayer resistance R_{BL} decreases from 1.6 to $0.06 \text{ M}\Omega\cdot\text{cm}^2$ which is a decrease by a factor of 26. This is indicated as arrow 1. It has to be noted that the fitted curve does not resemble measured values very well so that the absolute values should be handled with care. Nevertheless the qualitative difference between the two measured curves is apparent. Apart from this decrease in R_{BL} slowly a second time component can be identified as a shoulder in the Bode Plot at frequencies around 10^{-2} Hz which is indicated by arrow 2. This can be attributed to pores or bilayer perturbations induced by α -haemolysin where fast ion conductance takes place. For the α -Haemolysin to be fully functional it has to assemble into a heptameric aggregate. This assembly happens on the surface of the membrane and results in a cylindrical pore with a diameter of 2.6 nm. As mentioned in the beginning of this section the

membrane fluidity of the supported polymer bilayers is very low so that it will be hard for a comparably big protein to fully insert. From the EIS spectra one cannot tell whether the α -haemolysin completely inserts in the bilayer. What can be concluded is that α -haemolysin definitely interacts with the membrane architecture. It remains unclear if the effect on bilayer resistance is caused by the monomeric or the heptameric form. The capacitance also changes to a higher value which means that the surface structure is less dense. This is in accordance with a perturbation of the bilayer by the α -haemolysin.

To compare the effect of α -haemolysin in lipid and polymer bilayers impedance spectra were recorded on a tethered lipid bilayer described in more detail in literature.^[138] In short the architecture consists of an anchoring thiolipid called DPTL which self assembles on gold to form a dense lipid layer with a reservoir below. To complete the bilayer small unilamellar vesicles of diphytanoylphosphatidylcholine (DiPhyPC) are fused on top of this hydrophobic layer. After successful bilayer preparation α -haemolysin is directly added to the measurement cell (vol. 1 mL) as a small aliquot of 20 μ L. In Figure 30 A one can see how the bilayer resistance decreases (red curve) while the capacitance stays on the same value (Figure 30 B). Spectra were recorded directly before and after the addition of α -haemolysin. This shows how quick the insertion process is in a lipid system compared to the supported polymer bilayer.

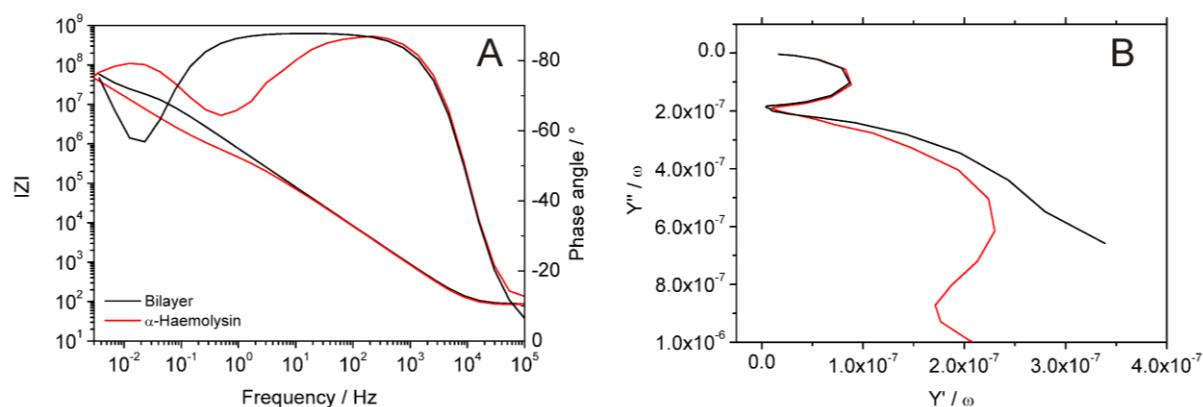


Figure 30: EIS Spectra of tethered bilayer lipid membrane before (black line) and after addition of α -HL (red line). (A) Bode plot (B) Admittance plot.

The comparison of the EIS-measurements in polymer system (Figure 29) and a lipid system (Figure 30) demonstrates that the effect of the α -haemolysin is very small in the polymer case. This can have several reasons. First the polymer layer is not defect free which leads to competing processes how charges can travel through the bilayer even without additional pores. Secondly the hydrophobic core of the polymer membrane is roughly a factor of two

thicker than a lipid bilayer. This results in a mismatch in hydrophobic length because proteins were optimized by nature for the cell membrane. This will reduce the driving force for the protein to incorporate in the membrane because a hydrophilic part of the has to . It is possible that the protein pore does not go into the membrane but still attaches or partly incorporates into the outer bilayer sheet which causes a perturbation detectable by EIS.

The interactions of the bilayer with alamethicin were also tested but did not shown any effect in the impedance spectra even after incubation over night. This is surprising since it was reported that it spontaneously incorporates into giant vesicles made from block-polyethylene-block-polyethyleneoxide (PEE-PEO).^[61] A possible explanation for the deviating observations could be the difference in PEO-head group, the slight chemical differences in the hydrophobic block and the reduced mobility of the planar architecture compared to vesicles.

4.4. Summary & Conclusion

In this chapter different approaches were presented to prepare supported bilayers from amphiphilic block copolymer through vesicle spreading. This can be induced through different interactions with the underlying support. The successful preparation of large scale supported polymer bilayers by vesicle spreading was achieved by a covalent coupling procedure of sulphur functionalized polymer on a gold surface. Under exertion of osmotic pressure and at high vesicle concentration, a full surface coverage was achieved. Due to sticking of vesicles or aggregates the structures are not as homogenous and smooth as the structures prepared via Langmuir techniques but they are much easier and faster to prepare. It could also be shown that two biological species namely polymyxin B and α -haemolysin can interact with this architecture. This is the first time that membrane active species were shown to interact with a supported polymer model membrane structure. The bilayer architecture presented here might prove useful as a matrix for protein based sensors because they combine biocompatibility and stability necessary for technical devices. In addition unfunctionalized PB-PEO vesicles were spread on hydrophilic glass surfaces. The degree of surface coverage was not as high as for the covalently bound species but by further optimization of spreading conditions and by utilizing higher vesicle concentrations full coverage should be achieved. These structures on transparent support offer the possibility to use optical microscopy for their

detailed investigation. They might serve as an easy platform to screen interactions of membrane active proteins with polymer surfaces.

5. Single Molecule Diffusion in Giant-Unilamellar-Polymer-Vesicles

The work in this chapter was done in cooperation with Matthias Geissbühler and Iwan Märki in the group of Prof. Theo Lasser at the EPFL Lausanne. Sample preparation, first characterization and data evaluation was carried out at the MPIP in Mainz while FCS measurements were done in Lausanne. The model peptide FGFR3-(TM) was provided and OCD measurements in polymer were recorded by the group of Prof. Kalina Hristova at Johns Hopkins University, Baltimore.

5.1. Introduction

Membrane proteins play a crucial role in a wide variety of cellular processes from transmembrane transport and energy transduction to sensing and signal transduction to catalysis at the cell surface. Many of these processes are highly dynamic. Lateral diffusion of integral and peripheral membrane proteins is an important factor in controlling the dynamics and functioning of the cell membrane.^[139] According to the early model proposed by Singer and Nicholson, biological membranes can be described as a fluid mosaic model where all membrane components can diffuse freely in two dimensions.^[2] It is now known that this simplified model does not fully represent the highly complex biological membrane with a protein area fraction of up to 35%.^[140] Due to formation of lipid rafts and supramolecular clusters diffusion can be significantly hindered.^[141] It is difficult to study diffusion of individual membrane components without perturbation or cross-talk in the cell membrane since native biological membranes are complex and involve numerous molecular species. Vesicles are a very good model system to probe membrane dynamics because in such self assembled aggregates the bilayer constituents and membrane proteins can diffuse freely within the bilayer plane. In contrast to supported bilayer architectures there are no additional interactions with the surface. Especially μm -sized giant unilamellar vesicles (GUV) proved useful for diffusion studies^[17] because they are easy to prepare and can be observed with a standard brightfield optical microscope which facilitates handling.

Lateral diffusion of small membrane components like lipids can be quantitatively described by the Saffman-Delbrück model which treats biomembranes as infinite plane sheets of a viscous fluid following Brownian motion.^[142] The model can also explain diffusion of membrane spanning species. Proteins are treated as cylinders incorporated into the 2D fluid following Brownian motion. Guigas *et al.* showed that the model does not hold anymore for high protein contents and objects with a diameter of more than ~ 3 nm.^[143] A very powerful technique to study lipid and membrane diffusion with single molecule sensitivity is fluorescence correlation spectroscopy (FCS). Several studies were carried out with FCS to investigate lipid-protein^[19] and protein-protein interactions in lipid model systems.^[144]

Apart from lipid architectures amphiphilic block copolymers came up in the past decade as alternative constituents for model membrane systems because it could be shown that they can form lipid-like membrane structures which are mechanically more stable in terms of maximal areal strain.^[55] Dynamic properties of polymeric 2D-membranes have been studied to some extent.^[93] In this paper Discher and co-workers studied the self-diffusion of dye labelled polymers in aspirated giant vesicles with fluorescence recovery after photobleaching (FRAP) measurements. A comparison was made between a short PEE-PEO diblock copolymer with a saturated hydrophobic block and a longer PB-PEO copolymer with an unsaturated hydrophilic block. They observed a significant decrease of the diffusion coefficient D_{Polymer} of at least a factor of 30 compared to lipids (SOPC). The huge difference in D (factor 50) between the two polymers which only vary by a factor of 2.6 in molecular weight M_w is remarkable. The authors propose transition from a scenario where the two opposing layers do not interpenetrate much for the short polymer to a situation where the two membrane sheets overlap in the hydrophobic core of the membrane. This interpenetration is thought to be the main factor for the increased stability compared to lipid systems. The self assembly behaviour of amphiphilic diblock copolymers was also studied by computer simulations.^[56] It could be shown theoretically that the interdigitation and the entanglement increase with longer hydrophilic blocks finally leading to a decreasing mobility. Most interesting, it could be shown that a membrane forming triblock copolymer system (PMOXA-PDMS-PMOXA) can host transmembrane proteins while remaining functional.^[58, 60] Besides that Vijayan *et al.* demonstrated the successful incorporation of the pore forming TM-helix gramicidin into vesicles of block polyethylene-block-polyethyleneoxide (PEE-PEO).^[61]

The transmembrane proteins and peptides used so far in the context of polymer bilayers are typically pores or selective channels which are able function as individual units. For many functional proteins it is absolutely necessary to transiently form clusters of two or more units

in order to be functional. For example neuronal^[145] and odorant^[146] receptors of the GPCR family need to have lateral mobility in order to induce a signal cascade. To introduce such functional proteins into polymer bilayers their mobility has to be ensured. To date no information is available about the diffusivity of external species in polymeric bilayer matrices.

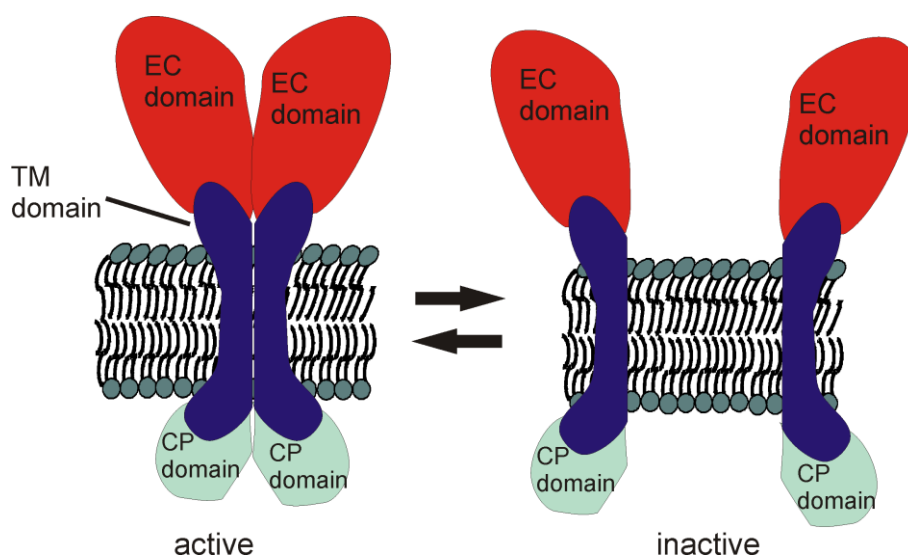
The objective of this chapter was to investigate the self-diffusion dynamics of polymer bilayer constituents as well as external probes on the single molecule level. The chapter can be subdivided into three different parts:

The first part is aiming to provide a well characterized reference system (chapter 5.3.1). It deals with the question how fast small fluorescent probes diffuse in a lipid environment and how is the probe diffusion related to lipid self-diffusion. To answer this, the diffusion of two different lipophilic dyes DID^[147] and Bodipy 630/650 was measured with fluorescence correlation spectroscopy (FCS). Both species spontaneously incorporate into lipid bilayers. A more detailed treatment of dye structure and orientation will be provided in the chapter Results and Discussion. To determine the lipid self-diffusion a Texas-Red (TR) labelled phosphatidylethanolamine lipid (DHPE) was added to a DiPhyPC bilayer in a molar ratio of 1:10⁵. By comparing the obtained values one can estimate how far the dye diffusion resembles lipid self-diffusion of the matrix. The lipid DiPhyPC was used for several reasons. On the one hand it produces more robust giant vesicles than e.g. DOPC. On the other hand the hydrophobic chains bare methyl side chains. This structure is more comparable to the polymers investigated later than an unbranched chain.

In the second part the lateral mobility of the polymer membrane was investigated (chapter 5.3.2). The polymers used for this study are hydroxyl terminated PB-PEO diblock copolymers known from previous chapters. In aqueous environment they form planar structures but also giant vesicle structures can be prepared via electroformation. Again two different approaches were tried. On the one hand the same two lipophilic dyes as above were observed in artificial polymer bilayers of two different molecular weights. This gives first insights into polymer bilayer diffusivity. In addition the measurement of polymer species of two different chain lengths provides information about possible molecular configurations. Again to compare the diffusion of the small fluorescent probes with the polymer self-diffusion dynamics a covalently labelled derivative of the polymer was used.

In the third part the question is addressed whether biologically relevant membrane spanning species can diffuse inside the completely artificial environment of neutral polymer chains (chapter 5.3.3). Since complicated transmembrane proteins are easily denatured and therefore

are not easy to handle it was decided to use simple and robust model system. The transmembrane (TM) domain of the *fibroblast growth factor receptor 3* (FGFR3) poses such a model system because its structure is not altered during drying or organic solvent treatment. The amino acid sequence adopts a single membrane spanning α -helix configuration. Transmembrane helices are a main building block of many more complex TM-proteins. The protein FGFR3 belongs to the family of receptor tyrosine kinases.^[148] The biochemical signalling cascade of FGFR3 is initiated by dimerization of two monomers in the membrane plane as depicted in Scheme 21.



Scheme 21: Simplified illustration of the dimerization of the *fibroblast growth factor receptor 3*.

The Cy5 labelled peptide consists of one membrane spanning α -helix that is very hydrophobic. The free energy of transfer from water to octanol for the membrane-embedded segment is estimated as 9.4 kcal/mol.^[149] The high hydrophobicity is thought to be advantageous for the incorporation into the hydrophobic bilayer core of non-natural structures because the reduction of free energy is a strong driving force. The diffusion dynamics for FGFR3-(TM) were determined in bilayers of two different molecular weights to see if there is an effect of the hydrophobic bilayer thickness. For better comparison FGFR3-(TM) diffusion was also measured in DiPhyPC vesicles for better comparison.

5.2. Materials and Methods

5.2.1. Materials

The polymers used for this work were synthesized by Serena Belegriou at the University of Basel in the group of Prof. Wolfgang Meier.

Polymers. Hydroxyl terminated polymers of two different molecular weights were synthesised. For details of the synthesis procedure see chapter 2. The molecular weight of the block copolymers was determined by gel permeation chromatography GPC and $^1\text{H-NMR}$ (nuclear magnetic resonance). First, a polybutadien (PB) aliquot, drawn prior to the sequential copolymerization, was analyzed by GPC with tetrahydrofuran THF as eluent. Polybutadiene standards (Polymer Standard Service) were used to calculate M_n , M_w , and the polydispersity index (PDI). The number of the ethylene oxide repeating units, thus the molecular weight, was calculated from the peak ratio in the $^1\text{H-NMR}$ spectrum of the block copolymer. The ratio of hydrophobic monomer units compared to the whole polymer were 64% and 67% for PB-PEO 01 and PB-PEO 03 respectively.

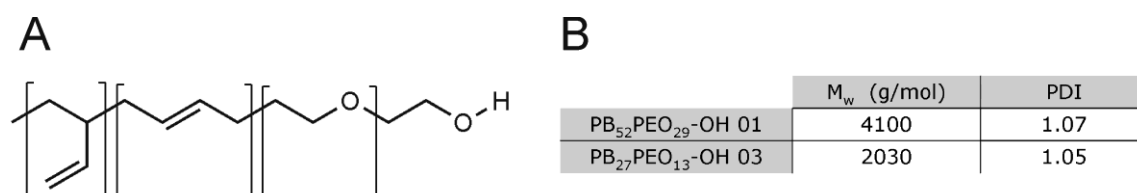
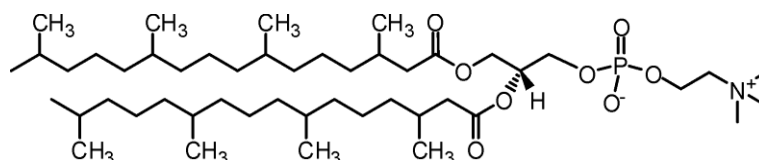


Figure 31: Structure of PB-PEO-OH. The polybutadiene block is a mixture of 1,2 and 1,4 connected butadiene units as indicated in the left part of the structure in two separate brackets(A) and the GPC results for the molecular weights(B).

The dye functionalized derivative of PB-PEO 01 was obtained by coupling tetramethylrhodamin-5-carbonylazide through an ester bond.

Lipids. L- α -phosphatidylcholine extract from soy bean (soy PC) DOPC (1,2-dioleoyl-*sn*-glycero-3-phosphocholine) and DiPhyPC (1,2-diphytanoyl-*sn*-glycero-3-phosphocholine, Scheme 22) were purchased from Avanti Polar Lipids (Alabaster, Alabama) and used without further purification. The head groupe labelled lipid Texas Red® 1,2-dihexadecanoyl-*sn*-glycero-3-phosphoethanolamine, triethylammonium salt (Texas Red® DHPE) was obtained from Invitrogen (Karlsruhe, Germany).

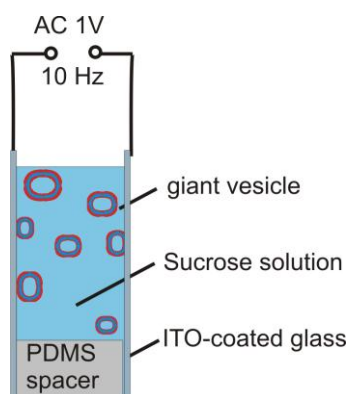


Scheme 22: Structural formula of DiPhyPC.

Lipophilic dyes. The commercial dyes Bodipy 630/650 SE and DID^[150] (Invitrogen, Karlsruhe) were each dissolved in chloroform to a concentration of 2 mg/mL. From these aliquots 1:1000 dilutions were prepared. For vesicle labelling 2 μ L of that diluted solution was added to 1 mL of amphiphile solution. The Bodipy derivative used here is a succinimidyl ester potentially reactive to amine groups. Because there are no amines present in the sample it is converted into the free acid by hydrolysis after several hours in water.

Transmembrane peptide FGFR3-(TM). The material was provided by the group of Prof. Kalina Hristova (Johns Hopkins University, Baltimore). The peptide was synthesized using solid phase peptide synthesis and purified using reverse high pressure liquid chromatography HPLC, as described in literature.^[149] The amino acid sequence of the wild type is DEAGSVYAGILSYGVGFFLFILVVAAVTLCRLR but in the studies presented here a labelled mutant (RRAGS-VYAGILSYGVGFFLFILVVEAVT-LCRLR-Cy5) was used. According to the SOSUI prediction software^[151] the transmembrane region consists of 23 amino acids which are VYAGILSYGVGFFLFILVVEAVT. The Results from the calculations can be found in Appendix A.

Giant vesicle preparation. All vesicle samples were prepared *via* electroformation. The setup used for this purpose is sketched in Scheme 23.



Scheme 23: Electroformation setup used for giant vesicle preparation.

A chloroform solution of the amphiphile (lipid 1 mg/mL; polymer 2 mg/mL) was drop coated on ITO coated glass electrodes and dried under vacuum over night. The two electrodes were clamped together only separated by a u-shaped PDMS (polydimethylsiloxan) spacer of 1 mm

thickness. The resulting gap was filled with 200 mM solution of sucrose and the electrodes were connected to an AC voltage generator. For lipid samples an amplitude of 1 V at 10 Hz was applied for 2 h followed by 30 min at 1 V and 5 Hz. For polymer samples the amplitude was 2 V and the frequency was kept at 10 Hz for at least 12 h before reducing to 4 Hz for 2 h. In all cases vesicles with a very broad size distribution were obtained as could be seen under an optical microscope.

FCS sample preparation. For diffusion measurements about 100 μL of a 200 mM glucose solution buffered with HEPES(2-(4-(2-Hydroxyethyl)-1-piperazinyl)-ethansulfonic acid) at 7.4 was given into a PDMS-sample cell. Then 5-10 μL of the vesicle/sucrose solution was added. The vesicles were allowed to sediment for about 5 min before measurements were started. In the case of peptide diffusion 5 μL of a saturated Trolox solution were added to increase the photostability and reduce fluorescence quenching of the Cy5 label. Trolox is a Hoffman-LaRoche's trade name for 6-hydroxy-2,5,7,8-tetramethylchroman-2-carboxylic acid, a water-soluble derivative of vitamin E that prevents photobleaching through triplet quenching.^[152]

Supported lipid bilayers on glass. 1 mL of a chloroformic solution of DiPhyPC (1 mg/mL) was given into a flask. The solvent was volatilized while stirring with a vortex stirrer to produce a thin film on the glass wall. The film was dried under a stream of nitrogen for 3 h. Then 1 mL of ultrapure water (MilliQ 18.2 $\text{M}\Omega\cdot\text{cm}^2$) was added to rehydrate the lipid film and produce a opaque lipid suspension. After strong stirring the vesicle suspension was extruded through a polycarbonate membrane with 100 nm pore size. 50 μL of extruded vesicles suspension was added to 500 μL of phosphate buffer in a measurement cell with a clean glass surface. After 1 h the surface was rinsed with 10 mL of buffer to yield a supported lipid bilayer on glass.

OCD measurements. 4 mg of the polymer was dissolved in 1 ml chloroform to prepare a 4 mg/ml polymer stock solution. FGFR3-(TM) peptide was dissolved in HFIP/MeOH (1:2), and the concentration was determined by CD to be 60 μM . FGFR3-(TM) was added to 125 μl polymer solution to yield a 5 mol-% (peptide/polymer) final concentration. Dropwise, the mixed polymer/FGFR3-(TM) solution was deposited on a quartz slide and the solvent was removed under a stream of nitrogen to form a multilamellar sample containing the peptides. The quartz slide with the deposited multilamellar sample was placed in a custom designed chamber. A drop of water was placed inside the chamber to hydrate the sample 30 minutes before starting the experiment. CD spectra were recorded while the sample was rotated

around the beam axis in increments of 45 degrees. The eight recorded spectra were averaged and corrected for polymer background.

5.2.2. Single Particle Tracking (SPT)

For the single particle tracking experiment of FGFR3-(TM) in DiPhyPC a homebuilt microscope at the Max-Planck-Institute for Polymer Research was used. The assembly and implementation of the microscope was done during the course of this thesis.

The output of a 10 mW Helium-Neon laser was coupled into a single mode fibre (Schaefer + Kirchhoff GmbH, Hamburg; Germany) to obtain a Gaussian beam profile. At the fibre output, the light was collimated and directed to the sample by a dichroic mirror (Q645 LP, Chroma Technology Corp.) through an objective (Leica, oil immersion, 100x, 1.4 NA). Fluorescence was collected through the same objective. Excitation light was blocked by a combination of a notch and a long pass filter (Semrock NF01 633U and Semrock LP02-633RS). Light was then focused by a tube lens to a CCD camera (Sensicam QE, PCO AG, Kelheim, Germany).

SPT data evaluation. Analysis of image series of diffusing molecules was done with the free software *Image J*. Trajectories were recorded as .tif files and then imported into the program. To denoise images the *spot enhancing filter* of Spot Tracker 2D^[153] was used. The actual tracking was done with the *Particle Detector & Tracker* plugin.^[154] First a recognition algorithm was used to identify particles and then trajectories were constructed by linking particles within a certain radius in subsequent frames. Then trajectories with 7 or more steps and no interruptions were selected by hand. From these trajectories mean square displacements (MSD) were calculated with a data evaluation routine in Igor Pro (Wavemetrics) according to Equation 20

$$MSD = \langle (x_{i+n} - x_i)^2 + (y_{i+n} - y_i)^2 \rangle$$

Equation 20

where (x_{i+n}, y_{i+n}) describes the particle position following a time interval, t , given by n times video frame time (0.4 sec) after starting at position (x_i, y_i) . i ranges from 1 to $N-n$, where N is the total number of particle positions recorded, and n takes on values 1, 2, 3 ... $n - 1$.^[155] MSDs were then plotted versus $4t$ and fitted linearly. According to Equation 21 the resulting slope then yields the diffusion coefficient D .

$$MSD(t) = 4Dt$$

Equation 21

5.2.3. Fluorescence Correlation Spectroscopy (FCS)

FCS measurements were done on a home-built fluorescence microscope in the group of Prof. Theo Lasser at the EPFL in Lausanne. For technical details of the used setup see chapter 2. This subchapter describes the experimental details for the performed diffusion measurements. For theoretical background the reader is referred to the general chapter Materials and Methods.

The FCS setup was calibrated using literature values for free Cy5 ($370 \mu\text{m}^2/\text{s}$)^[156] for red excitation. For the green excitation tetramethylrhodamine (TMR) was used. Literature states a value for Rhodamine 6G ($414 \mu\text{m}^2/\text{s}$)^[157] Because are chemically very similar in structure it was assumed that they have the same hydrodynamic radius and therefore the a similar diffusion behaviour. Free diffusion in a droplet of dye solution was measured repeatedly. Calibration measurements were fitted to a three dimensional Gaussian model taking the photochemical process of triplet excitation into account^[158] (Equation 22).

$$G(t) = 1 + \frac{1}{N} \cdot \left(\frac{1}{1 + \frac{t}{\tau_D}} \cdot \frac{1}{\sqrt{1 + \frac{1}{S^2} \cdot \frac{t}{\tau_D}}} + \frac{P_T}{1 - P_T} e^{-\frac{t}{\tau_T}} \right)$$

Equation 22: Autocorrelation function for a three dimensional Gaussian excitation volume. N = number of molecules in the focus, τ_D = diffusion time, τ_T = triplet time, P_T = triplet probability, t = lag time, S= Structure parameter.

The structure parameter $S = z_0/\omega_0$ in Equation 22 is a measure for the proportion of the focal volume where z_0 is the extension along the z-axis and ω_0 is the focus diameter. With the help of point spreads function calculation one can verify that the structural parameter is heavily increasing for increasing focal distance to the surface for our objective (NA = 1.45). Close to the cover slide $S \sim 2$ while at $10 \mu\text{m}$ it increases up to $S \sim 5.5$ (for $\lambda = 532 \text{ nm}$) and $S \sim 5$ (for $\lambda = 635 \text{ nm}$). With the known diffusion coefficient D and a measured diffusion τ_D time it is possible to calculate the focal width ω according to Equation 23.

$$\tau_D = \frac{\omega^2}{4D}$$

Equation 23: τ_D = mean diffusion time, ω = focal width, D = diffusion coefficient

FCS autocorrelation curves of the calibration solutions were recorded at different positions from the surface as can be seen in Figure 32. At position zero a long diffusion time around $47 \mu\text{s}$ indicates the retarding effect of the surface due to e.g. adsorption. When the focus is subsequently positioned in solution a linear increase in τ_D is observed. This stems from increasing aberrations: the objective is optimized for a focal distance of $d = 0$. By moving the focal plane further into solution the light has to travel through water with a lower refractive index than glass. This deforms and expands the focal volume leading to higher τ_D as can be seen in Figure 32. This effect is present in all objectives, but it is probably slightly stronger for high numerical aperture oil-immersion objectives (as used in this study $\text{NA} = 1.45$). This kind of lens system is optimized and corrected for total internal reflection fluorescence (TIRF) measurements directly at the glass surface. To take this into account the calibration measurements were done at a penetration depth of $10 \mu\text{m}$ because most measured vesicles were in this size range.

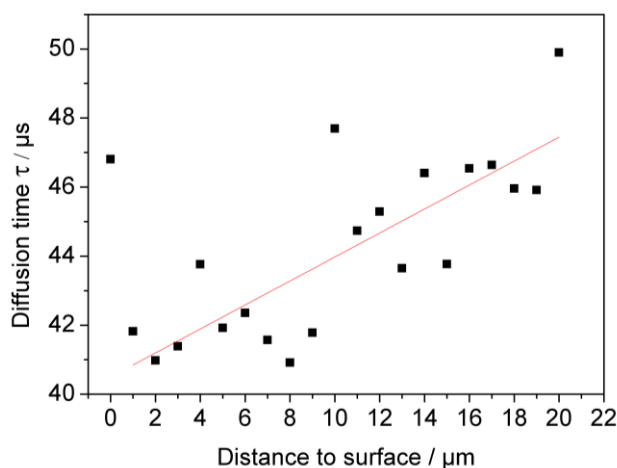


Figure 32: Influence of the focus distance from the surface on the diffusion time of TMR (10 nM).

FCS data collection. An aspect which has to be taken into account for the data evaluation is the inaccuracy in the z-positioning relative to the membrane plane. Various groups have shown the effect of the z-position on the active focal width ω and the diffusion coefficient.^[159] As a consequence the lowest value measured for diffusion time τ_D and particle number N should be the most accurate one because it corresponds to the lowest beam waist. Because an exact positioning was not possible due to slow drift and vesicle shape fluctuations the rough z-position was determined by eye in the fluorescence microscopy image and then the z-piezo of the sample holder was slightly moved around this position from one measurement to the next.

FCS data evaluation. Since all samples were not fixed on the sample but were only physisorbed, strong drift could be observed in some cases. This drift appears in the autocorrelation curve as a directed motion with its own typical transition time through the focal volume. This motion usually resulted in a time component in the time regime >1 sec. Whenever this slow component appeared the vesicle had moved its position as could be seen with the bright field microscope. For the data evaluation here, only correlation curves which did not show these second modes of motion were taken into account.

The preselected curves were then fitted with a model to obtain experimental diffusion times τ_D .^[158] For fitting 2D diffusion curves recorded on vesicle membranes a simplified model was used that excludes motion along the z-direction but takes triplet state excitation into account.

$$G(t) = 1 + \frac{1}{N} \cdot \left\{ \frac{1}{1 + t/\tau_D} + \frac{P_T}{1 - P_T} \exp(-t/\tau_T) \right\}$$

Equation 24: Fitting model for autocorrelation curves of two dimensional diffusion. N = number of molecules in the focus, τ_D = diffusion time, τ_T = triplet time, P_T = triplet probability, t = lag time.

For every species 50 correlation curves were recorded and fitted to the appropriate model. In principle the measurement with the fastest diffusion time and the lowest number of molecules in the focus should represent the best value. In order to take the z-positioning into account but also have some statistics from these 50 values the lowest 5 were selected and the average was calculated.

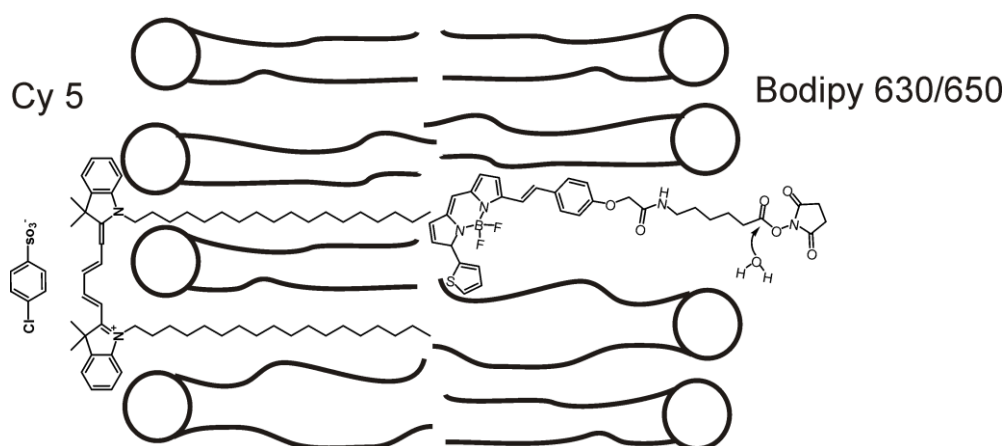
5.3. Results and Discussion

The aim of this work was to elucidate the dynamics of species incorporated into polymeric bilayer membranes and compare them to the diffusion behaviour in lipid environment. In the first step experiments in giant unilamellar lipid vesicles were done as a reference system. Then the same probes were used to characterize the diffusion in polymer bilayers of two different molecular weights. Additionally diffusion measurements of a covalently labelled polymer gave insights into the polymer self-diffusion. And finally, with the information gathered before it was then possible to measure the lateral mobility of a membrane spanning model peptide.

5.3.1. Diffusion in Lipid Bilayers

To have a well characterized reference system it was first analyzed how hydrophilic dyes and fluorescent lipid probes diffuse in an environment that closely resembles the biological membrane.

In order to study the 2D diffusion behaviour in lipids two different membrane probes were used that are known to selectively stain the hydrophobic core of the membrane. The two dyes DID and Bodipy 630/650-SE were used for this purpose. DID is a hydrocarbon chain modified derivative of the well known Cy5 dye which belongs to the cyanine family. Since it has a hydrophilic head group and two hydrophobic tails it will partition most likely at the interface between hydrophobic core and hydrophilic outer layer of a bilayer system as depicted in Scheme 24. The other membrane probe used in this work is Bodipy 630/650 SE. SE stands for succinimide ester which is reactive to free amine groups. Since there are no amine groups present in the system it is assumed that the activated ester slowly hydrolyses to form the free carboxylic acid when samples are prepared in aqueous solution. Bodipy 630/650 is not as hydrophobic as DID^[160] but also stains the hydrophobic core of the membrane. The exact conformation of the Bodipy probe inside the bilayer is not known but due to its amphiphilicity it most likely locates at the hydrophilic-hydrophobic interface with the conjugated π -system buried inside the membrane core (Scheme 24). On the contrary the conjugated π -system of DID is located at the hydrophilic-hydrophobic interface of the bilayer structure. So far no reference is known in literature where this exact compound was used to probe the diffusion dynamics of a membrane. For another Bodipy derivative (BODIPY® TR methyl ester) it is reported to serve as a good staining agent for cellular membranes^[161-162] but no description of the molecular conformation and the diffusion behaviour inside the hydrophobic core is available so far. Both dyes can either be incorporated during the vesicle formation procedure or they can be added to the solution after vesicle formation to selectively stain the vesicle shell. The main reason why two different dyes were used was to find out what influence the chemical structure of the probe has on the diffusion behaviour.



Scheme 24: Assumed conformation of the two utilized dyes in a lipid environment. In the case of Bodipy 630/650 (right) hydrolysis of the active ester is indicated.

FCS autocorrelation curves were recorded on fluorescently labelled vesicles composed of the saturated lipid diphytanoylphosphatidylcholine (DiPhyPC) and a lipid extract from soy bean (L- α -phosphatidylcholine soy PC) consisting mainly of unsaturated chains. It has to be noted that DiPhyPC produces much more stable vesicle samples which can be stored at 4°C for weeks while vesicles from Soy PC only survive one week at the most and also burst more easily when brought into contact with glass. For this reason DiPhyPC vesicles were chosen as a reference system.

Sample type	D / $\mu\text{m}^2/\text{s}$
DiPhyPC + Bodipy	5.60 ± 0.30
DiPhyPC + DID	5.05 ± 0.23
Soy bean PC + Bodipy	10.25 ± 0.022
DiPhyPC + TR-DHPE	5.41 ± 0.50

Table 5: Results from fitting the autocorrelation curves to the 2D model described above. Denoted errors are standard deviations. Autocorrelation curves can be found in Appendix B.

As can be seen Table 5 the diffusion of Bodipy varies a lot depending on the membrane constituting lipid. The difference in diffusion coefficient by a factor of 2 obviously stems from the difference in acyl chain saturation. While soy bean PC mainly consists of unsaturated chains (77%, according to Avanti Polar Lipids) DiPhyPC has completely saturated chains. The kinked configuration of double bonds in the soy bean lipids creates a higher degree of disorder so that they are less densely packed. On the other hand the diffusion

coefficients do not differ significantly depending on the probe used. Bodipy and DID exhibit diffusion coefficients between 5.05 and 5.6 $\mu\text{m}^2/\text{s}$ suggesting the location in a similar physico-chemical environment.

The question was how the diffusion behaviour of the two lipophilic relates to the self-diffusion of a natural lipid species. In the optimal case one would use a covalently labelled DiPhyPC species but since this was not commercially available lipid self-diffusion was checked by adding a small amount of the fluorescent lipid Texas Red-dihexadecanoylphosphatidyl-ethanolamine (TR-DHPE) to the lipid mixture. The obtained TR-DHPE diffusion coefficient of 5.4 $\mu\text{m}^2/\text{s}$ lies between the two values of Bodipy and DID indicating that all three probes sense the same environment in DiPhyPC. Presumably they are all located within one lipid bilayer sheet. A good agreement between lipid self diffusion and diffusion of lipophilic membrane markers was also reported in literature.^[163] There is no value known for DiPhyPC but the fully saturated dimyristoylphosphatidylcholine (DMPC)^[164] shows a diffusion coefficient of 5.82 $\mu\text{m}^2/\text{s}$ that fits well with our values for TR-DHPE of 5.4 $\mu\text{m}^2/\text{s}$ and DID of 5.6 $\mu\text{m}^2/\text{s}$.

5.3.2. Diffusion in Polymer Bilayers

The aim of this subchapter is to measure the diffusion dynamics of polymeric bilayers made from amphiphilic block copolymers. This is done in two ways. First the lateral diffusion of the same lipophilic dyes as in chapter 5.3.1. was measured in the polymer bilayers of two different chain lengths. Second the polymer self-diffusion of a dye-labelled derivative of PB-PEO 01 was determined and compared to the values of the free fluorescent probes.

Fluorescent probe diffusion. In the previous chapter the diffusion coefficients of both dyes in the lipid matrix were qualitatively the same. This proves that the diffusion of external probes is mainly governed by the bilayer constituting matrix. Values for DID and Bodipy also showed good agreement with the values for lipid self diffusion. Therefore the same approach is now used to test the diffusion dynamics of PB-PEO bilayers with two different molecular weights (PB-PEO 01: 4100 g/mol; PB-PEO 03: 2050 g/mol).

The FCS autocorrelation curves of Bodipy and DID in the two different polymers were recorded. Figure 33 A shows the autocorrelation curves of Bodipy 630/650 in the polymer with the corresponding fit curves (red and black line). For comparison to the lipid

measurements the correlation curve of Bodipy in DiPhyPC is plotted in blue. The table in Figure 33 B summarizes all obtained fit values for all four possible combinations.

In contrast to the fast Bodipy diffusion in a DiPhyPC bilayer ($\sim D = 5.6 \mu\text{m}^2/\text{s}$, blue curve) the diffusion in the polymer membranes is slowed down by approximately a factor of 4. This is expected since the long polymer chains will adopt a more coiled structure than the short acyl chains of lipids so that they are much more bulky. In literature polymer diffusion of the polymer PEE-PEO which is comparable in chemical composition and molecular weight was even reported to be a factor 30 lower than lipid diffusion.^[93]

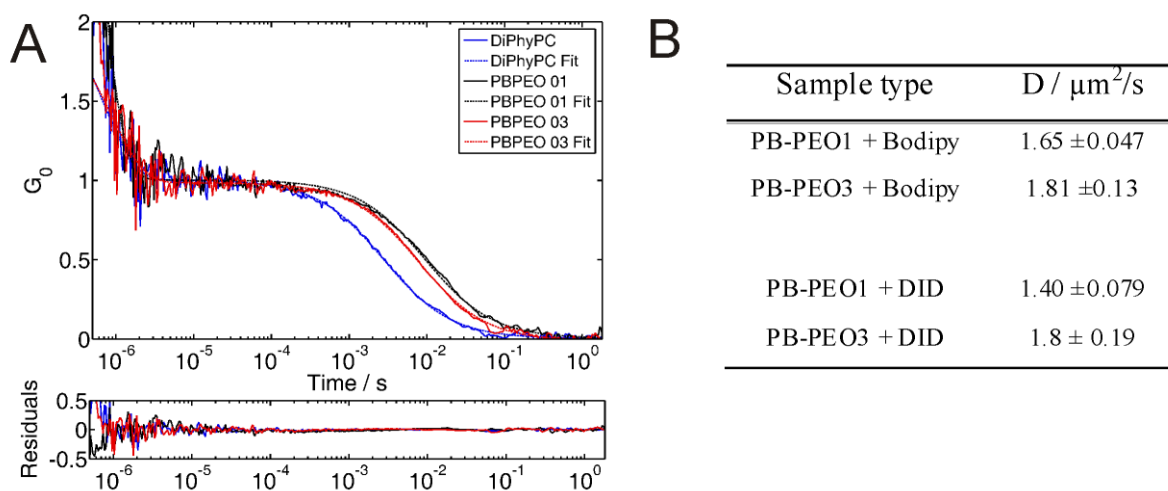


Figure 33: FCS autocorrelation curve of Bodipy 630/650 in vesicles of the two polymers of different M_w and in DiPhyPC vesicles (A) and the corresponding fit results for both lipophilic dyes in polymeric environment (B).

For both dyes the diffusion coefficients D only show small differences depending on what polymer they diffuse in. Bodipy diffusion is 10% and DID 30% slower in the longer polymer than in the short one. This is somewhat surprising since the chains of PBPEO-01 are twice as long as those of PB-PEO 03. It was suggested by Lee *et al.*^[93] that polymer chains of the used length can be described by the *Rouse* model. This implies that the diffusion coefficient D is proportional to the inverse of the number of monomer units N ($D \sim N^{-1}$). In a simplified way this means that the interactions between the polymers are just the sum of the friction of all monomer units. If this was the case one would expect larger differences between the two polymers. The low differences can have several reasons. The unsaturated carbon bonds in the polybutadiene backbone induce kinks in the polymer chains which lead to disorder and therefore a less dense packing. This can lead to entanglement with molecules from the same bilayer sheet or the polymer chains of one layer interpenetrate the opposing layer. Both cases lead to additional interactions so that diffusion does not follow an ideal *Rouse* scaling

anymore. Another point that has to be considered is that the diffusion of Bodipy and DID is not directly coupled to the chains of the polymer matrix. It could be that the dye diffusion is more to the polymer case. Most likely it is a combination of all mentioned aspects but to quantify or rule out the influences additional measurements are necessary with more different polymer chain lengths.

Polymer self-diffusion. The question remains if the diffusion of the block copolymer itself is significantly different from the diffusion behaviour of the external membrane probes. In the case of lipids it was demonstrated that lipid and dye diffusion coefficients are similar. To investigate polymer self-diffusion PB-PEO 01 was covalently labelled with the dye tetramethylrhodamin. The dye labelled polymer was mixed with unlabelled hydroxyl terminated PB-PEO 01 and subsequently giant vesicles were. Polymer self diffusion measurements were greatly complicated by a high amount of free dye not coupled to the PB-PEO chains. To remove the free dye it would be necessary to remove the free dye by preparative HPLC but due to a lack of time it was not possible to prepare new vesicle samples within the course of this thesis. Since tetramethylrhodamin is water soluble it is homogeneously distributed everywhere in the sample and not only in the bilayer plane. This produces a high background signal. It was still possible to position the focus roughly at the vesicle shell in widefield (WF) microscopy mode where FCS curves could be recorded. In WF-fluorescence microscopy single objects were visible by eye which are moving along the membrane plane. A typical FCS autocorrelation curve can be seen in Figure 34. Due to the high heterogeneity the algorithm written in MATLAB is not able to fit these curves with a reasonable accuracy. Therefore one can only extract qualitative information from the curve. What can be directly seen is that there is not only one diffusing species but shoulder in the correlation curve indicates a bimodal distribution of diffusion times. The main component has a diffusion time of about $650 \mu\text{s}$ which would correspond to $D = 35 \mu\text{m}^2/\text{s}$. This is about a factor 10 slower than the diffusion of free TMR but still too fast for a molecule to diffuse within the bilayer plane. A diffusion component in this range could result from the free TMR that sticks to the highly hydrated PEO chains of the bilayer. Additionally there is a second time component in the range of 10^{-2} s. This shoulder can be observed in all autocorrelation curves but does not appear in the background measurement next to a vesicle indicating a membrane related diffusion process.

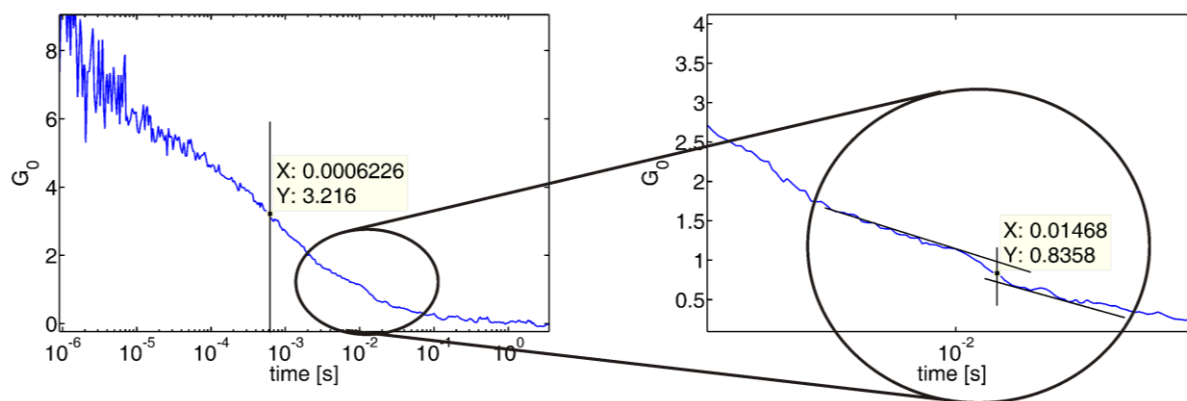


Figure 34: FCS autocorrelation curve of TMR-labelled PB-PEO-01.

By graphically estimating the inflexion point of the shoulder as presented in Figure 34 a diffusion time of 15 ± 10 ms is obtained that corresponds to a diffusion coefficient $D = 1 \mu\text{m}^2/\text{s}$. This estimated value is in the same range as the diffusion coefficients of the membrane markers in the giant polymer GUVs (Figure 33 B). It has to be stressed that this is only a rough estimate that give an idea about the order of magnitude because of the strong background and the low number of “membrane” events. Data so far indicate that PBPEO-01 has a diffusion coefficient which is a factor of 5 slower than the lipid diffusion in DiPhyPC vesicles. This decrease can be explained by the entanglement of polymer chains in the same bilayer sheet and also by a penetration of the chains into the opposing sheet. As described by Discher and co-workers^[93] at longer chain lengths the interpenetration of the opposing layers of the membrane gets so high that the two sheet model is not applicable any more. In literature there is one report from the group of Discher and co-workers that measured fluorescence recovery after photobleaching (FRAP) on a labelled diblock copolymer of polyethylene-polyethyleneoxide (PEE-PEO) of comparable molecular weight.^[93] This PEE₄₀PEO₃₇ block copolymer has a lower hydrophilic fraction (52%) compared to the PB-PEO 01 and PB-PEO 03 used here (64% and 67% respectively). The diffusion constants they obtained are a factor of 8-10 slower than the values in this work. This can have various reasons. First, their reference value for SOPC (stearoyl-oleoyl-phosphatidylcholine) ($3.8 \mu\text{m}^2/\text{s}$) is almost a factor of 2 slower than the value reported in literature ($6.6 \mu\text{m}^2/\text{s}$)^[165] pointing towards a systematic difference in the measurement. An aspect which is only speculation but is not discussed in the work by Discher is photobleaching. No time dependent fluorescence intensity is shown prior to photobleaching or after full recovery. Usually this should be part of a complete FRAP curve to rule out unwanted photobleaching caused by the excitation light. In the case of photobleaching all recovery curves would appear to be too slow because this is a contrary process to the recovery taking place. A second factor that could lead

to the difference in observed diffusion times is the chemical difference of the hydrophilic block compared to the polymer used here. The C=C double bonds present in PB-PEO are known to induce disorder which might lead to a less dense packing and therefore to a faster diffusion compared to PEE-PEO where the hydrophobic block is fully saturated.

5.3.3. Diffusion of the Model Peptide FGFR3-(TM)

In the first part it could be demonstrated that it is possible to introduce fluorescent membrane probes in the membrane matrix to evaluate the fluidity. It is now interesting to go a step further and see if biologically relevant transmembrane species can be incorporated into these polymeric structures to diffuse in the bilayer plane. Therefore a single α -helical transmembrane peptide from the TM-domain of the *fibroblast growth factor receptor 3* (FGFR3) was used as a model system.

Peptide diffusion in lipid bilayers. In the first step membrane diffusion of FGFR3 was measured in a lipid reference system of DiPhyPC GUVs (Figure 35). Again DiPhyPC was chosen as the membrane constituting lipid because it forms stable peptide modified vesicles which do not easily burst upon contact to glass.

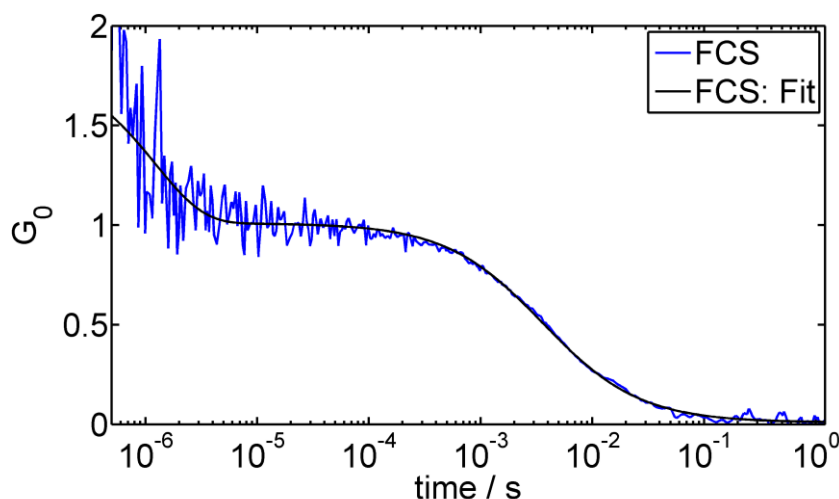


Figure 35: FCS autocorrelation curve of Cy5 labelled FGFR3-(TM) in a giant unilamellar vesicle composed of DiPhyPC in buffered glucose (pH 7.4). The fitted $\tau_D = 2.95 \pm 0.22$ ms translates to a diffusion coefficient of $D = 5.29 \pm 0.44 \mu\text{m}^2/\text{s}$.

The obtained diffusion coefficient for FGFR3-(TM) in DiPhyPC is $5.3 \mu\text{m}^2/\text{s}$. Within the error margin peptide and lipid diffusion are the same. This obtained value for peptide

diffusion lies well within the range of reported protein diffusion. Even higher diffusion coefficients were reported for much bigger proteins.^[144] It is somewhat surprising to see the same diffusivity for lipid and peptide because due to collisions of a membrane spanning peptide with lipid in both layers would be expected to be slowed down. Gambin *et al.* obtained a 10 times slower diffusion for a single helix than the bilayer constituting lipids.^[166] Probably the differences stem from chemical differences of the lipid bilayer and the used model peptide.

A possible explanation for the small differences in lipid and peptide diffusion could be that FGFR3-(TM) is not incorporated but only adsorbs on the lipid bilayer. To test whether the peptide is spanning the bilayer diffusion was measured in supported lipid bilayers on glass. If the peptide is only adsorbed on the bilayer diffusion should not be slowed down but if it is spanning the bilayer the contact to glass should significantly slow down the peptide diffusion.

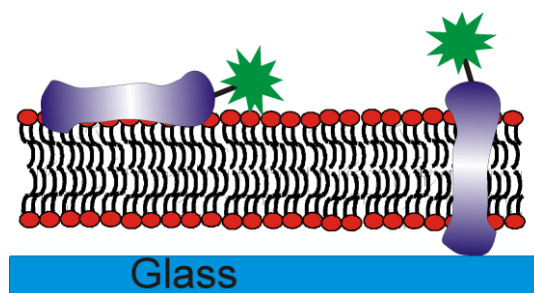


Figure 36: Two possible arrangements of FGFR3(TM) in a lipid bilayer. Parallel orientation on top of the lipid film (left) and transmembrane configuration (right).

Therefore the diffusion of FGFR3-(TM) was measured in supported lipid bilayer membranes (sBLM) with single molecule tracking (SMT). The setup for single molecule tracking was constructed and single molecule tracking capability was implemented during the course of this thesis. For very slow diffusion SMT is advantageous over FCS because it is a widefield technique that allows for measurement of many scattered particles at the same time. In an FCS experiment one would need to increase the measurement time drastically to obtain enough events in the small confocal observation volume. To prepare sBLMs small unilamellar vesicles from DiPhyPC with a small amount of labelled peptides (molar ration $10^5/1$) were prepared via film rehydration and subsequent extrusion. The lipid-peptide vesicles were then fused on a glass surface to form a supported lipid bilayer. This was now put in widefield fluorescence microscope and the field of view was completely bleached. Then the laser shutter was closed to allow mobile peptides to diffuse back into the observation area. By this only the mobile species can be measured while the immobile ones stay dark after bleaching. After approximately 5 min the excitation was switched back on and time traces of 50 images

were directly recorded with a sensitive CCD camera with a time lag of 400 ms. Trajectories were extracted (Figure 37 A and B) and the mean square displacement (MSD) was calculated. MSD is then plotted versus time as can be seen in Figure 37 C. From the slope of curves the diffusion coefficient can be extracted and a mean value of $D = 0.0075 \mu\text{m}^2/\text{s}$ was obtained. This is about three orders of magnitude slower than the expected 2D diffusion in the unperturbed vesicular system presented in Figure 35. The reason for the very low mobility is the strong coupling of the lipid matrix and the peptide with the underlying glass surface. The observed slow diffusion is a clear indication that FGFR3-(TM) is spanning the DiPhyPC bilayer because only when it stands transmembrane it can interact with the surface. A diffusion coefficient of FGFR3-(TM) comparable to the one obtained here was also found in literature by using fluorescence recovery after photobleaching (FRAP) of FGFR3-(TM) in a supported lipid bilayer of palmitoyl-oleoyl-phosphatidylcholine (POPC).^[86] The diffusion coefficient reported there was $D = 0.0055 \pm 0.0001 \mu\text{m}^2/\text{s}$ which compares well to the measurement presented in this work.

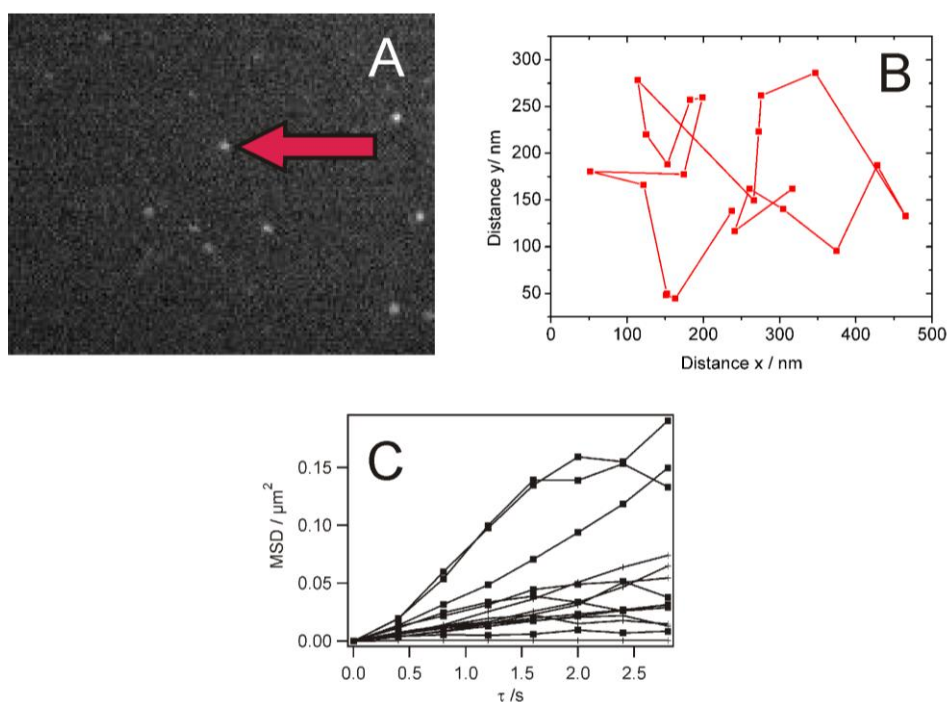
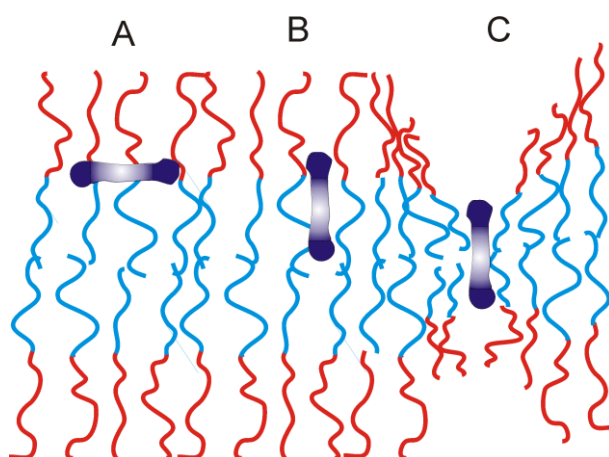


Figure 37: Single particle tracking of FGFR3-TM in a lipid bilayer. (A) Fluorescence image (B) exemplary trajectory of the indicated object in A. (C) calculated mean square displacements.

So in conclusion it can be stated that FGF3(TM) stands transmembrane in the lipid bilayer and diffuses freely with a diffusion coefficient similar to that of the lipid matrix.

Peptides orientation in polymer bilayers. The first question which has to be tested is if the model peptide incorporates into the polymer bilayer in a membrane spanning fashion. This is not trivial because there are two main factors which are fundamentally different in polymer structures compared to lipid systems. First and most important there is a mismatch in the thicknesses of the hydrophobic core of the bilayer and the TM-domain which might prevent the peptide from spanning the membrane. The hydrophobic part of a natural lipid bilayer has a thickness of approximately 3.5 nm while it is in the range of 9 nm in the polymer case. Secondly the used bilayer constituting species are completely neutral which can alter the interactions of the peptide with the hydrophilic part of the polymer film. Due to these changes in membrane architecture there are several possibilities how a hydrophilic helical peptide can associate with the bilayer to reduce its free energy. These possible configurations are depicted in Scheme 25. The first option is an alignment along the bilayer plane as shown in (A). Another possible configuration is a full incorporation of the peptide where one terminus is completely buried inside the bilayer core (B). Even though one hydrophilic tail would be in an unfavourable environment this might still result in gain in energy because the lipophilic transmembrane section of the peptide accounts for 70% of the whole amino acid chain. The last scenario that was also suggested in literature^[167] is full peptide incorporation with a membrane thinning around the peptide. This results in complete spanning of the polymer film(C).



Scheme 25: Illustration of the possible configurations of the hydrophobic peptide within a polymeric bilayer. (A) parallel to the membrane plane (B) perpendicular to the membrane plane.

Circular dichroism (CD) is a method to determine the chirality of optically active structures like proteins or peptides.^[168] Here the interactions of circular polarised light with optically active materials are exploited which show different absorption properties for the different

components of the polarized light. An extension of this technique is oriented circular dichroism (OCD).^[169] When chiral molecules are aligned in one direction OCD can provide information about the orientation relative to the excitation axis.^[170] Transmembrane peptides and proteins that adopt an α -helical conformation in a planar membrane are such aligned optically active materials. Therefore OCD spectroscopy is a suitable tool to analyse orientation of the TM domain of FGFR3 inside the polymer film. OCD spectra were measured on peptide doped polymer films which were drop casted from methylene chloride solution. The films were dried and rehydrated for 30 min before the measurement starts.

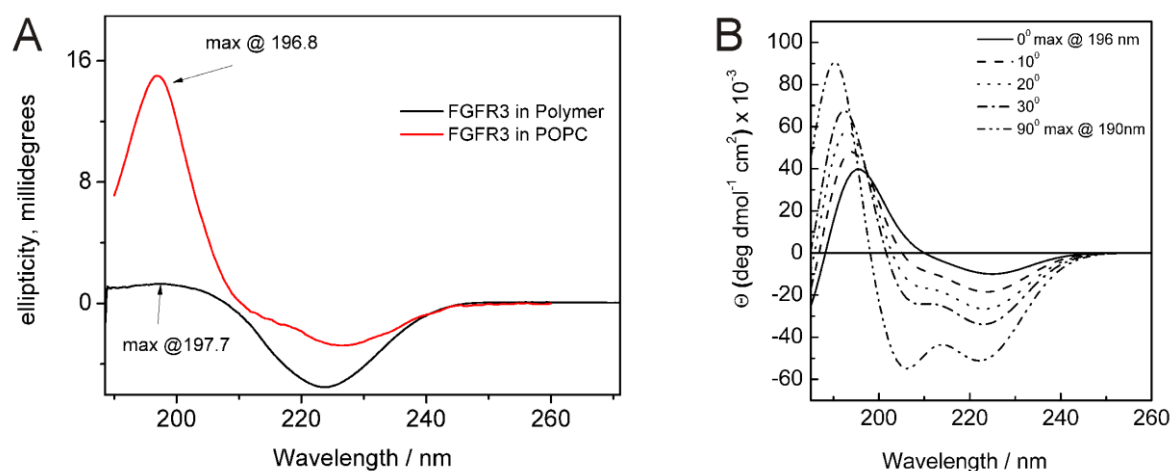


Figure 38: OCD spectra from FGFR3 in lipid (red) and polymer (black) membranes (A). Theoretical OCD spectra calculated for different helix tilt angles are shown in (B).

Figure 38 A shows the OCD spectra of the model peptide FGFR3 mixed in POPC (red line) and polymer bilayers (black line). For additional reference the OCD spectra of an α -helical peptide were calculated for different helix tilt angles according to methods described by Olah and co-workers^[169] (Figure 38B). The maxima of the measured curves are at 196.8 nm and 197.7 nm while the minima are at 226.2 nm and 224.0 nm for the lipid and polymer system respectively. Although the molar fraction of peptide in both samples was the same the signal intensity in the polymer case is much lower for the maximum. This results from the fact that the hydrophobic polybutadien block in the polymer carries a very high number of C=C double bonds which absorb the light in the relevant wavelength range (C-C=C-C $\lambda_{\text{max}}=186$ nm). Therefore the negative signal at around 225 nm gives more information about the peptide orientation. In the case of a peptide orientation at an angle of 90° to the excitation axis would result in an additional signal at around 205 nm. Also the completely random distribution of peptide orientations in a vesicle suspension would yield a second negative component of the signal at wavelengths slightly above 200 nm.^[169] The absence of a second peak at around

205 nm is a clear sign for peptide orientation parallel to the excitation axis and excludes the possibility of horizontally adsorbed peptide strands at the hydrophilic-hydrophobic interface (Scheme 25 A). What can also be seen is that the signal for the polymer-peptide system are broader than the for the lipid architecture which means that the sample is less homogenous. This can either result from inhomogeneity in the polymer film morphology or from a distribution of peptide tilt angles inside the polymer bilayer. A comparison of measured values and theory indicates a slight deviation from the 0° orientation with a helix tilt of maximum $\sim 20^\circ$.

The films for OCD spectroscopy were prepared via dropcasting from methylene chloride solution. It was reported that planar multilayer structures from polymers as well as lipids^[171-172] are obtained by this method. In a study by Reiter *et al.* multilayers were even demonstrated for a PB-PEO polymer comparable to the ones used in this work.^[173] To check whether the hydroxyl terminated PB-PEO 01 really forms multilamellar structures on glass AFM was measured at the edge of a dried and rehydrated film as shown in Figure 39.

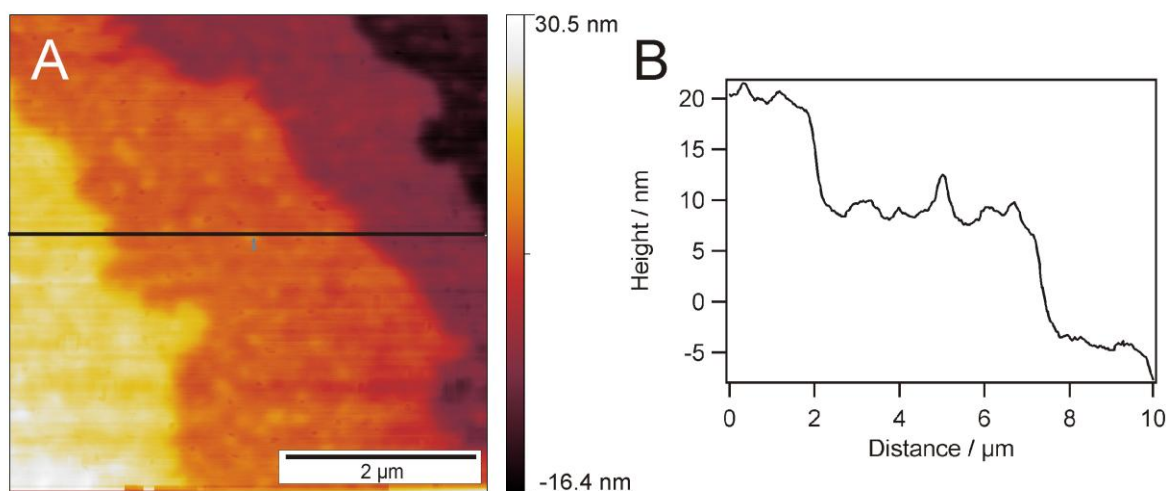


Figure 39: AFM image at the edge of a film from hydroxyl terminated PB-PEO-01 (A) and the corresponding height profile along the indicated line (B).

In Figure 39 A distinct steps indicating single layers are visible and the step heights measured in the profile in Figure 39 B are approximately 14 nm. This compares well to the layer thicknesses measured for polymer films characterised by AFM and SPR in the previous chapters. So this is a clear sign that the polymer films used for OCD experiments form stacks of bilayer structures parallel to the surface.

Peptide diffusion in polymer bilayers. Now that there is a strong indication that FGFR3-(TM) is incorporated in the bilayer peptide diffusion was also studied in vesicles of the two

amphiphilic block polymers introduced above. The fluorescence microscopy image in Figure 40 B shows the location of the fluorescent peptide exclusively along the shell of a giant unilamellar polymer vesicle. In video mode the motions along the shell can be seen.

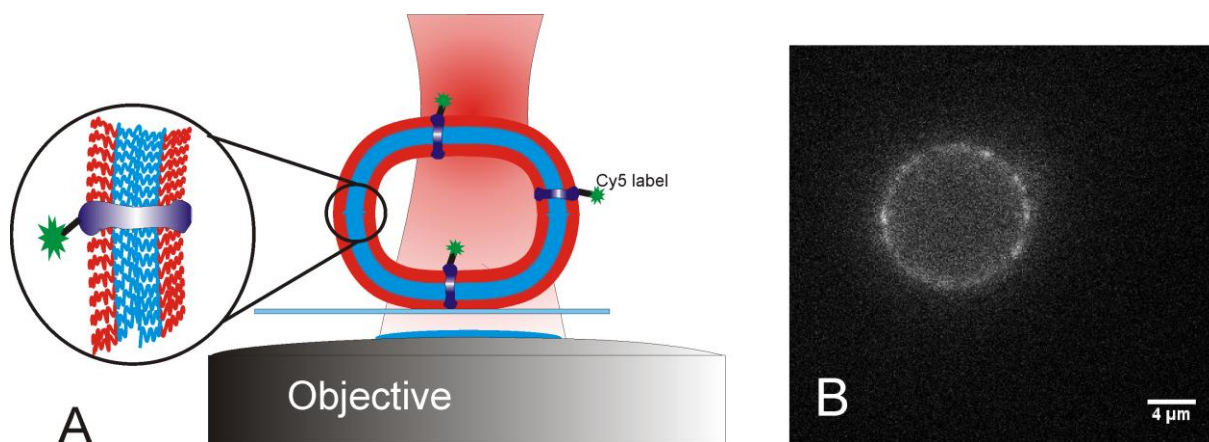


Figure 40: Fluorescently labelled peptide FGFR3-(TM) incorporated into a giant polymer vesicle membrane. (A) Schematic drawing. (B) Fluorescence microscopy image.

FCS measurements of Cy5-labelled FGFR3-(TM) in polymer GUVs of two different molecular weights are shown in Figure 41 A. Fitting of the autocorrelation curves (Figure 41 B) yields diffusion coefficients of 0.95 and 1.3 $\mu\text{m}^2/\text{s}$ for the long and the short polymer respectively. The difference in D between the short PB-PEO 03 and the longer PB-PEO 01 are 38%. About the same ratio of diffusion coefficients between the two polymer species was observed for the lipophilic dye Bodipy 630/650 in PB-PEO 01 and PB-PEO 03. Also the absolute values are almost exactly the same as for the two hydrophobic fluorophores and the estimated self-diffusion studied in the first part of this chapter. This is somehow surprising if one assumes that the peptide spans the full bilayer because then it should feel an increased friction leading to a slower diffusion. It rather suggests that FGFR3-(TM) is only located in one of the membrane sheets like the two lipophilic dyes. The comparison of the diffusion of FGFR3-(TM) in the lipid systems to the two polymer species shows a decrease in mobility of a factor of five. The same difference in mobility was also observed for the hydrophobic dyes in chapter 5.3.2.

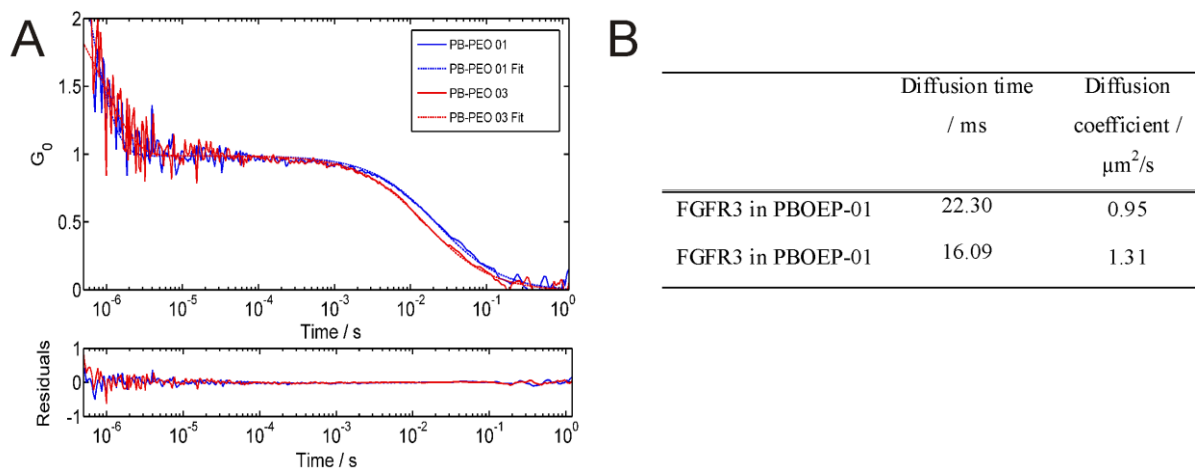


Figure 41: FCS autocorrelation curves of Cy5 labelled FGFR3-TM in giant polymer vesicles of two different molecular weights PB-PEO 01: $M_w = 4150$ g/mol; PBPEO 03: $M_w = 2050$ g/mol (A) and the results from the fitting procedure (B).

All the observations of the diffusion behaviour in combination with the OCD measurement suggest that FGFR3-(TM) is incorporated in the hydrophobic core but probably does not span the full bilayer because of the increased hydrophobic thickness. A situation where the α -helix is located in one bilayer sheet perpendicular to the bilayer plane (Scheme 25 B) seems to be the most likely scenario but a full spanning of the bilayer cannot be fully excluded.

5.4. Summary and Outlook

In this chapter the diffusion dynamics of fluorescent probes and an α -helical model peptide in lipid and polymeric giant unilamellar vesicles is described.

In the first section it was shown that the diffusion of the two lipophilic dyes Bodipy 630/650 and DID reflects the lipid self-diffusion in the bilayer. The same dyes were also measured in polymeric bilayers of two different chain length where they showed diffusion which was slowed down by a factor of 4 compared to the lipid environment. The molecular weights of the polymers with similar block ratios were 4100 g/mol and 2050 g/mol respectively. While the chain lengths differ by a 100% the diffusion in these polymers only varies 10-30%. If the dye diffusion in polymer reflects the mobility of the 2D matrix as well as it does in the lipid case, this contradicts a proposed *Rouse* scaling proposed in literature. Polymer self-diffusion was also analyzed but measurements were hampered by strong background of free tetramethylrhodamin dye in solution. This only allows a rough estimate of the diffusion coefficients. If the estimation is correct, the value of the diffusion coefficients is exactly in the

same range of the values for Bodipy and DID. In analogy to lipid experiments this would mean that measurement of dye diffusion is able to probe the diffusion dynamics of a polymer bilayer. Apart from dye diffusion also the lateral mobility of the transmembrane peptide FGFR3-(TM) in polymeric and lipid bilayers was measured. Successful membrane incorporation of the model peptide in lipid environment was demonstrated with single molecule tracking experiments in sBLMs which were performed on a self-constructed setup during the course of this thesis. The oriented circular dichroism spectra of the peptide in the polymer bilayer show that the peptide is oriented perpendicular to the bilayer plane which suggests a transmembrane configuration. The single molecule diffusion measurements of FGFR3-(TM) show full mobility of the peptide in the polymer bilayer plane of two different polymer chain lengths. The absolute peptide diffusion coefficients as well as the ratio between long and short polymer are comparable to the values for the lipophilic dyes in polymer.

For the first time the diffusion behaviour of two lipophilic dyes and a transmembrane peptide in polymer giant unilamellar vesicles was measured with single molecule techniques. Since the lateral mobility is a prerequisite for many transmembrane proteins to function, the results presented here should trigger further biofunctionalisation attempts of polymeric membranes with more complex protein structures. There are also some open questions which have to be answered. First the experiments on the self-diffusion of the polymer have to be repeated after removal of all unbound dye to get reliable data. The complete removal of the free dye label tetramethylrhodamin should be achieved by preparative HPLC.

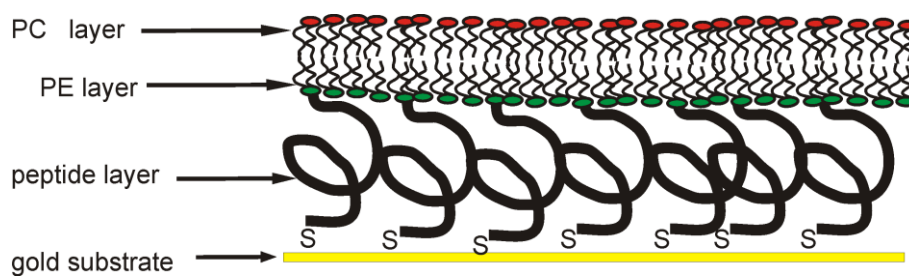
One hurdle that has to be overcome if more demanding proteins shall be incorporated in polymeric bilayer is the preparation of protein functionalised polymeric bilayers. Most proteins do not retain their structure when they are directly involved in the electroformation process. Here they are dissolved in organic solvents and dried on a glass support. Therefore new incorporation strategies for vesicle preparation have to be considered. A promising way for protein insertion after vesicle formation could be the so called *in vitro* expression.^[174] For this a cell extract containing all components necessary for protein translation/transcription is used together with the DNA coding for that protein. In the presence of a suitable model membrane the whole expression mechanism can then introduce the expressed protein directly into the bilayer structure. One advantage if this technique would be that no protein stabilizing detergents are needed.

6. On the Preparation of Planar Lipid Bilayers on Peptide Support

6.1. Introduction

Supported lipid bilayers also termed (sBLM) are a quick and easy route to planar lipid layers and they have proven their value in studies on lipid dynamics^[175-176], cell adhesion^[28] and many more.

Apart from the many advantages sBLM have there are some serious drawbacks. One is the limited stability of these model membrane systems. Typically they have to be freshly prepared and directly used since they decompose within days. Other problems arise when sBLMs are used for transmembrane protein studies. Since the bilayer is directly coupled to the surface there is no space for bulky domains reaching far outside the bilayer. The interactions of the protein with the glass support can immobilise them and thus lead to a loss of functionality. Also the lack of a reservoir for analytes and ions on the bottom side makes many transmembrane proteins studies impossible. For this purpose various ways were developed to decouple the bilayer from the support. As detailed the general introduction (chapter 1) there are polymer supported bilayers as well as tethered bilayers which use a synthetic anchor lipid. While polymer systems sometimes have a too loose support that complicates bilayer formation a SAM can form a support that is too closely packed. A compromise can be the so called peptide tethered bilayer membrane (Scheme 26). By using self assembly of a stiff α -helical thiopeptide on gold support a defined anchor region can be formed which still has enough space to introduce bulky TM-proteins.^[36] The peptide was subsequently functionalised with a lipid on the surface via amide bond formation in organic solvents like DMF. In the past an attempt has been made to prepare an alternative peptide tethered system in our group^[177] that only uses chemistry in aqueous solution. The reason why one wants to circumvent organic solvents in the preparation procedure is that some biological systems are highly sensitive towards these molecules and can result in a loss of function.



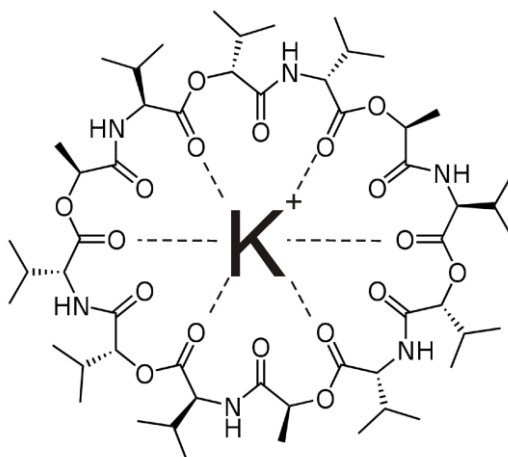
Scheme 26: Peptide tethered bilayer membrane target structure

In short the procedure for the aqueous coupling route is described. Self assembled monolayers of a thiopeptide (P19) derived from the α -laminin subunit were prepared from aqueous solution. The carboxylic acid groups at the C-termini of the peptide chain facing to the surface were converted into active esters with EDC/NHS chemistry.^[178] To the activated end groups dimyristoyl-phosphoethanolamine (DMPE) was added in a Triton-X 100 detergent solution to couple it to the surface forming a lipid monolayer. Vesicles were added to this surface to complete bilayer formation via vesicle spreading.

The procedure was carried out *in situ* in the sample cell and was followed with SPR spectroscopy. Plasmon spectra could be interpreted as a successful membrane built-up but a microscopic characterisation of the morphology was still pending. Now in this work the architecture was also analysed with AFM in liquid and combined SPR/EIS measurements.

In the first part of the results section the characterisation of the existing procedure is presented. Significant shortcomings of this procedure were found. For this reason in the second part an alternative preparation route to a peptide tethered lipid bilayer is shown. One main problem in the previous route is the low solubility of lipids in water so that they cannot be coupled under aqueous conditions. Therefore coupling was carried out in chloroform. By this sufficiently functionalised peptide layers with a hydrophobic surface could be generated. To complete the bilayer assembly the so called rapid solvent exchange method was used because it is known to form bilayers with a high surface coverage even on moderately hydrophobic support.

To confirm the successful bilayer built up on a large scale the mobile ion carrier peptide valinomycin was incorporated into the bilayer architecture. Valinomycin is an antibiotic from *Streptomyces fulvissimus*^[179] that consists of three identical units formed of D-valine, L-valine, L-lactic acid and D-hydroxyisovaleric acid. The chemical structure is depicted in Scheme 27.



Scheme 27: Structural formula of valinomycin

In the absence of potassium ions it can adopt various configurations.^[180] If there is potassium in solution the six ester carbonyl groups can complex the potassium so that the hydrophobic side groups the ring point outwards. Consequently the complex can pass the lipid bilayer which is not possible for the unshielded ion. In this complex the ion is in an environment that resembles the hydration shell. The lipophilic groups on the outer part now allow diffusion through the membrane barrier. The complexation geometry is optimised for potassium so that it has a selectivity over sodium of 1000/1.^[181] In medicine valinomycin can be used as an antibiotic that releases potassium from bacteria so that it interrupts protein synthesis.^[182] In artificial lipid bilayer systems it is often used as a robust model system to evaluate electrochemical properties.^[30]

6.2. Experimental

Surface preparation in aqueous environment The previous architecture was described by Wiltschi *et al.*^[177] The SPR flow cell (volume ~60 μ L) was filled with P19 solution (0,01 mg/ml in water) and incubated for 90 min. The surface was rinsed with 1 mL of ultra pure water and afterwards filled with a 1:1 mixture of NHS solution (0.1 M) and EDC solution (0.4 M). Surface was allowed to react for 10 min. To the activated surface a DMPE suspension (0.2 mg/ml in PBS with 0.1% Triton-X-100 (1mg/ml, 1,6 mM)) was added directly without an intermediate rinsing step and allowed to incubate for 90 min. After the reaction the cell was rinsed with 2 mL of phosphate buffer (PBS). Small unilamellar vesicles from soy bean PC were prepared by film rehydration and subsequent extrusion through a polycarbonate

membrane (50 nm pore size). The freshly prepared vesicle suspension was added directly and incubated for 90 min followed by rinsing with 2 mL of PBS.

Surface functionalisation for rapid solvent exchange. The coverage of the gold substrate with the thiopeptide P19 (CSRARKQAASIKVAVSADR;Cys-Laminin A chain from, Sigma Aldrich) was achieved by self assembly from aqueous solution with a concentration of 0.02 mg/mL. Freshly prepared gold slides were covered with a big drop of peptide solution and were incubated in a wet Petri dish for 16 h. The prepared monolayer was rinsed with ultrapure water.

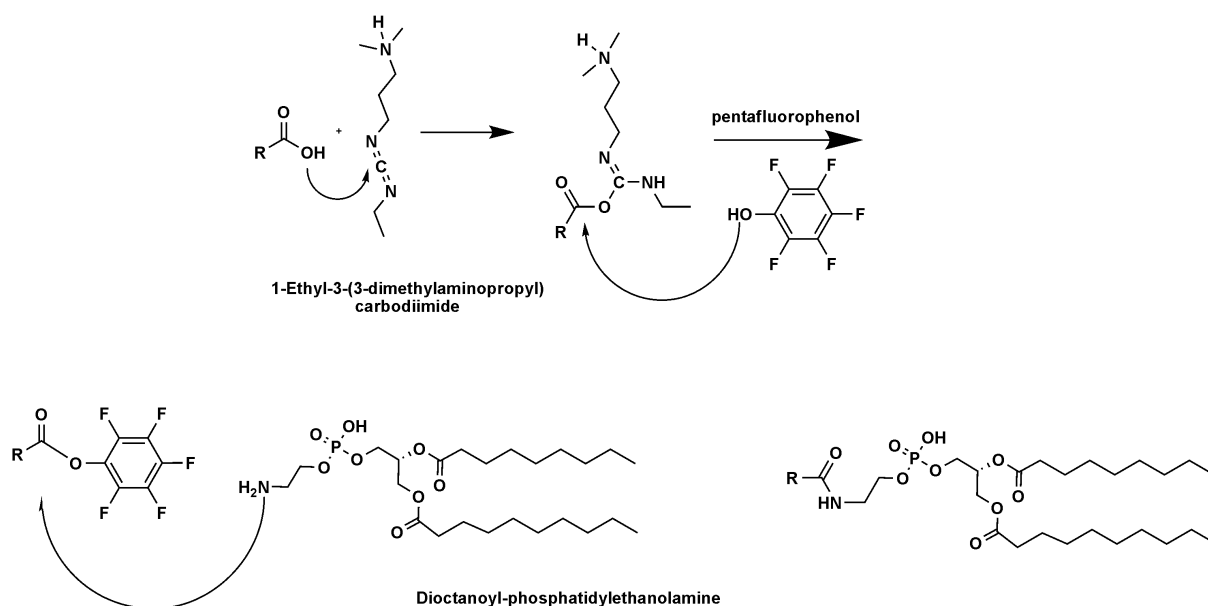
The conversion of the free carboxylic acid to an active ester was carried out in chloroformic solution (p.a. grade) to prevent hydrolysis. Different kinds of active esters were prepared.

10 mg of N-hydroxysuccinimid (NHS) were dissolved in 200 μ L of chloroform to yield a 0.42 M solution. 15 mg of 1-Ethyl-3-(3-dimethylaminopropyl) carbodiimid hydrochloride (EDC) was dissolved in 200 μ L of chloroform to yield a 0.39 M solution. The two were mixed together and directly applied to a fresh self assembled peptide layer.

Second 15 mg of sulfo-NHS were dissolved in 200 μ L of chloroform (0.35 M). The solution was mixed with the similar EDC solution as described in 1.

Pentafluorophenol (PFP) was heated to 60°C in a water bath to melt the solid. 10 μ L of PFP were added to 400 μ L of EDC solution (0.16 M) so that the ratio of PFP to EDC was 1.47:1. The fresh mixture was also directly applied to the peptide SAM.

The slide with the reaction droplet was put in a small Petri dish and tightly sealed to prevent evaporation of the chloroform. After for 45 min the surface was washed thoroughly with absolute ethanol. In the following step 500 μ L of 1,2-dioctanoyl-sn-glycero-3-phosphoethanolamine (DiOctPE) solution in chloroform (1 mg/mL) were incubated on the surface for 60-70 min.



Scheme 28: Reaction scheme of the peptide functionalisation using a pentafluorophenol active ester.

Rapid solvent exchange. To the lipopeptide functionalised surface 1 mL an ethanolic solution of DOPC (1,2-dioleoyl-*sn*-glycero-3-phosphocholine, 5 mg/mL) was added and incubated for 30-45 min in a flow cell. Then the surface was quickly rinsed with at least 20 mL of pure water by pressing it through the cell with a syringe. The produced surfaces were analysed by atomic force microscopy (AFM) and electrochemical impedance spectroscopy (EIS). For AFM imaging the flow cell was opened under water and transferred to a small Petri dish without exposing the surface to air. For EIS measurement the rapid solvent exchange step was carried out directly in the sample cell.

Combined EIS/SPR measurement. Measurements were done in a sample cell of 1 mL volume where the gold slide is monitored in the regular SPR configuration while it serves as the working electrode at the same time. Reference and counter electrode both reach into the sample volume through a small access from the side. EIS spectra were recorded with a regular Autolab System as used in single measurements.

6.3. Results and Discussion

6.3.1. Analysis of the Existing Surface Preparation Procedure

The AFM images were recorded at Veeco GmbH, Mannheim Germany together with Sandra Ritz, Massimiliano Luchi and Alexandre Berquand (Veeco).

AFM was measured on a Veeco Bioscope II in contact mode with a silicon nitride tip with a nominal spring constant of 0.01 N/m. Only vesicle adsorption was imaged in tapping mode. All experiments were carried out on flat gold surfaces prepared by template stripping (see chapter 2). The surface typically exhibits a mean surface roughness of 0.3 nm (RMS) over $1 \mu\text{m}^2$. Figure 42 shows the AFM image of the peptide covered gold substrate after self assembly. In the corresponding height profile it can be seen that peptide layer is homogeneous with some extra material adsorbed on the surface which could not be rinsed of. Small defects in the peptide layer can be measured in the cross sections when zooming in (graph not shown) which have a depth of about 2 nm.

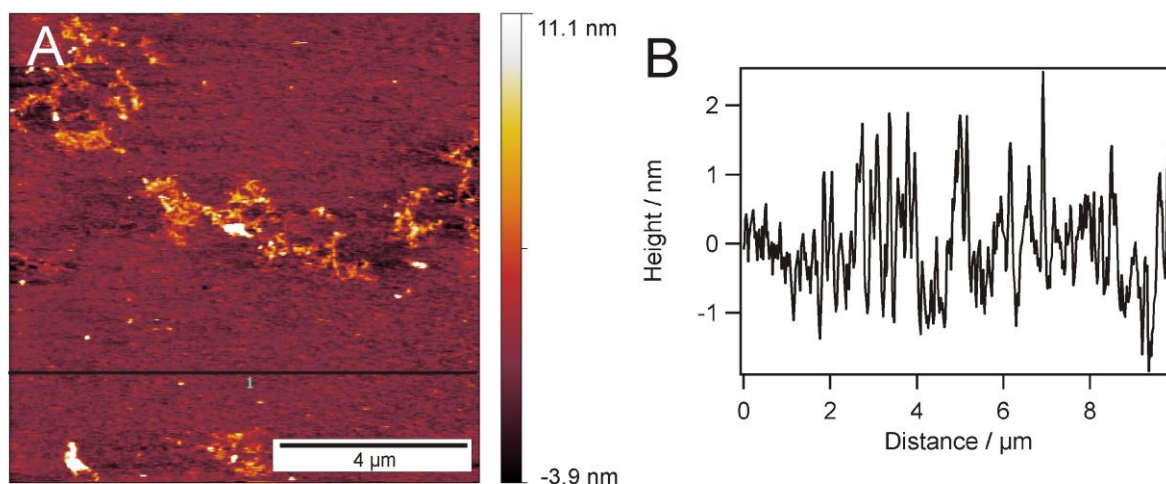


Figure 42: AFM image of the peptide covered gold substrate A) and the corresponding section B)

In the next step the acid end groups are activated with EDC/NHS in water for 10 min but no longer to prevent hydrolysis. To couple the DMPE to the active ester, a solution of the lipid in phosphate buffer (PBS, pH 7.4) was added directly to the surface without rinsing. Due to the insolubility of DMPE in water 0.1% (1 mg/mL, 1.6 mM) Triton-X 100 was added as a detergent. This concentration is more than seven times above the critical micelle

concentration of Triton ($CMC_{TritonX} = 0.22 \text{ mM}$) which means that a lot of micelles are present in solution and on the surface. The AFM image of the prepared surface in Figure 43 shows many little objects in the height range of 4-6 nm. This could either be pure Triton micelles or mixed DMPE/Triton micelles. The measured contact angle to water is 45° which is exactly the same value as for the pure P19 monolayer.

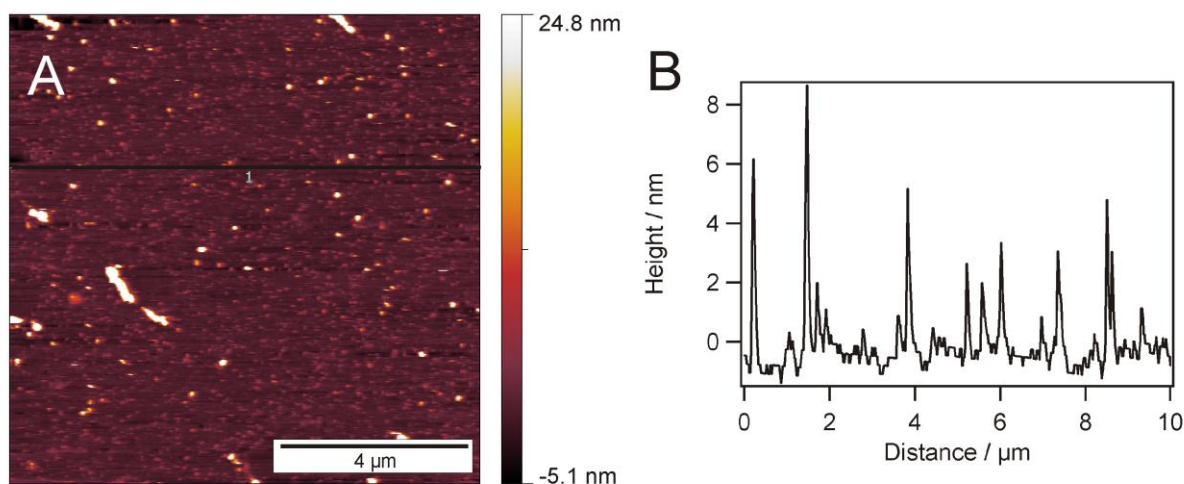


Figure 43 AFM image of the surface after the coupling procedure of DMPE (A) and the corresponding height profile (B).

In the final step a vesicle suspension of soy bean PC (1 mg/mL) was added to the surface to fuse on this support and incubated for 30 min. After rinsing the surface gently a picture was recorded which can be seen in Figure 44.

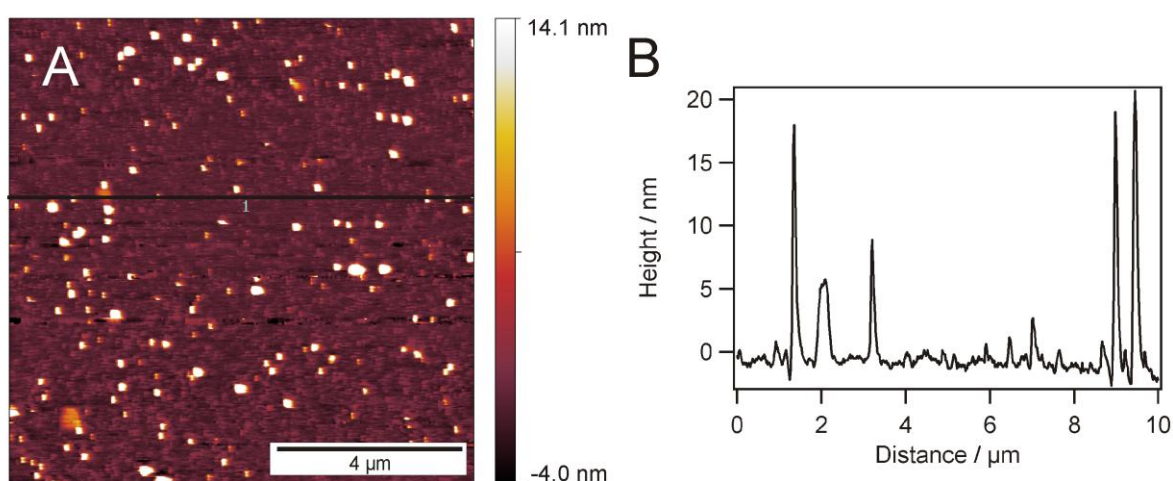


Figure 44: AFM image after vesicle addition (A) and the corresponding height profile along the indicated line (B)

Scattered objects can be seen on the surface which have a heights between 20 nm and 50 nm according to the height profiles. This corresponds to the height of intact vesicles which are adsorbed on the surface. In between the higher objects there are still the small objects visible that were already present after DMPE addition.

On the surface there are only very rare signs of vesicle fusion. For example in the lower left corner of Figure 44 A a small patch might be seen. In general there is no vesicle spreading occurring on the surface.

To validate the AFM results, a complementary measurement was carried out where the membrane preparation procedure was simultaneously monitored with SPR and EIS (Figure 45). The SPR kinetics measured at a constant angle is depicted in blue. The first steps of the architecture assembly were done in ultrapure water (MilliQ, 18.2 M Ω) to reduce the ion strength and reduce the likelihood of hydrolysis so that it was impossible to measure EIS until 280 min. The SPR signal shows adsorption of the material for every single step as described in the experimental part but no statement about the surface structure can be made.

- 0-200 min: adsorption of 19 and rinsing with water
- 200-210 min: incubation with NHS/EDC

The change in signal results from a change in refractive index of the solution and cannot be interpreted as high mass adsorption.

- 210-280 min: incubation with DMPE to couple to the active ester
- 280 min rinsing with PBS
- 300: addition of soy bean PC vesicles

The biggest increase appears when the soy bean PC vesicles were added in phosphate buffer. On the first sight the SPR-trace could be interpreted as a successive built-up of the layer system. On the contrary, the EIS signal in Figure 45 depicted in red shows that the resistance does not change upon vesicle addition and stays on a very low value of a mere 15 k Ω ·cm². This means that there is no electrochemical sealing and therefore no planar bilayer system. This is consistent with the AFM image in Figure 45 after vesicle addition which also showed no planar lipid layer structure.

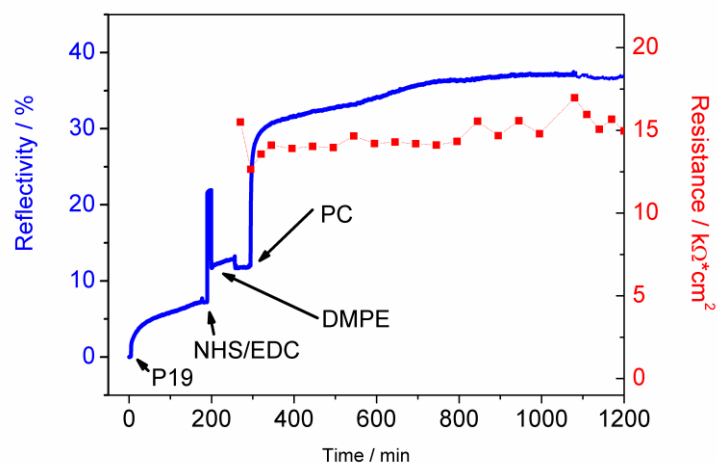
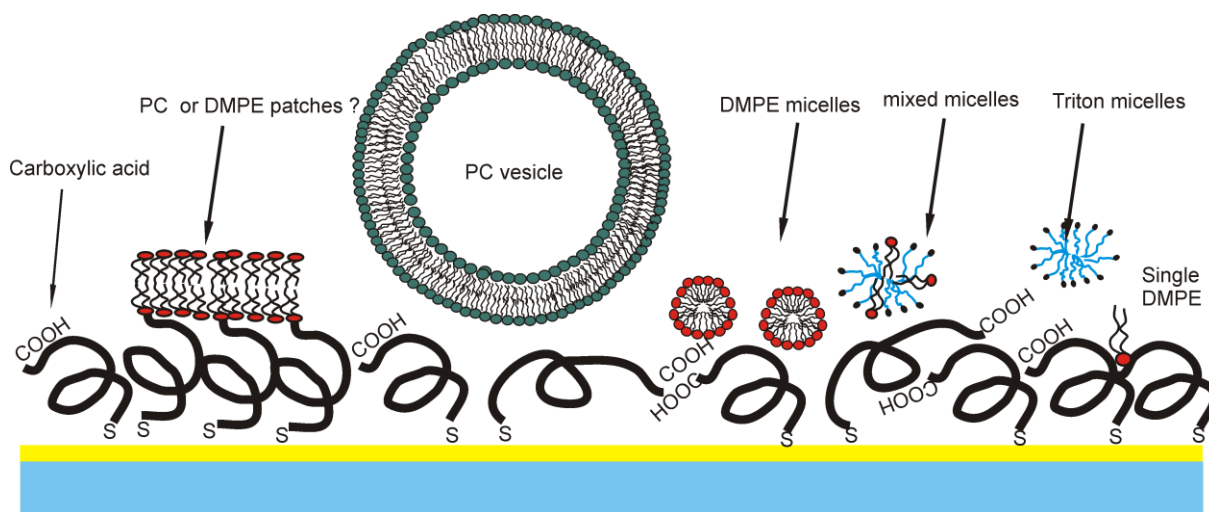


Figure 45: Combined SPR and EIS measurement of the membrane preparation procedure. EIS measurements of the resistance is shown as red symbols while the SPR reflectivity is depicted as the blue line.

So it can be concluded that the surface consists of adsorbed micelles of DMPE, Triton-X 100 micelles and adsorbed soy bean PC vesicles as depicted in Scheme 29. Also a few sparsely scattered membrane patches might be present.



Scheme 29: Schematic drawing of all the different species which are most likely present on the surface.

Previously this surface was used to study the in-vitro expression of an odorant receptor (OR5) from *rattus norvegicus*.^[183] Directed insertion of the receptor into a membrane structure was reported by selective labelling of the N- and C-terminus respectively. Also functionality of the receptor was shown as a change in signal of the amide I band upon addition of the ligand lilyal by surface enhanced infrared absorption spectroscopy (SEIRAS). For the protein insertion itself it does not make a difference if the surface consists of planar layers or vesicular structures as long as there are some kind of lipid bilayer structures present. All the

experimental observations so far can be explained with a system of sparsely adsorbed vesicles. Unfortunately due to the high surface heterogeneity it is simply impossible to tell in which of the possible surface structures the receptor is incorporated which is not suitable if single aspects of the expression mechanism or the protein behaviour shall be studied.

6.3.2. A New Route to Peptide Tethered Lipid Bilayers

Under the circumstances presented above, now the aim was to find a way to prepare a planar lipid bilayer on top of P19-peptide support which is homogeneous over large areas. Therefore every step in the preparation procedure was analysed and optimised. The work on the surface chemistry optimisation was carried out in cooperation with Alexander Körner during his diploma thesis which was done between November 2008 and July 2009 at the MPI for Polymer Research and is filed in the department of chemistry at the University of Mainz.

Optimisation of the coupling chemistry on the surface. The approach that was chosen to change the architecture from the undefined adsorption of various components to a planar bilayer system was to analyse and improve every single step of the procedure. In a first step the amount of P19-peptide was varied and the surface coverage was investigated by quartz crystal microbalance. No increase in surface coverage was observed by using higher thiopeptide concentration. Therefore it is assumed that the peptide concentration of 0.02 mg/mL is enough to fully cover the gold surface with the highest possible packing.

To increase the amount of lipid which is covalently bound to the carboxylic end group of the peptide layer, different coupling reagents were tested for their reactivity to ethanolamine lipids on the surface by contact angle measurements. The results are presented in Table 6.

	Contact angle / °
Pure P19-layer	43,0±4,1
P19-EDC/S-NHS _(CHCl₃) -DOctPE _(CHCl₃)	51,1±3,6
P19-EDC/NHS _(CHCl₃) -DOctPE _(CHCl₃)	51,0±2,8
P19-EDC/PFP _(CHCl₃) -DOctPE _(CHCl₃)	61,9±4,2

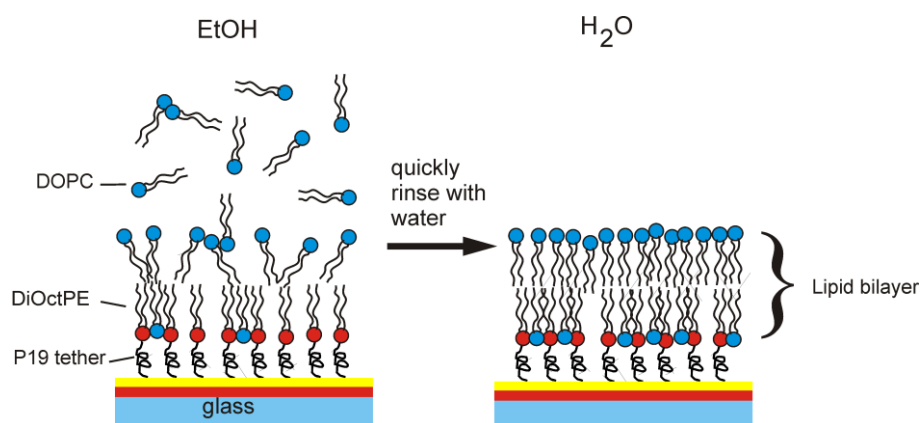
Table 6: Comparison of different ester activation methods by contact angle measurement.

The lipid coupling through pentafluorophenol (PFP) ester activation shows the highest contact angle of the three approaches. It is also reported in literature that PFP forms a more stable ester species towards hydrolysis only reactive to amine groups.^[184] For further surface preparation only the PFP-ester chemistry was used.

To further increase the number of lipids on the surface a modified version of the P19-thiopeptide bearing more carboxyl groups at the end than the native one was used. The last three amino acids of the natural form, alanine, aspartic acid and arginine were replaced by glutamine and two times aspartic acid. As a consequence two acid are groups available on the C-terminus instead of one. If the coupling procedure with PFP-ester and DiOctPE as described above was carried out on this surface the contact angle increased from $41.1 \pm 1.1^\circ$ for the pure P19 layer to $83.8 \pm 1.7^\circ$. The increased number of anchor groups and the resulting rise in surface hydrophobicity should improve the quality of a lipid layer significantly and facilitate membrane build-up.

6.3.3. Bilayer Formation via Rapid Solvent Exchange

In the past vesicle spreading on the peptide support was used to form a lipid bilayer. By AFM it could be shown that this leads only to adsorbed vesicles (Figure 44). An alternative method to produce lipid bilayers on top of this loose peptide support exhibiting a rather low hydrophobicity is the so called rapid solvent exchange which is drawn in Scheme 30. The basic principle is as follows. An ethanolic solution of a lipid is applied directly to a hydrophobic support at a relatively high concentration of 5-10 mg/mL. This solution is allowed to incubate for about 15 min. Then the lipid solution is quickly replaced by pure water or buffer solution. Most of the dissolved lipids are washed away but the ones which are in very close proximity to the surface can reduce their free energy by orienting towards the tethered lipids. This results in lipid bilayer structures. The method was first reported by Cornell *et al.*^[185] and Lösche and co-workers showed that this procedure also works on a moderately hydrophobic support.^[32]



Scheme 30: Schematic representation of the membrane formation via rapid solvent exchange.

Both the optimised P19-lipid layer as well as the lipid bilayer were characterised with AFM. Figure 46 shows the lipid functionalised P19-layer (A) and the corresponding height profile along the indicated line. The surface is more or less homogenous with some objects scattered on the surface which are up to 10 nm in height. These are probably aggregates/micelles of DiOctPE. Some of the roughness can also be attributed to the surface roughness of the underlying gold layer which was prepared by thermal evaporation.

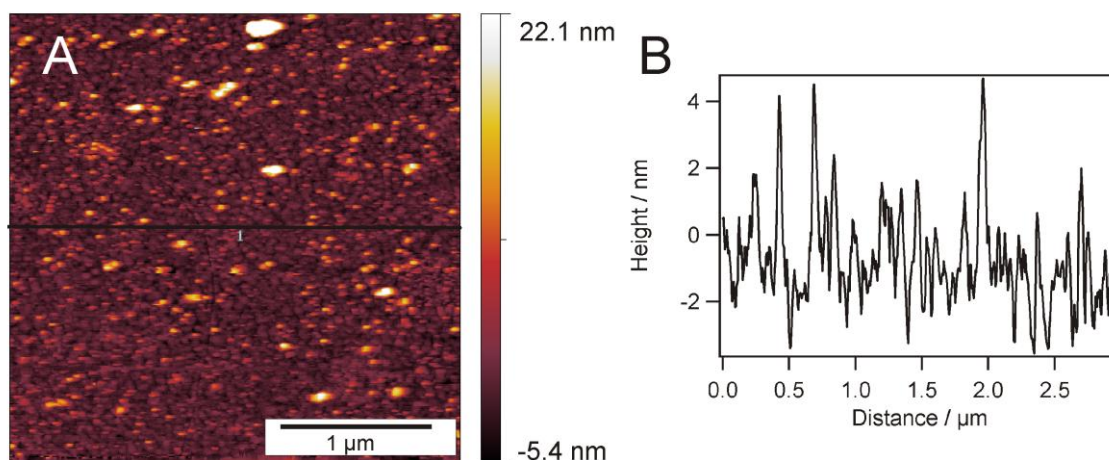


Figure 46: AFM image of the lipid functionalised peptide monolayer (A) and the corresponding height profile along the indicated line (B).

On a substrate from the same batch as the one in Figure 46 a lipid bilayer was formed by the rapid solvent exchange method. After incubating with the ethanolic lipid solution for 30 min and rapidly rinsing with ultrapure water the samples was imaged under the AFM in liquid as shown in Figure 47. Most of the small objects which were visible on the monolayer disappeared and a mostly homogeneous lipid layer has formed. The fact that the bilayer is really present can be seen in regions where the horizontal line defects along the fast scanning

axis are visible. These defects only occur when the deflection setpoint in intermittent contact mode is lowered which exerts a higher force on the sample. This leads to defects in the lipid bilayer which are induced by the cantilever and they only appear when the deflection setpoint is reduced which leads to higher force on the surface. The higher the force is the more often the cantilever snaps into the membrane and creates defects which have an average depth of 4.5 nm as can be seen in the height profile in Figure 47 B. This layer thickness is exactly what one would expect for a lipid bilayer.

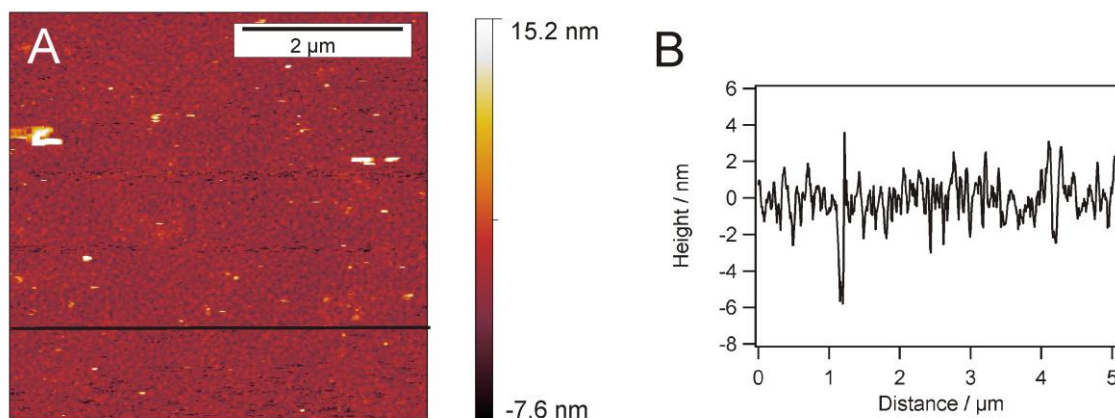


Figure 47: AFM image of the surface after rapid solvent exchange (A) and the corresponding height profile (B).

To gain some more insight into the mechanical properties of the two surfaces now force-distance curves were recorded. In Figure 48 A the F-d-curve on the monolayer shows no significant differences in the approach and retraction curve. This is the case when no strong adhesive or repulsive forces are present. This is the expected behaviour for the lipopeptide monolayer.

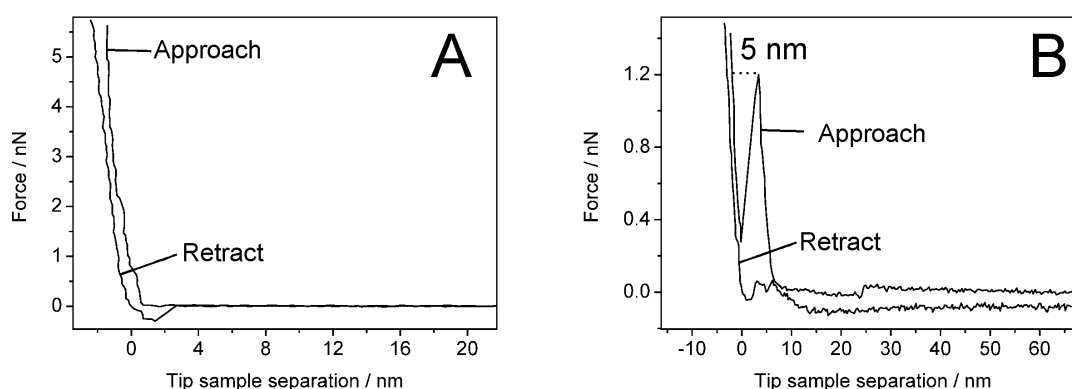
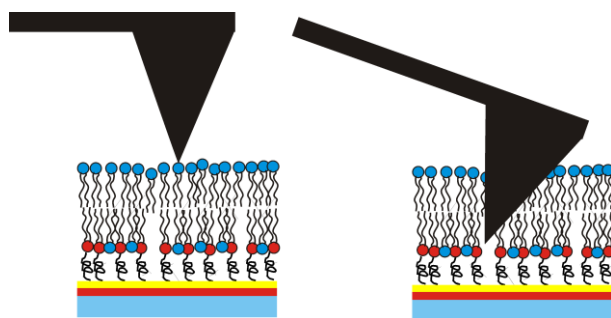


Figure 48: Force-distance measurements carried out on the thiopeptide monolayer (A) and the bilayer structure after rapid solvent exchange (B).

The force-distance curve recorded on the completed bilayer is presented in Figure 48 B and shows a completely different behaviour. Since there is a lateral pressure within the membrane plane that has to be overcome, a rise of the force curve can be observed at the beginning. At a certain point, the applied force is high enough and the cantilever snaps into the bilayer, which can be seen at a distance below 10 nm where the force temporarily decreases until the lower part of the substrate is reached. This is schematically drawn in Scheme 31. This step is characteristic for supported bilayers and has been observed for various lipid bilayer systems.^[110] What is also important is that the jump in the force-distance curve appears even after several approach-retract cycles which shows that the membrane is mobile enough to cure the small hole made by the cantilever. The width of the jump corresponds to approximately 5 nm, which is the thickness of a complete lipid layer. Since the cantilever was not calibrated and the nominal spring constant was taken for scaling, it was not possible to determine absolute force values from these measurements. However, a qualitative statement can be made and the presence of the bilayer can be confirmed.



Scheme 31: Sketch on how the AFM cantilever protrudes the lipid bilayer upon increased force.

In order to study the membrane preparation not only locally with AFM but also on a larger scale, upon addition of the second lipid layer electrochemical impedance spectroscopy was performed. The data representation in the Bode plot shows a large change in the phase angle as well as the impedance $|Z|$ (see Figure 49 A). The data is fitted to the equivalent circuit shown in Figure 49 C. Instead of a perfect capacitor in the RC-element a constant phase element (CPE) is used. This represents the inhomogeneity on the surface since a CPE can be described as many different valued capacitors distributed on the surface. The resistance increases by a factor of 5.5 from $3.5 \text{ M}\Omega\cdot\text{cm}^2$ to $19.4 \text{ M}\Omega\cdot\text{cm}^2$ while the capacitance decreases from $24 \mu\text{F}\cdot\text{cm}^2$ to $11 \mu\text{F}\cdot\text{cm}^2$. The big increase in the resistance shows that the surface gets really electrically sealed by the addition of a layer via rapid solvent exchange. Regarding the resistance of the created system the electrochemical sealing is high enough to see the small changes which might be introduced by charge transporting transmembrane-

proteins like carriers or pores. The high value of the capacitance is not typical for a complete lipid bilayer which means that there are still many defects in the architecture which lower the detected density of material. On the other hand the visible change from the monolayer to the bilayer shows that a significant amount of material is deposited on the surface.

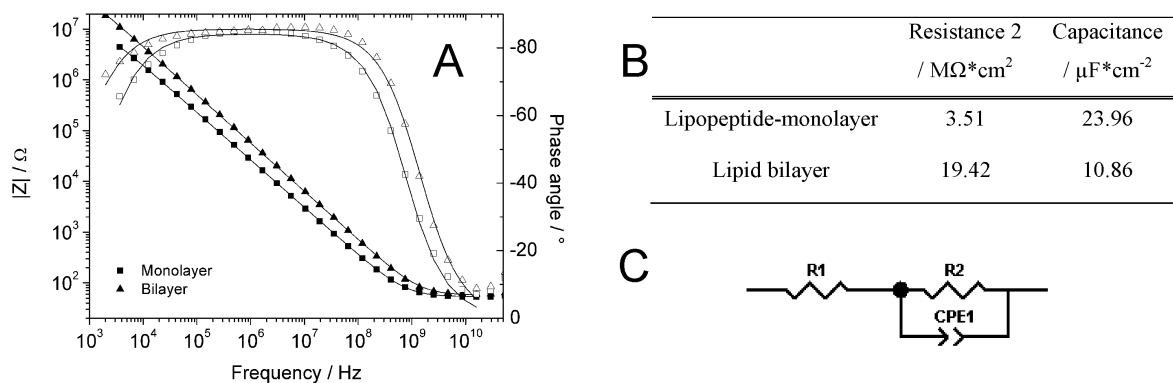


Figure 49: Bode plot of the impedance data (symbols) from the surface before and after membrane build-up via rapid solvent exchange and fitted curves (lines) (A) and the results of the fitting procedure (B). The equivalent circuit model used for fitting is shown in (C)

6.3.4. Interactions of Valinomycin with the Bilayer Membrane

Finally it was tested if the membrane peptide valinomycin can be incorporated into the lipid bilayer architecture in a functional way. Valinomycin is a cyclic model peptide with the ability to carry ions across the membrane. It is used as an antibiotic and it is selective for potassium ions over sodium ions. Upon addition of valinomycin to a lipid bilayer it spontaneously incorporates into the hydrophobic core and changes its electrochemical properties. By this it is possible to probe the large scale sealing properties. Only if the bilayer surface coverage is sufficiently high it is possible to see the reduction in resistance in the presence of potassium ions. In Figure 50 A the electrochemical impedance data are shown in the Bode plot. Symbols indicate measured data and lines show the fit results.

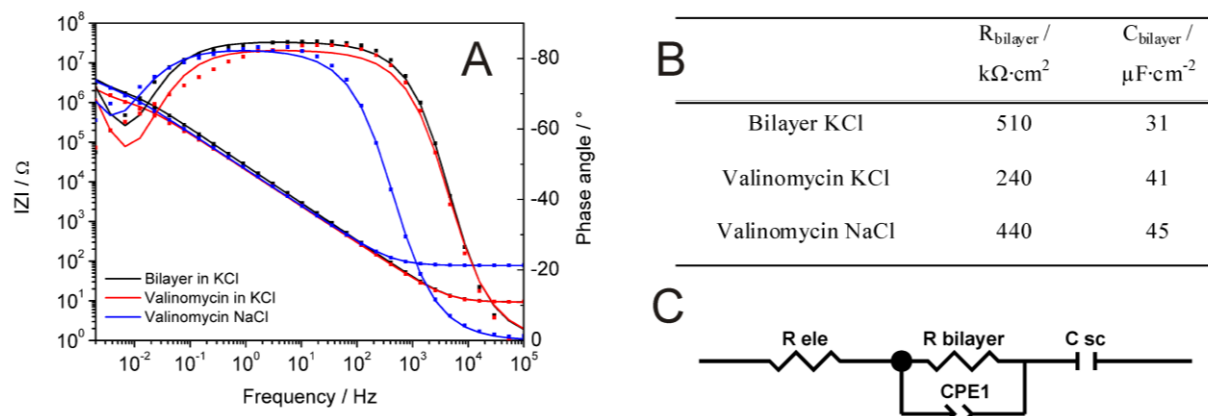


Figure 50: Electrochemical impedance spectra in the Bode plot representation (A) with the fit results (B) and the used equivalent circuit model.

The black curve represents the pure bilayer in the presence of 1 M KCl solution. This is a very high salt concentration resulting in a low electrolyte resistance of $28 \Omega \cdot cm^2$. The bilayer resistance of $510 k\Omega \cdot cm^2$ is rather low compared to the values obtained above but the high phase angle indicates reasonable homogeneity. Then $10 \mu L$ of valinomycin in ethanol ($0.5 mg/mL$) were added to the sample cell volume of 1 mL (red) which led to a decrease in resistance to $240 k\Omega \cdot cm^2$. After changing the electrolyte from KCl to 0.1 M NaCl the bilayer resistance returns to about $440 k\Omega \cdot cm^2$ corresponding to an 86% recovery of the initial value. The change in the curve at high frequencies is solely due to the change in electrolyte concentration and has no influence on the bilayer. This shows the successful incorporation of the potassium selective ion carrier peptide. The change in resistance is not as pronounced as would be expected for a defect free system. This can have several reasons. First the underlying P19-layer is not so densely packed which makes the support rough and therefore reduces the electrochemical sealing properties of an attached lipid bilayer. The more defects are present in the lipid matrix the more ions can migrate unhindered across the barrier. A second problem that can arise with the membrane built up through rapid solvent exchange is the formation of multilayer structures. Figure 51 shows the AFM image of additional bilayer patches adsorbed on top of a first layer. The fact that both layers are actually bilayers can be seen at the AFM cantilever induced defect sites in both layers. The height of the both layers can be measured at defects sites to be about 5 nm.

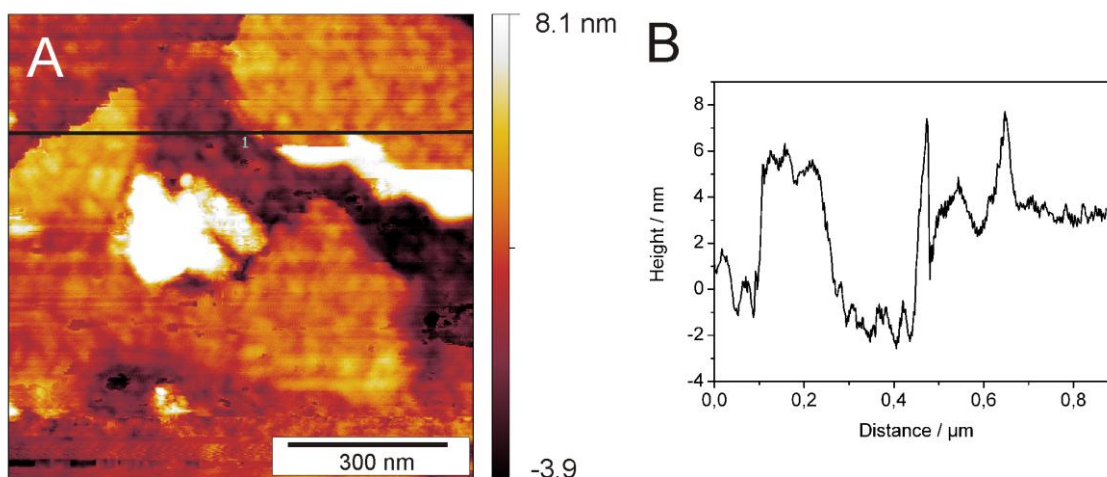


Figure 51: AFM image of patches of lipid multilayers on the peptide support (A) and the corresponding height profile along the indicated line(B). Step heights were measured to be 4.5 nm.

These multilayer structures surely reduce the visible effect of valinomycin because the incorporation of a peptide molecule into a top layer patch does not result in a change in resistance. On the other hand the presence of multilayer patches might be advantageous for fluorescence measurements because the increase distance to the gold surface reduces fluorescence quenching.

6.4. Summary

In summary it can be stated that the previously used peptide supported lipid bilayer architecture was thoroughly characterised which led to the conclusion that the surface is highly inhomogeneous and many different components and morphologies are present. As a solution a planar lipid bilayer on a P19-peptide support was successfully prepared on a large scale by the rapid solvent exchange method. This was monitored locally with AFM imaging as well as on the large scale by EIS measurements. The newly developed system was consecutively used to monitor the incorporation of the ion carrier valinomycin with electrochemical impedance spectroscopy. The experiment showed a reversible decrease of membrane resistance in the presence of potassium ions but no effect when potassium was exchanged by sodium proving the usefulness of the bilayer architecture as a platform for transmembrane protein research. Apart from the methods used here, due to the underlying gold film the system can also be used in future SPR studies with combined fluorescence detection.

7. General Summary and Conclusion

The aim of this work was to explore stable membrane model systems based on block copolymers. In this thesis the successful preparation of various model systems from the amphiphilic diblock copolymer polybutadien-polyethylenoxide and their in depth physicochemical characterization is presented. A peptide supported lipid bilayer systems was developed and characterized in addition to the work on polymer based systems.

In chapter 3 and 4 two complementary routes towards supported polymer bilayers were presented. First the built up through sequential Langmuir-Blodgett (LB) and Langmuir-Schaefer (LS) transfer was demonstrated. This produces well defined bilayer structures over several square centimetres with very few defects and without multilayer formation. Secondly vesicle spreading on various supports was explored as an alternative to the LB-LS transfer. Vesicle spreading on hydrophilic glass support through non-covalent interactions led to individual bilayer patches but no continuous polymer films were formed. On the contrary vesicle spreading on gold through covalent coupling of the polymer layer also led to bilayer structures with very high surface coverage. One advantage of the vesicle spreading approach is the ease of preparation and the possibility to prepare bilayers *in situ*. On the other hand vesicle spreading produces less defined architectures compared to LB-LS transfer because it leads to an increased number of defects and the presence of multilayer structures. Both preparation routes which use covalent coupling of the polymer to the support yield architectures with a thicknesses of 11 - 14 nm. The unambiguous existence of two individual membrane sheets was demonstrated by selective desorption the top layer with an effective solvent. Force-distance (F-d) measurements verify the existence of two individual layers where the top layer exhibits a certain degree of flexibility to cure manually created defects created by the AFM tip.

One key objective of this thesis was the generation of mechanically stable model membranes. Drying experiments of covalently bound bilayer structures showed stability against air for at least 1.5 hours. This is a significant improvement compared to lipid membrane models because they cannot stand such a long drying phase. Further drying for more than 12 hours led to disassembly of the bilayer. That suggests that the presence of residual water is necessary for the long term stabilisation.

Another important aspect that was investigated apart from stability is the possibility to introduce proteins into the presented artificial bilayers. The supported polymer bilayer

membranes were shown to interact with membrane active species. The cyclic peptide polymyxin B and the transmembrane pore α -haemolysin form transient holes and permanent pores in the bilayer respectively.

Knowledge of the diffusion properties of the planar polymer bilayers itself and of diffusing species is important to assess the possibility of proteins to incorporate into the bilayer. In most systems the close proximity of dyes in the bilayer to the gold film hampers fluorescence measurements due to quenching. In principle the polymer bilayers on transparent glass support that are prepared in this thesis pose an ideal alternative to measure diffusion properties with fluorescence techniques. Unfortunately the surface structure is not homogeneous enough to measure in-plane diffusion. Therefore in chapter 5 diffusion dynamics of membrane constituents and external probes was measured in bilayers of giant unilamellar vesicles. The state of the vesicular bilayer is not directly comparable to the diffusion in a supported system because there is no influence by the support. Nevertheless the performed measurements provide valuable insights into the interactions between polymers and incorporated species. Lateral diffusion of the α -helical transmembrane model peptide FGFR3-TM was measured with single molecule sensitivity. The membrane peptide appears to move freely inside the membrane plane. The polymer self-diffusion experiment was greatly hindered by a high fluorescence background so that the mobility of the polymer matrix can only be estimated. Preliminary results suggest a diffusion rate of the model peptide which is similar to that of the bilayer matrix. This points towards a strong coupling of the peptide to the bilayer and at least partly incorporation into the hydrophobic core. These results encourage further attempts to functionalise the polymer bilayer with more complex and sophisticated proteins.

In order to have an appropriate reference system for the polymer experiments described before, the last part of the thesis (chapter 6) deals with the preparation of a lipid based membrane model. Detailed analysis showed a high surface heterogeneity of the previously used system. As a part of this thesis a new route to a tethered lipid bilayer on a peptide support was developed. The bilayer formation on moderately hydrophobic support was achieved through the rapid solvent exchange method. Successful bilayer formation was verified on the microscopic as well as on the macroscopic scale. The applicability of the prepared system for the use in membrane protein research was proven by the functional insertion of the ion carrier valinomycin.

8. Outlook

A general problem all polymer architectures have in common is the question how to introduce proteins into the artificial bilayer environment. Two different strategies can be used.

1) Proteins can be introduced or mixed with the constituents prior to bilayer formation. This has the advantage that the polymer can directly arrange around the protein and host it in the emerging hydrophobic core. Unfortunately most bilayer preparation procedures involve organic solvents (e.g. injection method for polymer vesicles) which are not compatible with many proteins. This largely depends on the kind of polymer used. In a Langmuir film transfer proteins can in principle be introduced into the sub-phase at low surface pressure. The low surface pressure facilitates protein incorporation but the addition to the huge reservoir of the subphase would require unreasonably high amounts of protein which are often not available.

2) Proteins can be incorporated after bilayer formation so that organic solvents are circumvented. Many natural membrane proteins are known to spontaneously insert into lipid membranes. This spontaneous insertion is greatly hindered in polymers due to the decreased bilayer flexibility and the higher hydrophobic thickness. Even temporal destabilisation, e.g. with detergents, is not sufficient to allow protein integration in the hydrophobic core. After incorporation it can be difficult to remove the detergent completely. A way to circumvent detergents or other helping agents in the process of protein incorporation could be the so called *in-vitro* expression. For this method a cell extract containing all the components that are required for protein production, e.g. ribosomes, amino acids, etc., is added to the model membrane architecture. In the presence of the DNA coding for the desired protein the transcription and translation reaction will produce the pure target protein and can potentially insert it directly into the bilayer architecture.

A second aspect of polymer based model systems is bilayer stability. Several ways could lead to a further increase in polymer bilayer strength. The easiest way would be the use of a longer chain polymer which will result in increased interactions due to entanglement and layer interdigitation. This will most certainly be counterproductive for the incorporation of proteins because of the increased hydrophobic thickness mismatch and the increased bilayer rigidity. In an alternative approach could be the addition of ABA triblock copolymer. By introducing

chains which span the whole AB diblock copolymer bilayer the two bilayer sheets could be bound to each other without increasing the bilayer thickness.

The concept of supported polymer bilayers from two individual sheets was demonstrated in this work with PB-PEO diblock copolymers. Polymer synthesis offers a wide variety of polymer architectures. It might be interesting in the future to look for alternative bilayer forming amphiphilic polymer species. To further enhance protein incorporation it might be promising to use more flexible hydrophobic blocks with a lower glass transition temperature than polybutadiene. This would facilitate rearrangement of polymer chains around the hydrophobic domains of proteins. A higher flexibility is particularly interesting for supported bilayer systems with an inherently low mobility due to surface interactions. An example would be amphiphilic AB-diblock copolymers from PEO and poly-dimethylsiloxane (PDMS).

Another issue that has to be addressed in the future is the background of freely diffusing dyes in FCS measurement of the covalently labelled polymer (chapter 5). An appropriate method to remove the unbound dye molecules is preparative high pressure liquid chromatography (HPLC). If clean polymer samples are available reliable values for the polymer self-diffusion can be obtained.

9. References

- [1] *Wikipedia*. Available: http://en.wikipedia.org/wiki/Cell_membrane
- [2] S. J. Singer and G. L. Nicolson, "Fluid Mosaic Model of Structure of Cell-Membranes," *Science*, vol. 175, pp. 720-&, 1972.
- [3] G. Vereb, J. Szollosi, J. Matko, *et al.*, "Dynamic, yet structured: The cell membrane three decades after the Singer-Nicolson model," vol. 100, ed, 2003, pp. 8053-8058.
- [4] P. L. McNeil and R. A. Steinhardt, "PLASMA MEMBRANE DISRUPTION: Repair, Prevention, Adaptation," *Annual Review of Cell and Developmental Biology*, vol. 19, pp. 697-731, 2003.
- [5] R. A. Steinhardt, "The mechanisms of cell membrane repair - A tutorial guide to key experiments," *Cell Injury: Mechanisms, Responses, and Repair*, vol. 1066, pp. 152-165, 2005.
- [6] M. A. Yildirim, K.-I. Goh, M. E. Cusick, *et al.*, "Drug - target network," *Nature Biotechnology*, vol. 25, pp. 1119-1126, 2007.
- [7] A. Yethiraj and J. C. Weisshaar, "Why are lipid rafts not observed in vivo?," *Biophysical Journal*, p. biophysj.106.101931, 2007.
- [8] M. Edidin, "The State of lipid rafts: From Model Membranes to Cells," *Annual Review of Biophysics and Biomolecular Structure*, vol. 32, pp. 257-283, 2003.
- [9] I. Köper, S. M. Schiller, F. Giess, *et al.*, "Functional tethered bimolecular lipid membranes (tBLMs)," in *Advances in Planar Lipid Bilayers and Liposomes*. vol. 3, A. Leitmannova Liu, Ed., ed: Elsevier, 2006, pp. 37-53.
- [10] P. Mueller, D. O. Rudin, H. Ti Tien, *et al.*, "Reconstitution of Cell Membrane Structure in vitro and its Transformation into an Excitable System," *Nature*, vol. 194, pp. 979-980, 1962.
- [11] M. Montal and P. Mueller, "Formation of Bimolecular Membranes from Lipid Monolayers and a Study of Their Electrical Properties," *Proceedings of the National Academy of Sciences of the United States of America*, vol. 69, pp. 3561-3566, 1972.
- [12] A. Schulte, S. Ruamchan, P. Khunkaewla, *et al.*, "The Outer Membrane Protein VhOmp of *Vibrio harveyi*: Pore-Forming Properties in Black Lipid Membranes," *Journal of Membrane Biology*, vol. 230, pp. 101-111, Jul 2009.

- [13] G. Schmies, B. Luttenberg, I. Chizhov, *et al.*, "Sensory rhodopsin II from the haloalkaliphilic *Natronobacterium pharaonis*: Light-activated proton transfer reactions," *Biophysical Journal*, vol. 78, pp. 967-976, Feb 2000.
- [14] E. K. Schmitt, M. Vrouenraets, and C. Steinem, "Channel Activity of OmpF Monitored in Nano-BLMs," *Biophysical Journal*, vol. 91, pp. 2163-2171, 2006.
- [15] R. Kalmbach, I. Chizhov, M. C. Schumacher, *et al.*, "Functional Cell-free Synthesis of a Seven Helix Membrane Protein: In situ Insertion of Bacteriorhodopsin into Liposomes," *Journal of Molecular Biology*, 2007.
- [16] N. Kahya, D. Scherfeld, K. Bacia, *et al.*, "Probing Lipid Mobility of Raft-exhibiting Model Membranes by Fluorescence Correlation Spectroscopy," *Journal of Biological Chemistry*, vol. 278, pp. 28109-28115, 2003.
- [17] J. Korlach, P. Schwille, W. W. Webb, *et al.*, "Characterization of lipid bilayer phases by confocal microscopy and fluorescence correlation spectroscopy," *Proceedings of the National Academy of Sciences of the United States of America*, vol. 96, pp. 8461-8466, 1999.
- [18] S.-i. M. Nomura, S. Kondoh, W. Asayama, *et al.*, "Direct preparation of giant proteo-liposomes by in vitro membrane protein synthesis," *Journal of Biotechnology*, vol. 133, pp. 190-195, 2008.
- [19] S. A. Sanchez and E. Gratton, "Lipid-Protein Interactions Revealed by Two-Photon Microscopy and Fluorescence Correlation Spectroscopy," *Accounts of Chemical Research*, vol. 38, pp. 469-477, 2005.
- [20] C. Yoshina-Ishii and S. G. Boxer, "Arrays of Mobile Tethered Vesicles on Supported Lipid Bilayers," *Journal of the American Chemical Society*, vol. 125, pp. 3696-3697, 2003.
- [21] E. Sackmann, "Supported membranes: Scientific and practical applications," *Science*, vol. 271, pp. 43-48, Jan 1996.
- [22] A. A. Brian and H. M. McConnell, "Allogeneic stimulation of cytotoxic T cells by supported planar membranes," *Proceedings of the National Academy of Sciences of the United States of America*, vol. 81, pp. 6159-6163, 1984.
- [23] L. K. Tamm and H. M. McConnell, "Supported phospholipid bilayers," *Biophysical Journal*, vol. 47, pp. 105-113, 1985.
- [24] H. M. McConnell, T. H. Watts, R. M. Weis, *et al.*, "Supported Planar Membranes in Studies of Cell-Cell Recognition in the Immune-System," *Biochimica Et Biophysica Acta*, vol. 864, pp. 95-106, Jun 1986.

-
- [25] C. A. Keller, K. Glasmästar, V. P. Zhdanov, *et al.*, "Formation of Supported Membranes from Vesicles," *Physical Review Letters*, vol. 84, p. 5443, 2000.
- [26] K. Morigaki and K. Tawa, "Vesicle Fusion Studied by Surface Plasmon Resonance and Surface Plasmon Fluorescence Spectroscopy," vol. 91, pp. 1380-1387, 2006.
- [27] R. P. Richter, R. Berat, and A. R. Brisson, "Formation of Solid-Supported Lipid Bilayers: An Integrated View," *Langmuir*, vol. 22, pp. 3497-3505, 2006.
- [28] J. T. Groves and M. L. Dustin, "Supported planar bilayers in studies on immune cell adhesion and communication," *Journal of Immunological Methods*, vol. 278, pp. 19-32, 2003.
- [29] K. J. Seu, A. P. Pandey, F. Haque, *et al.*, "Effect of Surface Treatment on Diffusion and Domain Formation in Supported Lipid Bilayers," *Biophysical Journal*, vol. 92, pp. 2445-2450, 2007.
- [30] B. Raguse, V. Braach-Maksvytis, B. A. Cornell, *et al.*, "Tethered Lipid Bilayer Membranes: Formation and Ionic Reservoir Characterization," *Langmuir*, vol. 14, pp. 648-659, 1998.
- [31] S. M. Schiller, R. Naumann, K. Lovejoy, *et al.*, "Archaea Analogue Thiolipids for Tethered Bilayer Lipid Membranes on Ultrasoother Gold Surfaces," *Angewandte Chemie-International Edition in English*, vol. 42, pp. 208-211, 2003.
- [32] D. J. McGillivray, G. Valincius, D. J. Vanderah, *et al.*, "Molecular-scale structural and functional characterization of sparsely tethered bilayer lipid membranes," *Biointerphases*, vol. 2, pp. 21-33, 2007.
- [33] M. Tanaka and E. Sackmann, "Polymer-supported membranes as models of the cell surface," *Nature*, vol. 437, pp. 656-663, 2005.
- [34] M. L. Wagner and L. K. Tamm, "Tethered polymer-supported planar lipid bilayers for reconstitution of integral membrane proteins: Silane-polyethyleneglycol-lipid as a cushion and covalent linker," *Biophysical Journal*, vol. 79, pp. 1400-1414, Sep 2000.
- [35] M. Seitz, E. Ter-Ovanesyan, M. Hausch, *et al.*, "Formation of tethered supported bilayers by vesicle fusion onto lipopolymer monolayers promoted by osmotic stress," *Langmuir*, vol. 16, pp. 6067-6070, Jul 2000.
- [36] N. Bunjes, E. K. Schmidt, A. Jonczyk, *et al.*, "Thiopeptide-Supported Lipid Layers on Solid Substrates," *Langmuir*, vol. 13, pp. 6188-6194, 1997.
- [37] E. Reimhult and K. Kumar, "Membrane biosensor platforms using nano- and microporous supports," *Trends in Biotechnology*, vol. 26, pp. 82-89, 2008.
-

- [38] D. P. Nikolelis, G. Raftopoulou, P. Chatzigeorgiou, *et al.*, "Optical portable biosensors based on stabilized lipid membrane for the rapid detection of doping materials in human urine," *Sensors and Actuators B: Chemical*, vol. 130, pp. 577-582, 2008.
- [39] X. Song and B. I. Swanson, "Direct, Ultrasensitive, and Selective Optical Detection of Protein Toxins Using Multivalent Interactions," *Analytical Chemistry*, vol. 71, pp. 2097-2107, 1999.
- [40] H. Ringsdorf, B. Schlarb, and J. Venzmer, "Molecular Architecture and Function of Polymeric Oriented Systems - Models for the Study of Organization, Surface Recognition, and Dynamics of Biomembranes," *Angewandte Chemie-International Edition in English*, vol. 27, pp. 113-158, Jan 1988.
- [41] E. E. Ross, B. Bondurant, T. Spratt, *et al.*, "Formation of Self-Assembled, Air-Stable Lipid Bilayer Membranes on Solid Supports," *Langmuir*, vol. 17, pp. 2305-2307, 2001.
- [42] D. F. O'Brien, T. H. Whitesides, and R. T. Klingbiel, "The Photo-Polymerization of Lipid-Diacetylenes in Bimolecular-Layer Membranes," *Journal of Polymer Science Part C-Polymer Letters*, vol. 19, pp. 95-101, 1981.
- [43] S. Liu and D. F. O'Brien, "Stable Polymeric Nanoballoons: Lyophilization and Rehydration of Cross-linked Liposomes," *Journal of the American Chemical Society*, vol. 124, pp. 6037-6042, 2002.
- [44] R. Elbert, A. Laschewsky, and H. Ringsdorf, "Hydrophilic Spacer Groups in Polymerizable Lipids - Formation of Biomembrane Models from Bulk Polymerized Lipids," *Journal of the American Chemical Society*, vol. 107, pp. 4134-4141, 1985.
- [45] H. H. Hub, B. Hupfer, H. Koch, *et al.*, "Polyreactions in Ordered Systems .20. Polymerizable Phospholipid Analogs - New Stable Biomembrane and Cell Models," *Angewandte Chemie-International Edition in English*, vol. 19, pp. 938-940, 1980.
- [46] V. Subramaniam, G. D. D'Ambruso, H. K. Hall, *et al.*, "Reconstitution of Rhodopsin into Polymerizable Planar Supported Lipid Bilayers: Influence of Dienoyl Monomer Structure on Photoactivation," *Langmuir*, vol. 24, pp. 11067-11075, 2008.
- [47] A. Laschewsky, H. Ringsdorf, G. Schmidt, *et al.*, "Self-organization of polymeric lipids with hydrophilic spacers in side groups and main chain: investigation in monolayers and multilayers," *Journal of the American Chemical Society*, vol. 109, pp. 788-796, 1987.
- [48] T.-J. Jeon, N. Malmstadt, and J. J. Schmidt, "Hydrogel-Encapsulated Lipid Membranes," *Journal of the American Chemical Society*, vol. 128, pp. 42-43, 2005.

-
- [49] T.-J. Jeon, N. Malmstadt, J. L. Poulos, *et al.*, "Black lipid membranes stabilized through substrate conjugation to a hydrogel," *Biointerphases*, vol. 3, pp. FA96-FA100, 2008.
- [50] C. C. Ng, Y.-L. Cheng, and P. S. Pennefather, "Properties of a Self-Assembled Phospholipid Membrane Supported on Lipobeads," *Biophysical Journal*, vol. 87, pp. 323-331, 2004.
- [51] B. M. Discher, Y.-Y. Won, D. S. Ege, *et al.*, "Polymersomes: Tough Vesicles Made from Diblock Copolymers," *Science*, vol. 284, pp. 1143-1146, 1999.
- [52] J. N. Israelachvili, S. Marcelja, and R. G. Horn, "Physical Principles of Membrane Organization," *Quarterly Reviews of Biophysics*, vol. 13, pp. 121-200, 1980.
- [53] M. Antonietti and S. Forster, "Vesicles and liposomes: A self-assembly principle beyond lipids," *Advanced Materials*, vol. 15, pp. 1323-1333, Aug 2003.
- [54] H. Bermudez, D. A. Hammer, and D. E. Discher, "Effect of bilayer thickness on membrane bending rigidity," *Langmuir*, vol. 20, pp. 540-543, Feb 2004.
- [55] H. Bermudez, A. K. Brannan, D. A. Hammer, *et al.*, "Molecular Weight Dependence of Polymersome Membrane Structure, Elasticity, and Stability," *Macromolecules*, vol. 35, pp. 8203-8208, 2002.
- [56] G. Srinivas, D. E. Discher, and M. L. Klein, "Self-assembly and properties of diblock copolymers by coarse-grain molecular dynamics," *Nat Mater*, vol. 3, pp. 638-644, 2004.
- [57] G. Battaglia and A. J. Ryan, "Bilayers and Interdigitation in Block Copolymer Vesicles," *Journal of the American Chemical Society*, vol. 127, pp. 8757-8764, 2005.
- [58] W. Meier, C. Nardin, and M. Winterhalter, "Reconstitution of channel proteins in (polymerized) ABA triblock copolymer membranes," *Angewandte Chemie-International Edition*, vol. 39, pp. 4599-4602, 2000.
- [59] D. Wong, T. J. Jeon, and J. Schmidt, "Single molecule measurements of channel proteins incorporated into biomimetic polymer membranes," *Nanotechnology*, vol. 17, pp. 3710-3717, Aug 2006.
- [60] H.-J. Choi and C. D. Montemagno, "Artificial Organelle: ATP Synthesis from Cellular Mimetic Polymersomes," *Nano Letters*, vol. 5, pp. 2538-2542, 2005.
- [61] K. Vijayan, D. E. Discher, J. Lal, *et al.*, "Interactions of Membrane-Active Peptides with Thick, Neutral, Nonzwitterionic Bilayers," *The Journal of Physical Chemistry B*, vol. 109, pp. 14356-14364, 2005.
-

- [62] V. Pata and N. Dan, "The Effect of Chain Length on Protein Solubilization in Polymer-Based Vesicles (Polymersomes)," *Biophysical Journal*, vol. 85, pp. 2111-2118, 2003.
- [63] H.-J. Butt, T. Müller, and H. Gross, "Immobilizing Biomolecules for Scanning Force Microscopy by Embedding in Carbon," *Journal of Structural Biology*, vol. 110, pp. 127-132, 1993.
- [64] R. Naumann, S. M. Schiller, F. Giess, *et al.*, "Tethered Lipid Bilayers on Ultraflat Gold Surfaces," *Langmuir*, vol. 19, pp. 5435-5443, 2003.
- [65] S. Foerster and E. Kraemer, "Synthesis of PB-PEO and PI-PEO Block Copolymers with Alkylolithium Initiators and the Phosphazene Base t-BuP4," *Macromolecules*, vol. 32, pp. 2783-2785, 1999.
- [66] B. Esswein and M. Möller, "Polymerization of Ethylene Oxide with Alkylolithium Compounds and the Phosphazene Base tBuP4," *Angewandte Chemie-International Edition in English*, vol. 35, pp. 623-625, 1996.
- [67] R. Wiesendanger, *Scanning probe microscopy and spectroscopy methods and applications* vol. Reprinted, transferred to digital printing. Cambridge [u.a.]: Cambridge Univ. Press, 2001.
- [68] Wikipedia. http://en.wikipedia.org/wiki/Atomic_force_microscope.
- [69] N. Jalili and K. Laxminarayana, "A review of atomic force microscopy imaging systems: application to molecular metrology and biological sciences," *Mechatronics*, vol. 14, pp. 907-945, 2004.
- [70] B. Cappella and G. Dietler, "Force-distance curves by atomic force microscopy," *Surface Science Reports*, vol. 34, pp. 1-+, 1999.
- [71] H. Clausen-Schaumann, M. Seitz, R. Krautbauer, *et al.*, "Force spectroscopy with single bio-molecules," *Current Opinion in Chemical Biology*, vol. 4, pp. 524-530, 2000.
- [72] W. Knoll, "Interfaces and thin films as seen by bound electromagnetic waves," *Annual Review of Physical Chemistry*, vol. 49, pp. 569-638, 1998.
- [73] E. Kretschmann and H. Raether, "Radiative Decay of Non Radiative Surface Plasmons Excited by Light," *Zeitschrift Fur Naturforschung Part a-Astrophysik Physik Und Physikalische Chemie*, vol. A 23, pp. 2135-&, 1968.
- [74] I. K. Vockenroth, "Investigations of tethered bilayer lipid membranes for their potential use in biosensing devices," PhD, PhD Thesis, 2007.
- [75] J. Worm. (2001), <http://www.mpip-mainz.mpg.de/knoll/soft/>.

-
- [76] P. Yeh, *Optical waves in layered media*. New York: Wiley, 1988.
- [77] L. G. Schulz and F. R. Tangherlini, "Optical Constants of Silver, Gold, Copper, and Aluminum. II. The Index of Refraction n ," *J. Opt. Soc. Am.*, vol. 44, pp. 362-367, 1954.
- [78] J. Brandrup, *Polymer Handbook*, Second ed. New York: John Wiley & Sons, 1975.
- [79] J. R. Macdonald and E. Barsoukov, *Impedance spectroscopy theory, experiment, and applications* vol. 2nd ed. edited by Evgenij Barsoukov, J. Ross Macdonald. Hoboken, N.J.: Wiley-Interscience, 2005.
- [80] C. Steinem, A. Janshoff, W. P. Ulrich, *et al.*, "Impedance analysis of supported lipid bilayer membranes: A scrutiny of different preparation techniques," *Biochimica Et Biophysica Acta-Biomembranes*, vol. 1279, pp. 169-180, Mar 1996.
- [81] D. Magde, E. Elson, and W. W. Webb, "Thermodynamic Fluctuations in a Reacting System—Measurement by Fluorescence Correlation Spectroscopy," *Physical Review Letters*, vol. 29, p. 705, 1972.
- [82] L. Kastrop, H. Blom, C. Eggeling, *et al.*, "Fluorescence Fluctuation Spectroscopy in Subdiffraction Focal Volumes," *Physical Review Letters*, vol. 94, p. 178104, 2005.
- [83] M. Leutenegger, M. Gösch, A. Perentes, *et al.*, "Confining the sampling volume for Fluorescence Correlation Spectroscopy using a sub-wavelength sized aperture," *Opt. Express*, vol. 14, pp. 956-969, 2006.
- [84] E. Haustein and P. Schwille, "Single-molecule spectroscopic methods," *Current Opinion in Structural Biology*, vol. 14, pp. 531-540, 2004/10 2004.
- [85] J. A. Zasadzinski, R. Viswanathan, L. Madsen, *et al.*, "Langmuir-Blodgett films," *Science*, vol. 263, pp. 1726-1733, 1994.
- [86] M. Merzlyakov, E. Li, and K. Hristova, "Directed Assembly of Surface-Supported Bilayers with Transmembrane Helices," *Langmuir*, vol. 22, pp. 1247-1253, 2006.
- [87] K. Yu and A. Eisenberg, "Bilayer Morphologies of Self-Assembled Crew-Cut Aggregates of Amphiphilic PS-b-PEO Diblock Copolymers in Solution," *Macromolecules*, vol. 31, p. 3509, 1998.
- [88] D. E. Discher and A. Eisenberg, "Polymer Vesicles," *Science*, vol. 297, pp. 967-973, 2002.
- [89] F. H. Meng, Z. Y. Zhong, and J. Feijen, "Stimuli-Responsive Polymersomes for Programmed Drug Delivery," *Biomacromolecules*, vol. 10, pp. 197-209, Feb 2009.
- [90] A. Mecke, C. Dittrich, and W. Meier, "Biomimetic membranes designed from amphiphilic block copolymers," *Soft Matter*, vol. 2, pp. 751-759, 2006.
-

- [91] A. Taubert, A. Napoli, and W. Meier, "Self-assembly of reactive amphiphilic block copolymers as mimetics for biological membranes," *Current Opinion in Chemical Biology*, vol. 8, pp. 598-603, 2004.
- [92] B. M. Discher, H. Bermudez, D. A. Hammer, *et al.*, "Cross-linked Polymersome Membranes: Vesicles with Broadly Adjustable Properties," *The Journal of Physical Chemistry B*, vol. 106, pp. 2848-2854, 2002.
- [93] J. C. M. Lee, M. Santore, F. S. Bates, *et al.*, "From membranes to melts, rouse to reptation: Diffusion in polymersome versus lipid bilayers," *Macromolecules*, vol. 35, pp. 323-326, Jan 2002.
- [94] C. Nardin, J. Widmer, M. Winterhalter, *et al.*, "Amphiphilic block copolymer nanocontainers as bioreactors," *The European Physical Journal E: Soft Matter and Biological Physics*, vol. 4, pp. 403-410, 2001.
- [95] C. Nardin, S. Thoeni, J. Widmer, *et al.*, "Nanoreactors based on (polymerized) ABA-triblock copolymer vesicles," *Chemical Communications*, pp. 1433-1434, 2000.
- [96] E. Rakhmatullina and W. Meier, "Solid-Supported Block Copolymer Membranes through Interfacial Adsorption of Charged Block Copolymer Vesicles," *Langmuir*, vol. 24, pp. 6254-6261, 2008.
- [97] E. Rakhmatullina, A. Manton, T. Bürgi, *et al.*, "Solid-supported amphiphilic triblock copolymer membranes grafted from gold surface," *Journal of Polymer Science Part A: Polymer Chemistry*, vol. 47, pp. 1-13, 2009.
- [98] J. C. M. Lee, H. Bermudez, B. M. Discher, *et al.*, "Preparation, stability, and in vitro performance of vesicles made with diblock copolymers," *Biotechnology and Bioengineering*, vol. 73, pp. 135-145, Apr 2001.
- [99] Y.-Y. Won, A. K. Brannan, H. T. Davis, *et al.*, "Cryogenic Transmission Electron Microscopy (Cryo-TEM) of Micelles and Vesicles Formed in Water by Poly(ethylene oxide)-Based Block Copolymers," *The Journal of Physical Chemistry B*, vol. 106, pp. 3354-3364, 2002.
- [100] R. Matmour, R. Francis, R. S. Duran, *et al.*, "Interfacial Behavior of Anionically Synthesized Amphiphilic Star Block Copolymers Based on Polybutadiene and Poly(ethylene oxide) at the Air/Water Interface," *Macromolecules*, vol. 38, pp. 7754-7767, 2005.
- [101] R. Matmour, T. J. Joncheray, Y. Gnanou, *et al.*, "Two-Dimensional Polymeric Nanomaterials through Cross-linking of Polybutadiene-b-Poly(ethylene oxide) Monolayers at the Air/Water Interface," *Langmuir*, vol. 23, pp. 649-658, 2007.

-
- [102] T. Miyashita, "Recent Studies on Functional Ultrathin Polymer-Films Prepared by the Langmuir-Blodgett Technique," *Progress in Polymer Science*, vol. 18, pp. 263-294, 1993.
- [103] D. J. Crisp, "Surface Films of Polymers .2. Films of the Coherent and Semi-Crystalline Type," *Journal of Colloid Science*, vol. 1, pp. 161-184, 1946.
- [104] G. Jura and W. D. Harkins, "Equations for the pressure (π)-area (Δ) relations (Isotherms) of liquid expanded and intermediate monolayers on water," *Journal of Chemical Physics*, vol. 12, pp. 113-114, Mar 1944.
- [105] A. M. Goncalves da Silva, E. J. M. Filipe, J. M. R. d'Oliveira, *et al.*, "Interfacial Behavior of Poly(styrene) Poly(ethylene oxide) Diblock Copolymer Monolayers at the Air Water Interface. Hydrophilic Block Chain Length and Temperature Influence," *Langmuir*, vol. 12, pp. 6547-6553, 1996.
- [106] W. D. Harkins, "The physical chemistry of surface films," *The physical chemistry of surface films*, p. xvi+413 pp., 1952 1952.
- [107] S. M. Baker, K. A. Leach, C. E. Devereaux, *et al.*, "Controlled Patterning of Diblock Copolymers by Monolayer Langmuir-Blodgett Deposition," *Macromolecules*, vol. 33, pp. 5432-5436, 2000.
- [108] C. L. Brosseau, J. Leitch, X. Bin, *et al.*, "Electrochemical and PM-IRRAS a Glycolipid-Containing Biomimetic Membrane Prepared Using Langmuir-Blodgett/Langmuir-Schaefer Deposition," *Langmuir*, vol. 24, pp. 13058-13067, 2008.
- [109] D. K. Schwartz, "Langmuir-Blodgett film structure," *Surface Science Reports*, vol. 27, pp. 241-334, 1997 1997.
- [110] I. Pera, R. Stark, M. Kappl, *et al.*, "Using the Atomic Force Microscope to Study the Interaction between Two Solid Supported Lipid Bilayers and the Influence of Synapsin I," *Biophysical Journal*, vol. 87, pp. 2446-2455, 2004.
- [111] R. F. Roskamp, I. K. Vockenroth, N. Eisenmenger, *et al.*, "Functional Tethered Bilayer Lipid Membranes on Aluminum Oxide," *ChemPhysChem*, vol. 9, pp. 1920-1924, 2008.
- [112] I. K. Vockenroth, P. P. Atanasova, J. R. Long, *et al.*, "Functional incorporation of the pore forming segment of AChR M2 into tethered bilayer lipid membranes," *Biochimica et Biophysica Acta (BBA) - Biomembranes*, vol. 1768, pp. 1114-1120, 2007.
-

- [113] F. Albertorio, V. A. Chapa, X. Chen, *et al.*, "The alpha, alpha-(1 -> 1) linkage of trehalose is key to anhydrobiotic preservation," *Journal of the American Chemical Society*, vol. 129, pp. 10567-10574, Aug 2007.
- [114] F. Albertorio, A. J. Diaz, T. Yang, *et al.*, "Fluid and Air-Stable Lipopolymer Membranes for Biosensor Applications," *Langmuir*, vol. 21, pp. 7476-7482, 2005.
- [115] Y. Deng, Y. Wang, B. Holtz, *et al.*, "Fluidic and air-stable supported lipid bilayer and cell-mimicking microarrays," *Journal of the American Chemical Society*, vol. 130, pp. 6267-6271, May 2008.
- [116] S. Belegriou, J. Dorn, M. Kreiter, *et al.*, "Biomimetic Supported Membranes from Amphiphilic Block Copolymers," *Soft Matter*, p. in print, 2010.
- [117] T. Schmidt, G. J. Schutz, W. Baumgartner, *et al.*, "Imaging of single molecule diffusion
10.1073/pnas.93.7.2926," *PNAS*, vol. 93, pp. 2926-2929, April 2, 1996 1996.
- [118] D. J. Muller and A. Engel, "Strategies to prepare and characterize native membrane proteins and protein membranes by AFM," *Current Opinion in Colloid & Interface Science*, vol. 13, pp. 338-350, 2008.
- [119] Y. F. Dufrêne and G. U. Lee, "Advances in the characterization of supported lipid films with the atomic force microscope," *Biochimica et Biophysica Acta (BBA) - Biomembranes*, vol. 1509, pp. 14-41, 2000.
- [120] D. Constantin, U. Mennicke, C. Li, *et al.*, "Solid-supported lipid multilayers: Structure factor and fluctuations," *European Physical Journal E*, vol. 12, pp. 283-290, 2003.
- [121] C. Nardin, M. Winterhalter, and W. Meier, "Giant free-standing ABA triblock copolymer membranes," *Langmuir*, vol. 16, pp. 7708-7712, Oct 2000.
- [122] R. A. Dixon and I. Chopra, "Polymyxin B and polymyxin B nonapeptide alter cytoplasmic membrane permeability in Escherichia coli," *Journal of Antimicrobial Chemotherapy*, vol. 18, pp. 557-563, 1986.
- [123] J. J. Kasianowicz, T. L. Nguyen, and V. M. Stanford, "Enhancing molecular flux through nanopores by means of attractive interactions," *Proceedings of the National Academy of Sciences*, vol. 103, pp. 11431-11432, 2006.
- [124] T. Tomita, M. Watanabe, and T. Yasuda, "Influence of membrane fluidity on the assembly of Staphylococcus aureus alpha-toxin, a channel-forming protein, in liposome membrane," *Journal of Biological Chemistry*, vol. 267, pp. 13391-13397, 1992.

-
- [125] L. Song, M. R. Hobaugh, C. Shustak, *et al.*, "Structure of Staphylococcal alpha - Hemolysin, a Heptameric Transmembrane Pore," *Science*, vol. 274, pp. 1859-1865, 1996.
- [126] H. Duclohier and H. Wróblewski, "Voltage-Dependent Pore Formation and Antimicrobial Activity by Alamethicin and Analogues," *Journal of Membrane Biology*, vol. 184, pp. 1-12, 2001.
- [127] A. Spaar, C. Münster, and T. Salditt, "Conformation of Peptides in Lipid Membranes Studied by X-Ray Grazing Incidence Scattering," *Biophysical Journal*, vol. 87, pp. 396-407, 2004.
- [128] F.-Y. Chen, M.-T. Lee, and H. W. Huang, "Evidence for Membrane Thinning Effect as the Mechanism for Peptide-Induced Pore Formation," *Biophysical Journal*, vol. 84, pp. 3751-3758, 2003.
- [129] A. L. Plant, "Self-assembled phospholipid/alkanethiol biomimetic bilayers on gold," *Langmuir*, vol. 9, pp. 2764-2767, 2002.
- [130] D. Stamou, C. Duschl, E. Delamarche, *et al.*, "Self-assembled microarrays of attoliter molecular vessels," *Angewandte Chemie-International Edition*, vol. 42, pp. 5580-5583, 2003.
- [131] M. Maskos, "Influence of the solvent and the end groups on the morphology of cross-linked amphiphilic poly(1,2-butadiene)-b-poly(ethylene oxide) nanoparticles," *Polymer*, vol. 47, pp. 1172-1178, 2006.
- [132] T. B. He, B. C. Li, and S. J. Ren, "Glass-Transition Temperature and Chain Flexibility of 1,2-Polybutadiene," *Journal of Applied Polymer Science*, vol. 31, pp. 873-884, Feb 1986.
- [133] E. National Research Council. Committee on Polymer Science and, *Polymer science and engineering the shifting research frontiers*. Washington: National Acad. Press, 1994.
- [134] O. Prucker, S. Christian, H. Bock, *et al.*, "On the glass transition in ultrathin polymer films of different molecular architecture," *Macromolecular Chemistry and Physics*, vol. 199, pp. 1435-1444, Jul 1998.
- [135] O. Wesolowska, K. Michalak, J. Maniewska, *et al.*, "Giant unilamellar vesicles - a perfect tool to visualize phase separation and lipid rafts in model systems," *Acta Biochimica Polonica*, vol. 56, pp. 33-39, 2009.
- [136] A. Wiese, M. Münstermann, T. Gutsmann, *et al.*, "Molecular Mechanisms of Polymyxin B-Membrane Interactions: Direct Correlation Between Surface Charge
-

- Density and Self-Promoted Transport," *Journal of Membrane Biology*, vol. 162, pp. 127-138, 1998.
- [137] D. C. Morrison and D. M. Jacobs, "Binding of polymyxin B to the lipid A portion of bacterial lipopolysaccharides," *Immunochemistry*, vol. 13, pp. 813-818, 1976.
- [138] I. K. Vockenroth, P. P. Atanasova, A. T. A. Jenkins, *et al.*, "Incorporation of alpha-hemolysin in different tethered bilayer lipid membrane architectures," *Langmuir*, vol. 24, pp. 496-502, Jan 2008.
- [139] P. Ronchi, S. Colombo, M. Francolini, *et al.*, "Transmembrane domain-dependent partitioning of membrane proteins within the endoplasmic reticulum," *The Journal of Cell Biology*, vol. 181, pp. 105-118, 2008.
- [140] A. D. Dupuy and D. M. Engelman, "Protein area occupancy at the center of the red blood cell membrane," *Proceedings of the National Academy of Sciences*, vol. 105, pp. 2848-2852, 2008.
- [141] P. Sharma, R. Varma, R. C. Sarasij, *et al.*, "Nanoscale Organization of Multiple GPI-Anchored Proteins in Living Cell Membranes," *Cell*, vol. 116, pp. 577-589, 2004.
- [142] P. G. Saffman and M. Delbruck, "Brownian Motion in Biological Membranes," vol. 72, ed, 1975, pp. 3111-3113.
- [143] G. Guigas and M. Weiss, "Size-Dependent Diffusion of Membrane Inclusions," *Biophysical Journal*, vol. 91, pp. 2393-2398, 2006.
- [144] S. Ramadurai, A. Holt, V. Krasnikov, *et al.*, "Lateral Diffusion of Membrane Proteins," *Journal of the American Chemical Society*, vol. 131, pp. 12650-12656, 2009.
- [145] A. Baker, A. Sauliere, F. Dumas, *et al.*, "Functional membrane diffusion of G-protein coupled receptors," *European Biophysics Journal*, vol. 36, pp. 849-860, Oct 14-19 2007.
- [146] S. C. Prinster, C. Hague, and R. A. Hall, "Heterodimerization of G Protein-Coupled Receptors: Specificity and Functional Significance," *Pharmacological Reviews*, vol. 57, pp. 289-298, 2005.
- [147] Invitrogen, "Title," unpublished].
- [148] A. O. M. Wilkie, G. M. Morriss-Kay, E. Yvonne Jones, *et al.*, "Functions of fibroblast growth factors and their receptors," *Current Biology*, vol. 5, pp. 500-507, 1995.
- [149] T. Iwamoto, M. You, E. Li, *et al.*, "Synthesis and initial characterization of FGFR3 transmembrane domain: consequences of sequence modifications," *Biochimica et Biophysica Acta (BBA) - Biomembranes*, vol. 1668, pp. 240-247, 2005.

-
- [150] Invitrogen, "1,1'-dioctadecyl-3,3,3',3'-tetramethylindodicarbocyanine, 4-chlorobenzenesulfonate salt."
- [151] T. Hirokawa, S. Boon-Chieng, and S. Mitaku, "SOSUI: classification and secondary structure prediction system for membrane proteins," *Bioinformatics*, vol. 14, pp. 378-379, 1998.
- [152] T. Cordes, J. Vogelsang, and P. Tinnefeld, "On the Mechanism of Trolox as Antiflickering and Antibleaching Reagent," *Journal of the American Chemical Society*, vol. 131, pp. 5018-5019, 2009.
- [153] D. Sage, F. R. Neumann, F. Hediger, *et al.*, "Automatic tracking of individual fluorescence particles: Application to the study of chromosome dynamics," *Ieee Transactions on Image Processing*, vol. 14, pp. 1372-1383, 2005.
- [154] I. F. Sbalzarini and P. Koumoutsakos, "Feature point tracking and trajectory analysis for video imaging in cell biology," *Journal of Structural Biology*, vol. 151, pp. 182-195, 2005.
- [155] G. M. Lee, A. Ishihara, and K. A. Jacobson, "Direct Observation of Brownian Motion of Lipids in a Membrane," *PNAS*, vol. 88, pp. 6274-6278, July 15, 1991 1991.
- [156] A. Loman, T. Dertinger, F. Koberling, *et al.*, "Comparison of optical saturation effects in conventional and dual-focus fluorescence correlation spectroscopy," *Chemical Physics Letters*, vol. 459, pp. 18-21, 2008.
- [157] C. B. Muller, A. Loman, V. Pacheco, *et al.*, "Precise measurement of diffusion by multi-color dual-focus fluorescence correlation spectroscopy," *EPL (Europhysics Letters)*, vol. 83, p. 46001, 2008.
- [158] J. Widengren, U. Mets, and R. Rigler, "Fluorescence correlation spectroscopy of triplet states in solution: a theoretical and experimental study," *The Journal of Physical Chemistry*, vol. 99, pp. 13368-13379, 1995.
- [159] A. J. García-Sáez and P. Schwille, "Fluorescence correlation spectroscopy for the study of membrane dynamics and protein/lipid interactions," *Methods*, vol. 46, pp. 116-122, 2008.
- [160] V. Buschmann, K. D. Weston, and M. Sauer, "Spectroscopic Study and Evaluation of Red-Absorbing Fluorescent Dyes," *Bioconjugate Chemistry*, vol. 14, pp. 195-204, 2002.
- [161] J. S. Rossman, N. G. Stoicheva, F. D. Langel, *et al.*, "POLKADOTS Are Foci of Functional Interactions in T-Cell Receptor-mediated Signaling to NF- κ B," *Molecular Biology of the Cell*, vol. 17, pp. 2166-2176, 2006.
-

- [162] M. Goodin, S. Yelton, D. Ghosh, *et al.*, "Live-Cell Imaging of Rhabdovirus-Induced Morphological Changes in Plant Nuclear Membranes," *Molecular Plant-Microbe Interactions*, vol. 18, pp. 703-709, 2007.
- [163] N. Kahya and P. Schwille, "Fluorescence correlation studies of lipid domains in model membranes (Review)," *Molecular Membrane Biology*, vol. 23, pp. 29-39, 2006.
- [164] G. Orädd, G. Lindblom, and P. W. Westerman, "Lateral Diffusion of Cholesterol and Dimyristoylphosphatidylcholine in a Lipid Bilayer Measured by Pulsed Field Gradient NMR Spectroscopy," *Biophysical Journal*, vol. 83, pp. 2702-2704, 2002.
- [165] G. Lindblom and G. Orädd, "Lipid lateral diffusion and membrane heterogeneity," *Biochimica et Biophysica Acta (BBA) - Biomembranes*, vol. 1788, pp. 234-244, 2009.
- [166] Y. Gambin, R. Lopez-Esparza, M. Reffay, *et al.*, "Lateral mobility of proteins in liquid membranes revisited," *Proceedings of the National Academy of Sciences of the United States of America*, vol. 103, pp. 2098-2102, 2006.
- [167] K. Kita-Tokarczyk, J. Grumelard, T. Haefele, *et al.*, "Block copolymer vesicles--using concepts from polymer chemistry to mimic biomembranes," *Polymer*, vol. 46, pp. 3540-3563, 2005/5/11 2005.
- [168] N. Sreerama and R. W. Woody, "On the analysis of membrane protein circular dichroism spectra," *Protein Science*, vol. 13, pp. 100-112, Jan 2004.
- [169] Y. Wu, H. W. Huang, and G. A. Olah, "Method of oriented circular dichroism," *Biophysical Journal*, vol. 57, pp. 797-806, 1990.
- [170] K. Hristova, C. E. Dempsey, and S. H. White, "Structure, Location, and Lipid Perturbations of Melittin at the Membrane Interface," *Biophysical Journal*, vol. 80, pp. 801-811, 2001.
- [171] Y. Wu, K. He, S. J. Ludtke, *et al.*, "X-ray diffraction study of lipid bilayer membranes interacting with amphiphilic helical peptides: diphytanoyl phosphatidylcholine with alamethicin at low concentrations," *Biophysical Journal*, vol. 68, pp. 2361-2369, 1995.
- [172] M. Seul and M. J. Sammon, "Preparation of surfactant multilayer films on solid substrates by deposition from organic solution," *Thin Solid Films*, vol. 185, pp. 287-305, 1990.
- [173] G. Reiter, G. Castelein, P. Hoerner, *et al.*, "Morphologies of diblock copolymer thin films before and after crystallization," *European Physical Journal E*, vol. 2, pp. 319-334, Aug 2000.

-
- [174] D. Schwarz, C. Klammt, A. Koglin, *et al.*, "Preparative scale cell-free expression systems: New tools for the large scale preparation of integral membrane proteins for functional and structural studies," *Methods*, vol. 41, pp. 355-369, 2007.
- [175] T. Schmidt, G. J. Schutz, W. Baumgartner, *et al.*, "Characterization of Photophysics and Mobility of Single Molecules in a Fluid Lipid-Membrane," *Journal of Physical Chemistry*, vol. 99, pp. 17662-17668, Dec 1995.
- [176] W.-C. Lin, C. D. Blanchette, T. V. Ratto, *et al.*, "Lipid Asymmetry in DLPC/DSPC-Supported Lipid Bilayers: A Combined AFM and Fluorescence Microscopy Study," *Biophysical Journal*, vol. 90, pp. 228-237, 2006.
- [177] B. Wiltschi, M. Schober, S. D. Kohlwein, *et al.*, "Sterol Binding Assay Using Surface Plasmon Fluorescence Spectroscopy," *Analytical Chemistry*, vol. 78, pp. 547-555, 2005.
- [178] N. L. Benoiton, *Chemistry of peptide synthesis*. Boca Raton: CRC Press, 2006.
- [179] S. Kim, S. Morimoto, E. Koh, *et al.*, "Comparison of effects of a potassium channel opener BRL34915, a specific potassium ionophore valinomycin and calcium channel blockers on endothelin-induced vascular contraction," *Biochemical and Biophysical Research Communications*, vol. 164, pp. 1003-1008, 1989.
- [180] Y. A. Ovchinnikov, "Second febs--ferdinand springer lecture membrane active complexones. chemistry and biological function," *FEBS Letters*, vol. 44, pp. 1-21, 1974.
- [181] P. Lauger, "Carrier-Mediated Ion Transport: Electrical relaxation experiments give insight into the kinetics of ion transport through artificial lipid membrane," *Science*, vol. 178, pp. 24-30, 1972.
- [182] H. D. Holtje, "[Breathing and oxidative phosphorylation]," *Pharm Unserer Zeit*, vol. 6, pp. 123-7, 1977.
- [183] R. Robelek, E. S. Lemker, B. Wiltschi, *et al.*, "Incorporation of in vitro synthesized GPCR into a tethered artificial lipid membrane system," *Angewandte Chemie-International Edition*, vol. 46, pp. 605-608, 2007.
- [184] K. R. Gee, E. A. Archer, and H. C. Kang, "4-Sulfotetrafluorophenyl (STP) esters: New water-soluble amine-reactive reagents for labeling biomolecules," *Tetrahedron Letters*, vol. 40, pp. 1471-1474, 1999.
- [185] B. A. Cornell, V. L. B. Braach-Maksvytis, L. G. King, *et al.*, "A biosensor that uses ion-channel switches," *Nature*, vol. 387, pp. 580-583, 1997.
-

10. Appendix

Appendix A

Calculation of the hydrophobic domains of the FGFR3-(TM) mutant with the web based program SOSUI (http://bp.nuap.nagoya-u.ac.jp/sosui/sosui_submit.html)

SOSUI Result

Query title : None

Total length : 33 A. A.

Average of hydrophobicity : 1.130303

**This amino acid sequence is of a MEMBRANE PROTEIN
which have 1 transmembrane helix.**

No.	N terminal	transmembrane region	C terminal	type	length
1	6	VYAGILSYGVGFFLFILVVEAVT	28	PRIMARY	23

Display Options

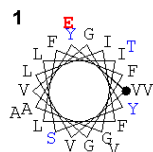
[Hydropathy profile]



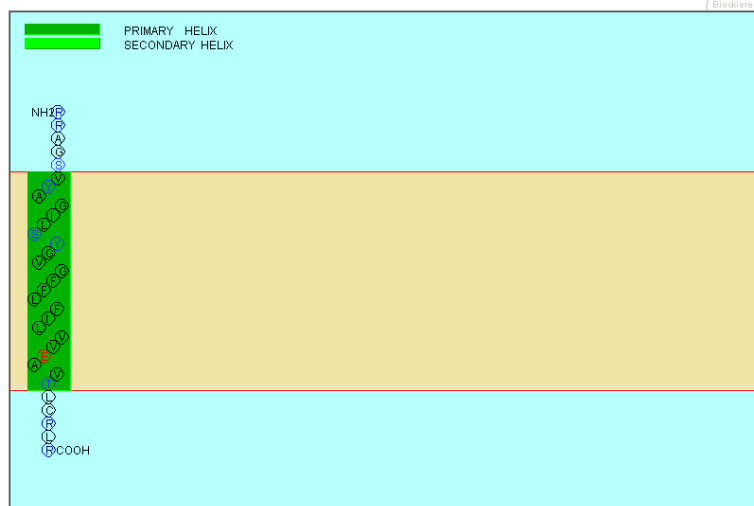
[Blockieren]

[Helical wheel diagram of predicted segments]

Hydrophobic residue: Black
Polar residue: Blue
Charged residue: Bold blue(+) Bold red(-)



[Blockieren]



Appendix B

FCS autocorrelation curves corresponding to data in Table 5. Measurements are not plotted in one graph since they were recorded during different measurement sessions with different calibrations.

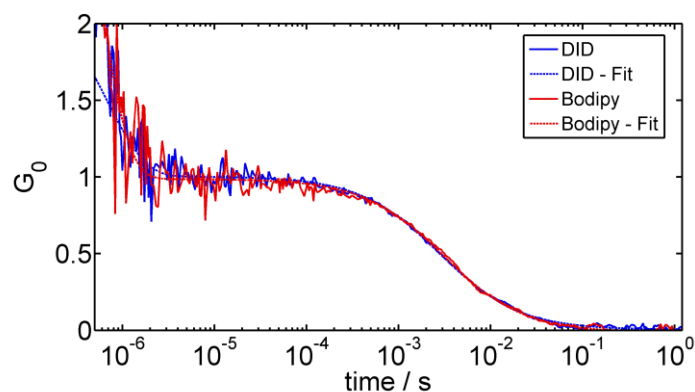


Figure 52: Autocorrelation curves of DID and Bodipy 630/650 inside a DiPhyPC lipid bilayer.

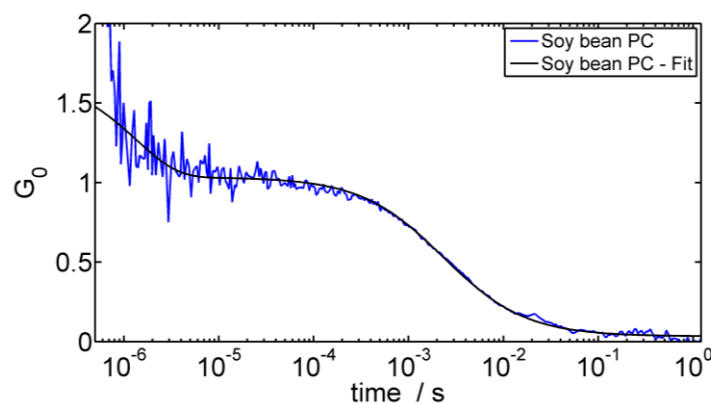


Figure 53: Autocorrelation curves of Bodipy 630/650 inside a Soy bean PC lipid bilayer.

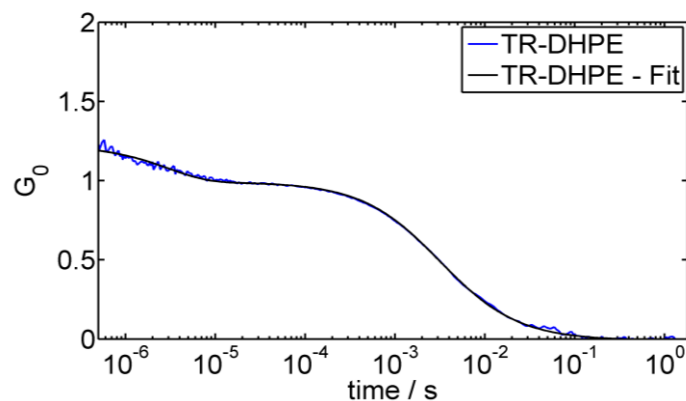


Figure 54: Autocorrelation curves of the fluorescent lipid Texas Red-DHPE

Acknowledgement

Without the help of many people this work would not have been possible.

I want to thank my supervisors for giving me the opportunity to carry out my PhD studies at the MPIP. Furthermore I want to thank them for the interesting and challenging project and their support throughout the last three years.

I also want to thank all my collaboration partners at the institute and abroad for their very productive cooperation.

Many thanks go to all members of the Materials Research Group at the MPIP for the great atmosphere and the many helpful discussions. I especially want to thank the diploma and internship students who helped me with my projects for the nice cooperation and their input.

During my PhD studies I used a lot of different techniques and equipment. I thank the scientific staff for always providing great support. This really produces excellent conditions to carry out research.

Furthermore I want to thank the technical service and the electronic / mechanical workshop for their uncomplicated help with many lab issues.

Last but not least I want to thank my wife for her constant support and her unceasing energy to motivate me even when experiments were not going so well in the lab.

Publications

1. Belegriou, S. *, **Dorn, J.** *, Kreiter, M., Kita-Tokarczyk, K., Sinner, E. K., and Meier, W. (2010) Biomimetic supported membranes from amphiphilic block copolymers, *Soft Matter* 6, 179-186.
* (equal contributions)
2. **Dorn, J.** , Belegriou, S., Kreiter, M., Sinner, E. K., and Meier, W. (2010) Vesicle spreading – An easy route to biomimetic planar polymer bilayers, (**to be submitted**)
3. Dorn, J. Geissbühler, M. , Märki, I. , Kreiter. M. , Sinner, E. K. , Lasser, T. Transmembrane peptide diffusion in giant unilamellar polymer vesicles (**in preparation**)